

**DEVELOPMENT OF LOW ALKALINITY ACTIVATED
CONSTRUCTION AND DEMOLITION WASTE BASED
GEOPOLYMER BINDER SYSTEMS FOR 3D PRINTING
APPLICATION**

**ÜÇ BOYUTLU BASKI UYGULAMASI İÇİN DÜŞÜK
ALKALİNİTE İLE AKTİVE EDİLMİŞ İNŞAAT VE YIKINTI
ATIĞI ESASLI JEOPOLİMER BAĞLAYICILI
SİSTEMLERİN GELİŞTİRİLMESİ**

HÜSEYİN İLCAN

PROF. DR. MUSTAFA ŞAHMARAN

Supervisor

Submitted to

Graduate School of Science and Engineering of Hacettepe University

as a Partial Fulfillment to the Requirements

for be Award of the Degree of **Doctor of Philosophy**

in Civil Engineering

2024

ABSTRACT

DEVELOPMENT OF LOW ALKALINITY ACTIVATED CONSTRUCTION AND DEMOLITION WASTE BASED GEOPOLYMER BINDER SYSTEMS FOR 3D PRINTING APPLICATION

HÜSEYİN İLCAN

Doctor of Philosophy, Department of Civil Engineering

Supervisor: Prof. Dr. Mustafa ŞAHMARAN

May 2024, 149 pages

The extent of environmental damage caused by construction activities executed to address the increasing population's housing and infrastructure needs and to construct a more livable world has been more clearly observed in recent years, especially as the magnitude of encountered natural phenomena is witnessed. The rises in greenhouse gas emissions, escalating soil and water pollution, the excavation use of clean and arable lands, significant depletion of natural resources, and various other factors can be detected as aspects missed by the construction sector in its pursuit of building a more livable world. Concrete stands out as the dominant material in the construction sector, with an annual global consumption of approximately 30 billion tons, making it the most commonly utilized material in the world after water. This widespread use contributes significantly to the consumption of Portland cement, the primary binder in traditional concrete production, which is energy-intensive and has high carbon emissions. To slow down this negative trend and lower the environmental burdens associated with the construction sector, various steps have been taken. At this point, some studies are being conducted on decreasing the clinker ratio in cement production, changing fuels and raw materials in cement production, substituting industrial by-products

for cement, utilizing waste in cementitious systems, and developing alternative binding systems to cement.

As a result of these studies, it has been discovered that a new generation binding system, synthesized through the alkali activation of precursor materials called geopolymers, which reduces the environmental impact of cementitious systems, can be used as an alternative to cementitious systems in the construction sector. Its ability to utilize industrial waste as precursor materials in synthesis has led to rapid progress in its use as a construction material, providing both environmental and economic benefits. While the precursors used in traditional geopolymer synthesis are industrial by-products, their elevated demand by the cement/concrete industry, as they can serve as substitutes, has diminished the ready availability of these materials and climbed their costs. Increasing costs and supply-related issues have induced researchers to explore the incorporation of innovative aluminosilicate precursors in geopolymer synthesis. The objective is to use easily accessible and affordable materials while dealing with the challenge of currently unvalorized wastes. These dual objectives endeavor to design more economical and environmentally friendly materials while simultaneously addressing issues coupled with generated wastes. In this context, considering that construction and demolition wastes (CDW) are predominantly composed of aluminum, silicon, and calcium sources, coupled with the global prevalence of CDW generation where it is mostly either disposed of in appointed landfill areas or used for low-tech applications, the incorporation of CDW-based materials in geopolymer production emerges as a promising avenue for effective and innovative material development, along with the high-quality valorization of wastes.

In addition to material-sourced issues in the construction sector, despite holding a considerable market share among industrial sectors, the construction industry has fallen behind in keeping pace with emerging technology in the past few decades and has been indecisive in taking required steps in traditional production processes to improve productivity compared to the other sectors. The growing demand for housing because of ongoing population growth, disasters, and wars, has resulted in the recognition in recent years by academics and companies that manufacturing processes in the construction sector required to be more efficient, cheap, and fast. Given this context, three-dimensional additive manufacturing (3D-AM), whose usage is rapidly gaining popularity due to the numerous advantages it offers in other sectors, has started to be employed in the construction industry.

3D-AM systematically constructs tailored structures through the successive deposition of layers following the digital models, offering a high degree of design freedom. With the adaptation of 3D-AM in the construction industry, digitalization, automation and individualization in built environments can be acquired. The key benefits provided by the 3D-AM technique involve the reduction of production-related errors, shortened production time, decreased occupational safety risks, reduced need for skilled workforce, increased customization, and lowered costs. Furthermore, 3D-AM which provides moldless production and the reduced generation of waste materials during the operation process, contributes significantly to mitigating the high environmental burdens caused by the construction sector.

Considering all these circumstances, within the scope of this thesis, studies have been conducted to (i) evaluate the effects of incorporation of the industrial wastes into CDW-based geopolymer mixtures, (ii) to provide comprehensive insights and knowledge about tailoring the fresh and hardened properties of the CDW-based geopolymer mixtures considering environmental burdens, (iii) to develop more environmentally friendly, economical, sustainable, and value-added 3D-AM-compatible geopolymer binder systems using CDW, (iv) to minimize the use of alkaline activators and maximize waste materials, (v) to investigate the effects of various additives on the engineering properties of geopolymer mortars, (vi) to mitigate shrinkage-related crack formation in 3D-printed filaments and efflorescence issues in CDW-based geopolymer mixtures, (vii) to investigate reinforcing strategies for 3D-printed structures and possibility of modular system in 3D-printed construction. The study utilized a comprehensive testing approach, encompassing a range of assessments such as flow table, setting time, flow curve, three-interval thixotropy, ram extruder, LCA, compressive and flexural strength, direct tensile, water absorption, sorptivity, efflorescence, drying shrinkage, wet-dry and freeze-thaw cycling tests. This comprehensive methodology facilitated a thorough exploration of the properties and performance of the geopolymer mixtures, effectively fulfilling the research objectives.

Keywords: Construction and demolition wastes, geopolymer, 3D-AM, waste upcycling, circularity in built environment

ÖZET

ÜÇ BOYUTLU BASKI UYGULAMASI İÇİN DÜŞÜK ALKALİNİTE İLE AKTİVE EDİLMİŞ İNŞAAT VE YIKINTI ATIĞI ESASLI JEOPOLİMER BAĞLAYICILI SİSTEMLERİN GELİŞTİRİLMESİ

HÜSEYİN İLCAN

Doktora, İnşaat Mühendisliği Bölümü

Tez Danışmanı: Prof. Dr. Mustafa ŞAHMARAN

Mayıs 2024, 149 sayfa

Artan nüfusun barınma ve altyapı ihtiyaçlarının karşılanması ve daha yaşanabilir bir dünya inşa edilmesi amacıyla gerçekleştirilen inşaat faaliyetlerinin çevreye verdiği zararın boyutları, özellikle karşılaşılan doğa olaylarının büyüklüğüyle birlikte son yıllarda daha iyi gözlemlenmektedir. Sera gazlarının emisyonlarındaki artışlar, artan toprak ve su kirlilikleri, temiz ve tarıma elverişli arazilerin hafriyat amaçlı kullanılması, doğal kaynakların yüksek miktarlarda tüketilmesi vb. gibi bir çok husus inşaat sektörünün daha yaşanabilir bir dünya inşa etmek isterken gözden kaçırdığı noktalar olarak hanesine yazılabilir. Beton, yıllık yaklaşık 30 milyar tonluk küresel tüketimiyle inşaat sektörünün baskın malzemesi olarak öne çıkmaktadır ve dünyada sudan sonra en çok kullanılan malzemedir. Bu yaygın kullanım, geleneksel beton üretiminde birincil bağlayıcı olan enerji yoğunluğu yüksek ve yüksek karbon salımına sahip Portland çimentosunun önemli miktarlarda tüketilmesine katkıda bulunmaktadır. Bu kötü gidişatı yavaşlatabilmek ve inşaat sektörünün sahip olduğu çevresel yükleri azaltmak için çeşitli adımlar atılmaya başlanmıştır. Bu noktada, çimento üretiminde klinker oranının azaltılması, çimento üretiminde yakıt ve hammadde değişimi, endüstriyel yan ürünlerin çimentoya ikamesi, atıkların çimentolu sistemlerde değerlendirilmesi ve çimentoya alternatif bağlayıcı sistemlerin geliştirilmesi üzerine bir takım çalışmalar yürütülmektedir.

Yapılan bu çalışmalar neticesinde, çimentolu sistemlerin çevresel etkisini azaltacak, jeopolimer olarak adlandırılan, öncül malzemelerin alkali aktivasyonu yoluyla sentezlenen yeni nesil bağlayıcı sistemin inşaat sektöründe çimentolu sistemlere alternatif olarak kullanılabileceği keşfedilmiştir. Sentezinde endüstriyel atıkların öncül malzeme olarak kullanılabirliği sayesinde sağlamış olduğu hem çevresel hem de ekonomik pozitif etkiler yapı malzemesi olarak kullanımı noktasında hızlı ilerlemeler kaydetmesini sağlamıştır. Fakat, geleneksel jeopolimer sentezi için kullanılan öncüller endüstriyel yan ürünler olsa da, bu malzemelerin çimento/beton endüstrisindeki artan talep nedeniyle hazır bulunabilirlikleri azalmış ve maliyetleri artmıştır. Artan maliyetler ve tedarikle ilgili sorunlar, araştırmacıları jeopolimer sentezi için yenilikçi alüminosilikat öncüllerinin kullanımını incelemeye yönlendirmiştir. Hedef, kolayca ulaşılabilir ve uygun maliyetli malzemeler kullanarak mevcut değerlendirilmemiş atıkların zorluğuyla başa çıkmaktır. Bu çift hedef, daha ekonomik ve çevre dostu malzemeler tasarlamayı amaçlar ve aynı zamanda üretilen atıklarla ilişkili sorunları ele almayı hedeflemektedir. Bu bağlamda, inşaat ve yıkım atıklarının (IYA) çoğunlukla alüminyum, silikon ve kalsiyum kaynaklarından oluştuğu, küresel olarak IYA üretiminin yaygın olduğu ve genellikle belirlenmiş depolama alanlarında bertaraf edildiği veya düşük teknoloji uygulamalarında kullanıldığı göz önüne alındığında, IYA kaynaklı malzemelerin jeopolimer üretimine entegrasyonu, etkili ve yenilikçi malzeme geliştirmek için umut vadeden bir yol olarak ortaya çıkmaktadır ve aynı zamanda atıkların yüksek kaliteli değerlendirilmesini sağlamaktadır.

İnşaat sektöründe malzeme kaynaklı sorunlara ek olarak, endüstri sektörleri arasında önemli bir pazar payına sahip olmasına rağmen, inşaat endüstrisinin son birkaç on yılda ortaya çıkan teknolojiye ayak uydurmakta geride kalmış ve diğer sektörlerle kıyasla üretkenliği artırmak için gerekli adımları atmada kararsız kalmış olması karışımıza çıkmaktadır. Süregelen nüfus artışı, felaketler ve savaşlar nedeniyle konut talebinin artması, son yıllarda akademisyenler ve şirketler tarafından inşaat sektöründeki üretim süreçlerinin daha verimli, ucuz ve hızlı olması gerektiği yönünde bir farkındalığa yol açmıştır. Bu bağlamda, diğer sektörlerde sunduğu birçok avantaj nedeniyle hızla popülerlik kazanan üç boyutlu katmanlı üretim (3B-Eİ), inşaat sektöründe de kullanılmaya başlanmıştır. 3B-Eİ, dijital modellere uygun olarak katmanları ardışık bir şekilde biriktirerek özel yapılar oluşturmaktadır. 3B-Eİ tekniği tarafından sağlanan temel avantajlar, üretimle ilgili hataların azaltılması, üretim süresinin kısaltılması, iş güvenliği risklerinin azaltılması, nitelikli işgücüne duyulan ihtiyacın

azaltılması, özelleştirmenin artırılması ve maliyetlerin düşürülmesidir. Ayrıca, 3B-Eİ, kalıpsız üretim ve işlem sırasında atık malzeme oluşturma azaltılması ile inşaat sektörü tarafından neden olan yüksek çevresel yükleri önemli ölçüde azaltmaya katkıda bulunmaktadır.

Bu tez kapsamında, (i) endüstriyel atıkların İYA tabanlı jeopolimer karışımlarına dahil edilmesinin etkilerini değerlendirmek, (ii) çevresel yükleri göz önünde bulundurarak İYA tabanlı jeopolimer karışımlarının taze ve sertleşmiş özelliklerini şekillendirmeye yönelik kapsamlı bilgi ve anlayış sağlamak, (iii) İYA kullanarak daha çevre dostu, ekonomik, sürdürülebilir ve katma değerli 3B-Eİ-uyumlu jeopolimer bağlayıcı sistemler geliştirmek, (iv) alkali aktivatörlerin kullanımını en aza indirgeyerek atık malzemeleri maksimum düzeyde kullanmak, (v) jeopolimer harçlarının mühendislik özellikleri üzerinde çeşitli katkı maddelerinin etkilerini araştırmak, (vi) 3B-baskılı yapılarda kuruma ile ilişkili çatlak oluşumunu ve İYA tabanlı jeopolimer karışımlarındaki kuma sorunlarını azaltmak, (vii) 3B-baskılı yapıların güçlendirme stratejilerini ve 3B-baskılı inşaat için modüler sistem olasılığını araştırmak amacıyla çalışmalar yapılmıştır. Bu kapsamlı metodoloji, akış tablosu, priz süresi, akış eğrisi, üç aralıklı tiksotropi, ram ekstrüder, yaşam döngüsü analizi, basınç ve eğilme dayanımı, doğrudan çekme, su emilimi, emme yeteneği, kuma deneyi, kuruma büzülmesi, ıslanma-kuruma ve donma-çözülme döngüsü gibi çeşitli değerlendirmeleri içeren bir dizi testi içermiştir. Bu kapsamlı metodoloji, jeopolimer karışımlarının özelliklerini ve performansını detaylı bir şekilde keşfetmeyi sağlamış ve araştırma hedeflerini etkili bir şekilde yerine getirmiştir.

Anahtar Kelimeler: İnşaat ve yıkıntı atıkları, jeopolimer, 3B-Eİ, atık değerlendirme, yapı çevre döngüsellik.

ACKNOWLEDGEMENT

Foremost, I would like to extend my sincere gratitude to my supervisor, Mustafa ŞAHMARAN, for his invaluable guidance and unwavering support throughout this endeavor. He provided consistent support during my thesis, sharing his extensive experience and knowledge. It has been an honor to be his student.

Also, I would like to express my gratitude to Prof. Dr. Berna UNUTMAZ, Prof. Dr. İlhami DEMİR, Assoc. Prof. Dr. Mustafa Kerem KOÇKAR and Assoc. Prof. Dr. Oğuzhan ŞAHİN for their participation as members of my thesis jury.

I express my sincere gratitude to the entire team at the Hacettepe University Advanced Concrete Research Laboratory for their consistent and invaluable support.

I would like to thank TÜBİTAK Department of Science Fellowships and Grant Programs (BİDEB) thanks to its support within the scope of the 2211-Domestic Doctoral Scholarship Program.

Lastly, I extend heartfelt thanks to my family for their generous support throughout this study. A special acknowledgment goes to my wife, whose unwavering support and assistance were indispensable during the thesis work. This achievement would not have been possible without them.

HÜSEYİN İLCAN

May 2024, Ankara

TABLE OF CONTENTS

| | |
|---|------|
| ABSTRACT | ii |
| ÖZET | v |
| ACKNOWLEDGEMENT | viii |
| TABLE OF CONTENTS | ix |
| LIST OF FIGURES | xi |
| LIST OF TABLES | xiv |
| SYMBOLS AND ABBREVIATIONS | xv |
| 1. INTRODUCTION | 1 |
| 1.1. Problem Definition | 1 |
| 1.2. Scope and Objectives | 3 |
| 1.3. Thesis Outline..... | 4 |
| 2. LITERATURE REVIEW | 5 |
| 2.1. Geopolymer Binder System | 5 |
| 2.1.1. Mainstream Precursors-based Geopolymer..... | 6 |
| 2.1.2. CDW-based Geopolymer | 17 |
| 2.2. 3D-AM in Built Environment | 23 |
| 2.2.1. Test Methods for Performance Assessment of 3D-AM | 24 |
| 2.3. Utilization of Geopolymers in 3D-AM | 27 |
| 3. EXPERIMENTAL PROGRAM..... | 31 |
| 3.1. CDW-based Geopolymer Paste Mixture | 31 |
| 3.1.1. CDW-based Materials | 31 |
| 3.2. CDW-based Geopolymer Mortar Mixture | 32 |
| 3.2.1. CDW-based Materials | 32 |
| 3.3. Industrial Waste-based Materials | 34 |
| 3.4. Alkaline Activators..... | 36 |
| 3.4.1. NaOH..... | 36 |
| 3.4.2. Ca(OH) ₂ | 36 |
| 3.4.3. Na ₂ SiO ₃ | 36 |
| 3.5. Mixture Preparation Procedure..... | 37 |
| 3.5.1. Small-scale production | 37 |
| 3.5.2. Large-scale production | 37 |

| | |
|---|-----|
| 3.6. Curing Condition..... | 38 |
| 4. RESULTS AND DISCUSSIONS | 39 |
| 4.1. Effect of Industrial Waste-Based Precursors on Performance of CDW-Based Geopolymer Paste..... | 39 |
| 4.1.1. Introduction | 39 |
| 4.1.2. Experimental Studies..... | 40 |
| 4.1.3. Experimental Results and Discussion | 45 |
| 4.2. Low-Alkaline Activated CDW-Based Geopolymer Mortars | 55 |
| 4.2.1. Introduction | 55 |
| 4.2.2. Experimental Studies..... | 56 |
| 4.2.3. Experimental Results and Discussion | 60 |
| 4.3. 3D-Printable CDW-based Geopolymer: Investigating the Effects of Additives on Engineering Properties | 80 |
| 4.3.1. Introduction | 80 |
| 4.3.2. Experimental Studies..... | 81 |
| 4.3.3. Experimental Results and Discussion | 84 |
| 4.4. Reinforcement Strategies and Modular System for 3D-Printed CDW-Based Geopolymer Structures | 96 |
| 4.4.1. Introduction | 96 |
| 4.4.2. Experimental Studies..... | 97 |
| 4.4.3. Experimental Results and Discussion | 105 |
| 5. CONCLUSION | 115 |
| 5.1. Effect of Industrial Waste-Based Precursors on Performance of CDW-Based Geopolymer Paste..... | 115 |
| 5.2. Low-Alkaline Activated CDW-Based Geopolymer Mortars | 116 |
| 5.3. 3D-Printable CDW-based Geopolymer: Investigating the Effects of Additives on Engineering Properties | 116 |
| 5.4. Reinforcement Strategies and Modular System for 3D-Printed CDW-Based Geopolymer Structures | 117 |
| 6. REFERENCES | 119 |

LIST OF FIGURES

| | |
|---|----|
| Figure 1.1. Chart diagram for a) disadvantages of conventional manufacturing, and b) advantages of advanced manufacturing methods. | 2 |
| Figure 2.1. A theoretical framework for geopolymerization [31]. | 9 |
| Figure 2.2. The phase involving rupture of Si-O-Si bonds and formation of Si-O ⁻ -Na ⁺ bonds. | 9 |
| Figure 2.3. The stage in which dissolved aluminum species create intricate formations.... | 10 |
| Figure 2.4. The stage in which monomers interact to construct polymers. | 10 |
| Figure 2.5. Model suggested for the precipitation of geopolymerization product of N-A-S-H gel [47]. | 11 |
| Figure 2.6. Common composition ranges of the raw materials utilized in the manufacturing of alkaline cements [49]. | 12 |
| Figure 3.1. Digital and SEM images of precursors. | 31 |
| Figure 3.2. PSD curves of CDW-based precursors. | 32 |
| Figure 3.3. Digital and SEM images of precursors and aggregates. | 33 |
| Figure 3.4. PSD of precursors and RCAs. | 34 |
| Figure 3.5. Digital and SEM images of industrial waste-based precursors. | 35 |
| Figure 3.6. PSD of industrial waste-based precursors. | 35 |
| Figure 3.7. The mixer used for small-scale production. | 37 |
| Figure 3.8. The mixer used for large-scale production. | 38 |
| Figure 3.9. Digital images of samples cured under ambient conditions. | 38 |
| Figure 4.1. View of the ram extruder setup. | 42 |
| Figure 4.2. LCA framework based on ISO standards. | 43 |
| Figure 4.3. Rheological test results of (a) flowability and buildability, (b) yield stresses.. | 46 |
| Figure 4.4. Compressive strength test results. | 50 |
| Figure 4.5. Distribution of the input variables for the various impact categories. | 52 |

| | |
|--|----|
| Figure 4.6. Flow table test results. | 60 |
| Figure 4.7. Rheometer tests results a) Flow curve, b) 3ITT..... | 63 |
| Figure 4.8. Setting time (Vicat test) results..... | 64 |
| Figure 4.9. Compressive strength of mixtures. | 66 |
| Figure 4.10. Flexural strength test results. | 67 |
| Figure 4.11. Water absorption test results of 28-day aged mixtures..... | 69 |
| Figure 4.12. Representative close-up views of coarse RCAs. | 70 |
| Figure 4.13. Sorptivity coefficient of mixtures. | 71 |
| Figure 4.14. Efflorescence test results: a) strength loss comparison among developed mixtures, b) visual representation of cracks observed in the 100% CDW-based mixture, c) representative images showing effloresced specimens with emphasis on the extent of efflorescence and its appearance. | 73 |
| Figure 4.15. Drying shrinkage test results..... | 75 |
| Figure 4.16. Wet-Dry resistance of CDW-based geopolymer mixture..... | 77 |
| Figure 4.17. Freeze-Thaw resistance of CDW-based geopolymer mixture, a) test results, b) representative images of tested specimen. | 79 |
| Figure 4.18. Details of a) the gantry type 3D printer and b) two-layered specimen..... | 84 |
| Figure 4.19. Compressive strength test results..... | 88 |
| Figure 4.20. Flexural strength test results. | 89 |
| Figure 4.21. Test results of a) water absorption and b) sorptivity for CDW-based geopolymer mortars..... | 91 |
| Figure 4.22. Visual inspection of efflorescence in CDW-based geopolymer mortars..... | 92 |
| Figure 4.23. Representative digital images and close-up views of cracks occurred in 3D-printed filaments. (<i>*area of $3.2 \times 2.4 \text{ mm}^2$</i>)..... | 94 |
| Figure 4.24. Visualization of a) G-code for the designed structure in software, b) bond region of consecutive layers, c) 3D-printed structure. | 96 |

| | |
|--|-----|
| Figure 4.25. Schematic representation of printed specimen a) 6-layered reference (BS), b) fiber-reinforced (BS-FR), c) single steel-reinforced (BS-SSR), d) multiple steel-reinforced (BS-MSR). | 99 |
| Figure 4.26. Schematic representation of a) simple box wall (OOP-B), b) zigzag inner wall (OOP-Z), c) crosstie reinforced wall (OOP-RS). | 100 |
| Figure 4.27. Schematic representation of a) continuously printed 6-layered specimen (FCA), b) 3+3 printed specimen with no treatment (PCA), c) 3+3 printed specimen with wetting treatment (PCA-W), d) 3+3 printed specimen with chipping treatment (PCA-C), e) 3+3 printed specimen with shear studs (PCA-S). | 101 |
| Figure 4.28. Schematic representation of a) monolithic 3D-printed wall (MW), b) modular 3D-printed wall (MoDW) and joint details. | 102 |
| Figure 4.29. Three-point bending test setup. | 103 |
| Figure 4.30. Compressive strength test setup for a) simple box wall (OOP-B), b) zigzag inner wall (OOP-Z), c) crosstie reinforced wall (OOP-RS). | 104 |
| Figure 4.31. Direct tensile test setup for a) monolithic 3D-printed wall (MW), b) modular 3D-printed wall (MoDW). | 104 |
| Figure 4.32. Bending strength: Three-point bending test results. | 106 |
| Figure 4.33. Typical failure patterns of bended specimens a) BS specimen, b) BS-FR specimen, c) BS-SSR specimen, d) BS-MSR specimen. | 107 |
| Figure 4.34. Out-of-plane strength: Compressive test results. | 108 |
| Figure 4.35. Typical failure patterns under compressive loading a) OOP-B specimen, b) OOP-Z specimen, and c) OOP-RS specimen. | 108 |
| Figure 4.36. Interlayer bond strength: Three-point bending test results. | 111 |
| Figure 4.37. Typical failure patterns of bended specimens a) FCA specimen, b) PCA specimen, c) PCA-W specimen, d) PCA-C specimen, e) PCA-S specimen. | 112 |
| Figure 4.38. Modular construction: Tensile test results. | 113 |
| Figure 4.39. Typical failure patterns of a) MW specimen, b) MoDW specimen. | 113 |

LIST OF TABLES

| | |
|--|----|
| Table 2.1. The bibliographic timeline of noteworthy developments related to alkali-activated binders (Revised after Pacheco-Torgal et al. [25]). | 6 |
| Table 2.2. Precursors used in geopolymer [48]. | 11 |
| Table 2.3. Challenges of 3D printing in built environments (Revised after El-Sayegh et al. [112]). | 24 |
| Table 2.4. Common test methods applied to performance assessment of 3D-AM (Revised after Robayo-Salazar et al. [113] and Kaliyavaradhan et al. [114]). | 25 |
| Table 3.1. Chemical compositions of precursors. | 31 |
| Table 3.2. Chemical composition of precursors. | 33 |
| Table 3.3. Chemical composition of precursors. | 35 |
| Table 3.4. Characteristics of NaOH. | 36 |
| Table 3.5. Characteristics of Ca(OH) ₂ . | 36 |
| Table 3.6. Characteristics of Na ₂ SiO ₃ . | 36 |
| Table 4.1. Details of mixes. | 40 |
| Table 4.2. Transportation details of the precursors and alkaline activators. | 44 |
| Table 4.3. Consumed electrical energies of machines. | 44 |
| Table 4.4. Mixtures proportion details. | 57 |
| Table 4.5. Detailed information regarding the additives. | 81 |
| Table 4.6. Mixtures proportion details for 1000g. | 82 |
| Table 4.7. Visual inspection of cracks in 3D-printed filaments. | 94 |
| Table 4.8. Details of geopolymer mortar mixture (1000g precursor). | 97 |

SYMBOLS AND ABBREVIATIONS

Symbols

| | |
|----------------------------------|-----------------------------|
| °C | Centigrade Degree |
| % | Percent |
| Å | Ångström |
| D | Layer Height-Diameter Ratio |
| g | Gram |
| µm | Micrometer |
| mm | Millimeter |
| cm | Centimeter |
| min | Minute(s) |
| M | Molarity |
| MPa | Megapascal |
| Al | Aluminum |
| Si | Silicon |
| Ca | Calcium |
| OH | Hydroxide |
| CO ₂ | Carbon Dioxide |
| NaOH | Sodium Hydroxide |
| KOH | Potassium Hydroxide |
| Ca(OH) ₂ | Calcium Hydroxide |
| Na ₂ SiO ₃ | Sodium Silicate |
| SiO ₂ | Silicon Dioxide |
| Al ₂ O ₃ | Aluminum Oxide |
| Na ₂ O | Sodium Oxide |
| Na ₂ SO ₄ | Sodium Sulfate |
| CaO | Calcium Oxide |
| Na ₂ CO ₃ | Sodium Carbonate |
| CaCO ₃ | Calcium Carbonate |
| NaCl | Sodium Chloride |
| Fe ₂ O ₃ | Ferric Oxide |
| MgO | Magnesium Oxide |

| | |
|--------------------------------|---|
| SO ₃ | Sulfur Trioxide |
| K ₂ O | Potassium Oxide |
| TiO ₂ | Titanium Dioxide |
| P ₂ O ₅ | Diphosphorus Pentoxide |
| Cr ₂ O ₃ | Chromium (III) Oxide |
| Mn ₂ O ₃ | Trimanganese Trioxide |
| p-value | Statistical Measurement Used to Validate a Hypothesis Against Observed Data |

Abbreviations

| | |
|-------|--|
| PC | Portland Cement |
| CDW | Construction and Demolition Wastes |
| USA | United States of America |
| EU-18 | European Union Countries |
| 3D | Three-Dimensional |
| AM | Additive Manufacturing |
| 3D-AM | Three-Dimensional Additive Manufacturing |
| 3D-CP | Three-Dimensional Concrete Printing |
| ASTM | American Society for Testing Materials |
| w/c | Water-to-Cement Ratio |
| w/s | Water-to-Solid Ratio |
| mm/s | Millimeter per Second |
| cm/s | Centimeter per Second |
| b/s | Binder-to-Sand Ratio |
| w/b | Water-to-Binder Ratio |
| a/b | Aggregate-to-Binder Ratio |
| kN/s | Kilonewton per Second |
| N/s | Newton per Second |
| C-S-H | Calcium-Silicate-Hydrate |
| SEM | Scanning Electron Microscopy |
| GGBFS | Ground Granulated Blast Furnace Slag |
| BFS | Blast Furnace Slag |

| | |
|---------|------------------------------------|
| FA | Fly Ash |
| RHA | Rice Husk Ash |
| SF | Silica Fume |
| PVA | Polyvinyl Alcohol |
| N-A-S-H | Sodium-Alumino-Silicate-Hydrate |
| XRD | X-ray Diffraction |
| EDX | Energy-dispersive X-ray |
| 3ITT | Three Interval Thixotropy Test |
| HB | Hollow Brick |
| RCB | Red Clay Brick |
| RT | Roof Tile |
| G | Glass |
| C | Concrete |
| BW | Brick Waste |
| CW | Concrete Waste |
| EN | European Norm |
| W | Water |
| XRF | X-ray Fluorescence |
| PSD | Particle Size Distribution |
| RCA | Recycled Concrete Aggregate |
| C-A-S-H | Calcium-Aluminate-Silicate-Hydrate |

1. INTRODUCTION

1.1. Problem Definition

Concrete stands most extensively utilized artificial material globally, serving as a pivotal element in addressing the requirements of infrastructure growth. The yearly global consumption of concrete is estimated to reach almost 30 billion tons, surpassing per person usage of any other material [1]. Annually, the fabrication of cement, the primary constituent of concrete, is documented to exceed 4 billion tons [2]. The remarkable scale of cement production has raised significant environmental apprehensions, given its contribution to approximately 5–8% of global CO₂ emissions. Studies indicate that in 2019, the cement industry's global process related CO₂ emissions amounted to 1.57 gigatons [3], while the overall carbon emissions from cement manufacturing reached almost 2.9 gigatons in 2021 [4].

Global temperatures in 2020 were roughly 1 °C above pre-industrial levels, and there are anticipations of a further rise to around 3 °C by the year 2100 [5] due to ongoing industrial activities. Initiatives are being made globally to take steps to prevent the increase in global temperatures. Achieving internationally targeted climate change goals hinges on the decarbonization of industries that are challenging to transition away from high carbon emissions. The manufacturing of cement and concrete exemplifies the difficulties faced in decarbonizing industries, primarily because of the chemical process of de-calcinating limestone and significant energy requirements inherent in cement production. Compounded by the widespread global production and consumption, these factors present substantial challenges in the decarbonization pathways of this industry [6]. To deal with this strategic challenge, rising number of studies have centered on mitigation strategies in the cement & concrete industries [7].

Alongside environmental challenges because of the manufacturing of construction materials, the management of construction and demolition wastes (CDW) has become a topic that needs consideration. As the world's population continues to grow and cities undergo a transformation, the escalation in new construction projects, infrastructure development, building renovations, and the demolition of end-of-life structures have intensified the problem of CDW. When examined from a numerical standpoint, the magnitude of the issue becomes even more apparent. The global generation of CDW surpasses 10 billion tons each

year and accounts for approximately 35% of the world's deposition areas, as a significant portion of these wastes ends up in landfills [8–10]. The deposition of these wastes in landfills presents significant economic and environmental challenges as it occupies limited clean landfills that could otherwise be utilized for alternative purposes, while also carrying the inherent risks of air, soil, and water contamination. To address these issues and unlock the potential benefits of low quality CDW, endeavors are being made to utilize them in value-added applications, rather than discarding them or employing them in low-tech utilization methods.

In addition to material-related environmental burdens, there are certain deficiencies in the traditional production techniques of the construction sector as illustrated in Figure 1.1. Each industrial sector has taken noteworthy steps to integrate rapidly evolving technological applications into manufacturing techniques to address quickly and cost-effectively the increasing needs of the growing population [11,12]. Particularly, the trend towards digitization has further extended with the fast development of technology in recent years, escalating transitions to Industry 4.0. However, despite holding a substantial market share among industrial sectors, the construction industry has fallen behind in keeping pace with emerging technology in the past few decades and has been indecisive in taking required steps in traditional production processes to improve productivity compared to the other sectors.

To overcome the disadvantages of the construction sector, it is imperative to embrace advanced manufacturing techniques and foster the development of geopolymer derived from CDW. This strategic shift is crucial for ensuring sustainability in built environments.

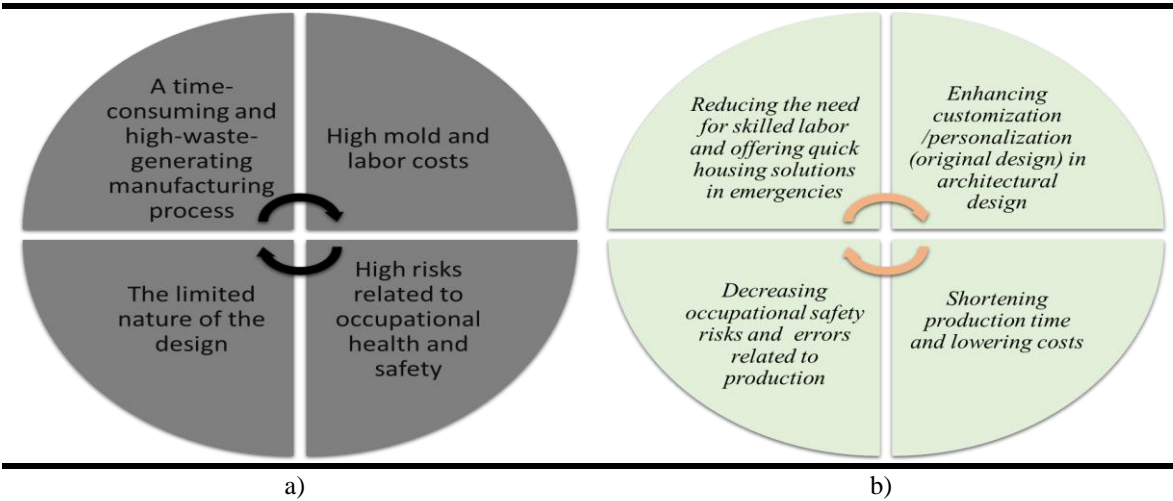


Figure 1.1. Chart diagram for a) disadvantages of conventional manufacturing, and b) advantages of advanced manufacturing methods.

1.2. Scope and Objectives

This dissertation research focuses on research involving the geopolymer material technology, emerging as an alternative to cementitious systems with high environmental burdens and energy-intensive production processes. In the synthesis of geopolymer materials, efforts were made to resolve the globally growing problem of Construction and Demolition Waste (CDW) by incorporating it into geopolymer production as a sustainable and environmentally friendly solution. Within this scope, the synthesis of geopolymers was conducted using CDW-based waste. Additionally, the effects of different industrial-waste-based precursors on CDW-based geopolymer systems were investigated to find out optimal usage ratios. As known, one of the major environmental and economic burdens in the geopolymerization process arises from the activators used. In this context, research was conducted in the thesis on the synthesis of low-alkaline activated CDW-based geopolymer. Furthermore, beyond material-related improvements, the goal was to combine the developed mixtures using the three-dimensional (3D) additive manufacturing (AM) method, an advanced production technique, to pave the way for more sustainable housing in the built environment. The thesis also examined the impact of different chemicals on the engineering features of the developed mixtures. Ultimately, to enhance the mechanical strength of the printed products, various reinforcing strategies in the 3D-AM system were explored, and preliminary studies were conducted on the feasibility of developing modular systems in structures manufactured with 3D-AM.

As part of the thesis studies, the following specific objectives have been targeted:

- Reducing the environmental and economic burden of construction activities.
- Transforming CDW into high value-added construction building materials.
- Evaluating the effects of incorporating industrial wastes into CDW-based geopolymer mixtures.
- Determining parameters that are influential in terms of environmental impact in mixture design.
- Developing a low-alkaline activated 3D-printable CDW-based geopolymer
- Exploring possibility of tailoring the engineering properties of CDW-based geopolymer through additives.
- Investigating the reinforcing strategies and possibility of modular system in 3D-printed CDW-based geopolymer structures.

1.3. Thesis Outline

This thesis comprises five primary parts, each detailed below.

In the initial section titled 'Introduction,' the thesis outlines the primary issues addressed within its scope, clarifies the goals, scope, objectives, and the overall content of the dissertation study.

In the second section, titled 'Literature Review,' an extensive review of the literature is provided, covering topics such as geopolymerization, the geopolymerization capability of CDW-based precursors, 3D-printing and the integration of geopolymer with 3D-AM.

In the third section, designated as the 'Experimental Program,' detailed knowledge is given about the materials utilized in this dissertation study, the procedure for mixture preparation, and the curing period condition.

In the fourth section, titled 'Results and Discussions,' the outcomes originating from the experimental studies carried out in the framework of the dissertation study are given, accompanied by discussions on the potential reasons behind the observed results. This section includes four main sub-sections: i) Effect of Industrial Waste-Based Precursors on the Performance of CDW-Based Geopolymer Mixtures, ii) Low-Alkaline Activated CDW-Based Geopolymer Mortars, iii) 3D-Printable CDW-based Geopolymer: Investigating the Effects of Additives on Engineering Properties, iv) Reinforcement Strategies and Modular System for 3D-Printed CDW-Based Geopolymer Structures.

In the fifth section, titled 'Conclusion,' the findings from the experimental studies performed in the thesis are concisely outlined.

2. LITERATURE REVIEW

2.1. Geopolymer Binder System

Concrete stands out as the predominant material in the construction sector, with an annual global consumption of around 30 billion tons [1]. This extensive use contributes to the depletion of substantial amount of ordinary Portland cement (OPC), the primary binder in traditional concrete fabrication. Nevertheless, the fabrication of cement causes severe environmental concerns, including the vigorous usage of natural raw materials and the emission of hazardous gases. Roughly 1.5 tons of source materials are necessary to manufacture 1 ton of OPC, resulting in approximately 0.55 tons of CO₂ emissions directly. Additionally, the burning of fuels in the process releases nearly 0.4 tons of CO₂, leading to an overall emission ranging from 0.8 to 1.0 tons of CO₂ [13]. Additionally, the cement industry is a prominent user of fossil fuels, accounting for approximately 12–15% of industrial energy [14]. On a global scale, the manufacture of OPC is projected to release approximately 1.35 billion tons of gases annually, accounting 6–9% of the total greenhouse gas emissions [15]. These emissions are mainly credited to fuel combustion, the decarbonation of limestone, and the usage of energy.

In the last thirty years, there has been an increasing understanding of the environmental issues related to the production of conventional concrete. This has motivated scientists and the cement industry to explore alternative methods for developing environmentally sustainable materials. Lately, the World Green Building Council set forth plans and ways for formulating sustainable construction with the aim of achieving a 40% reduction in carbon footprints by 2030 and ultimately reaching zero CO₂ emissions by 2050. Key proposed measures include the utilization of alternative fuels, CO₂ capture, enhanced energy efficiency in furnaces, integration of nanoparticles as a cement substitute, and the development of low-impact green building materials and technology [16].

Geopolymers, falling under the category of the latter option, have emerged as effective option to OPC-based binders and materials. Their appeal lies in the positive environmental impact, mitigating energy usage and utilizing waste materials [17]. Additionally, their outstanding mechanical and durability properties, potential for cost reduction [18], and excellent resistance to acids and high temperatures are also the appealing [19,20]. Substituting OPC with geopolymers not only provides environmental benefits but also

contributes to an overall mitigation in the CO₂ footprint in comparison to conventional concrete.

Geopolymers belong to category of alkali-activated binders and are generated by polymerizing various aluminosilicate precursors through activation processes [21,22]. The precursors may be originated from natural sources [23] or from industrial by-products. These by-products are now seen as valuable resources rather than waste materials as they have found prevalent and accomplished use in the cement & concrete industry as pozzolanic ingredients. The precursors, whether from natural or by-product sources, can be utilized individually or in combination. As a result, there is a growing emphasis on investigating alternative precursors that can be effectively incorporated into geopolymers, aiming to reduce the significant demand for by-products. Table 2.1 provides a historical overview of noteworthy developments in the area of alkali-activated materials [24].

Table 2.1. The bibliographic timeline of noteworthy developments related to alkali-activated binders (Revised after Pacheco-Torgal et al. [25]).

| Author Name | Year | Work |
|-----------------------|-------------|---|
| Feret | 1939 | Slags utilized for cement |
| Purdon | 1940 | Alkali-slag blends |
| Glukhovskiy | 1959 | Theoretical basis and development of alkaline cements |
| Glukhovskiy | 1965 | First called "alkaline cements" |
| Davidovits | 1979 | "Geopolymer" term |
| Davidovits and Sawyer | 1985 | Patent of "Pyrament" cement |
| Talling & Brandstetr | 1989 | Alkali-activated slag |
| Wu et al. | 1990 | Slag cement activation |
| Roy et al. | 1991 | Rapid setting alkali-activated cements |
| Roy & Silsbee | 1992 | Alkali-activated cements: a summary |

2.1.1. Mainstream Precursors-based Geopolymer

The interaction between a solid aluminosilicate and an aqueous solution of alkali hydroxide or silicate brings about development of alkali aluminosilicate material commonly named as 'geopolymer,' as termed by Davidovits [26]. However, it might be more fittingly categorized as an instance of what is more generally labeled as an 'inorganic polymer' [27]. These substances have the potential to deliver performance similar to conventional cementitious binders across various applications, offering the additional benefit of considerably reduced greenhouse gas emissions [28]. Depend on the used materials and the conditions of processing, geopolymers can show various properties and performance. These may encompass elevated compressive strength, minimal shrinkage, rapid or gradual setting, resistance to acids, resilience to fire, and decreased thermal conductivity. While the term

'geopolymer' is generally employed to characterize amorphous to crystalline geopolymerization products resulting from the formation of alkali aluminosilicates through reactions with alkaline activator, the resulting products are also mostly known by various other names. These cover 'low-temperature aluminosilicate glass' [29], 'alkali-activated cement' [30], 'geocement' [31], 'alkali-bonded ceramic' [32], 'inorganic polymer concrete' [31], and 'hydroceramic' [33]. In spite of the diverse range of terms used, all these designations refer to materials that share a common synthesis process. This process can be characterized as an intricate system including dissolution and precipitation within a reaction environment.

During 1950s, Glukhovsky [34] initiated an extensive reaction procedure for the alkali activation of precursors, mainly consisting of silica and reactive alumina. The Glukhovsky classifies the procedure in three progressive sections: (a) destruction-coagulation; (b) coagulation-condensation; and (c) condensation-crystallization. In recent times, various authors have expanded upon and extended the theories proposed by Glukhovsky. They have also used the accumulated understandings into zeolite synthesis to offer a more comprehensive explanation of the geopolymerization process[35–39]. Figure 2.1 demonstrates simple reaction steps of geopolymerization. This depiction describes the fundamental processes participating in the conversion of an aluminosilicates to a alkali aluminosilicate. It is important to note that the possible need for processing precursor materials through methods like grinding and thermal processing to adjust the chemical activity of aluminum is not illustrated in the diagram for clarity. While illustrated in a linear fashion, these processes are largely interconnected and take place simultaneously. The aluminosilicate source experiences dissolution through alkaline hydrolysis, utilizing water, causing the formation of aluminate and silicate species. It is crucial to state that the presumed mechanism driving the transformation of particles during geopolymerization includes the dissolution of these particles at the surface, yielding to the discharge of aluminate and silicate, as in a monomeric form. The definitive conversion process has not been verified under the strongly alkaline and insufficiently solvated conditions characteristic of geopolymer formation. In the absence of a conclusive mechanistic comprehension of particle conversion, this simplistic mechanistic model supposes surface dissolution. After dissolution, the species are assimilated into the aqueous phase, which might already have silicate from the solution. This leads the formation of an intricate mixes of silicate, aluminate, and aluminosilicate species. The equilibria of speciation within these solutions

have been extensively explored [40,41]. The rapid dissolution of aluminosilicates takes place at elevated pH levels, quickly leading to the creation of a supersaturated aluminosilicate solution. This leads gel creation as the oligomers create prevalent networks through condensation. During all this steps, water, initially utilized during dissolution, is discharged. Consequently, water work as a reaction environment, residing within pores in the gel. Formed gel is often termed bi-phasic, where the aluminosilicate material and water constitute the two phases. The duration need for the creation of a continuous gel from the supersaturated aluminosilicate solution notably varies regarding to the material processing, solution context, and reaction conditions [42,43]. However, in some systems, gelation never happens. These are typically more diluted systems, where the intensity of dissolved silicon and aluminum oscillates because of the sluggish response of the system distant from balance [44]. Following gelation, the system experiences continuous rearrangement and reorganization, yielding a rise in the connectivity of the gel network. This process brings about the formation of the three-dimensional aluminosilicate network mostly associated with geopolymers. In Figure 2.1, the geopolymerization is described as a result of two subsequent stages. Nucleation, including the dissolution of the aluminosilicate precursors and the generation of polymeric species, is mainly depended on thermodynamic and kinetic variables. It involves initial two steps offered by Glukhovsky. The subsequent stage is growth, during which the nuclei attain a critical size, and crystals commence development. Structural reorganization processes are essential in assigning the microstructure and pore network, considerably affecting numerous physical properties [45,46].

The Si-O-Al bonds are affected by the OH⁻ groups (Figure 2.3): dissolved aluminum species result in complex formations, mainly Al(OH)₄⁻ anions.

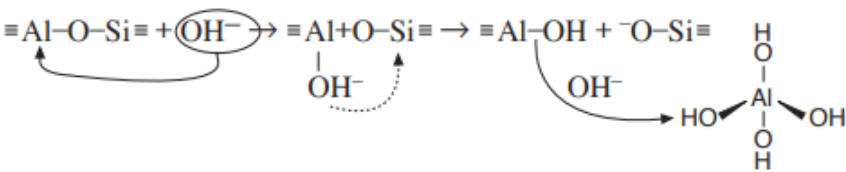


Figure 2.3. The stage in which dissolved aluminum species create intricate formations.

In the subsequent stage, coagulation-condensation, the buildup of ionic components fosters interaction among the fragmented components, commencing polycondensation and yielding the formation of coagulated structures. Silica monomers interact to generate dimers, producing Si-O-Si bonds, which subsequently give reaction with other monomers to create polymers (Figure 2.4). This stage is assisted by the presence of OH⁻. The clusters stemming from the polymerization of silicic acid commence to expand in every direction, creating colloids. Aluminates also engaged in polymerization, isomorphically substituting the silicon tetrahedra. While the alkaline works as a catalyst in the initial stage, in the subsequent stage, it serves as a structural element.

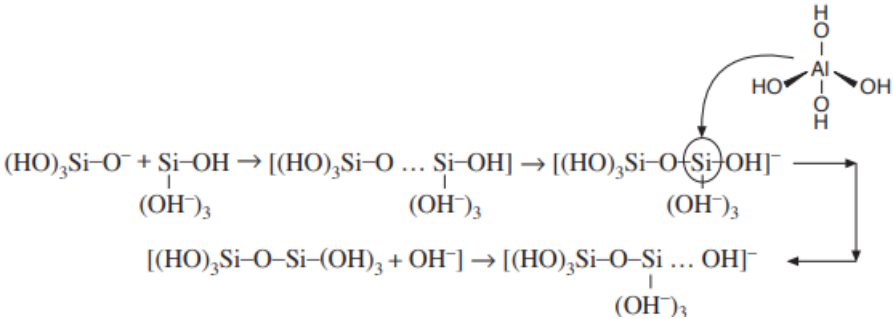


Figure 2.4. The stage in which monomers interact to construct polymers.

In the final stage, condensation-crystallization happens. The content of formed products is dependent on the mineralogy and chemical properties of the primary precursors, the activator type, and the curing procedure.

In subsequent studies, revisions have been done to this model, outlining the geopolymerization process as follows. Based on the revised model (refer to Figure 2.5), the precipitation of N-A-S-H gel includes a sequence of stages that could be concisely summarized. Upon interaction with the alkaline, the aluminosilicate source dissolves into various components, mainly silica and alumina monomers. These monomers participate in

interactions, yielding to the creation of dimers, which later give reaction with other monomers to bring about trimers, tetramers, and so forth. When the solution becomes saturated, an aluminosilicate gel, particularly N-A-S-H gel, is formed. This product at first shows aluminum-rich characteristics, termed Gel 1, representing a metastable intermediate reaction product [36]. The creation of this gel can be described by the elevated content of Al^{3+} ions during the first steps of the chemical process (from the initial minutes to the early hours). This can be ascribed to the fast dissolution of reactive aluminum compared to silicon, given that Al-O bonds are less robust than Si-O bonds. As the reaction improves, more Si-O groups in the original aluminosilicate source dissolve, increasing the silicon availability in the reaction environment and its ratio in the N-A-S-H gel (referred to as Gel 2). This process of structural reorganization plays an essential role in determining the final form of the polymer, along with the microstructure and structure of pores. These factors are significant in affecting various physical features of the resulting cement.

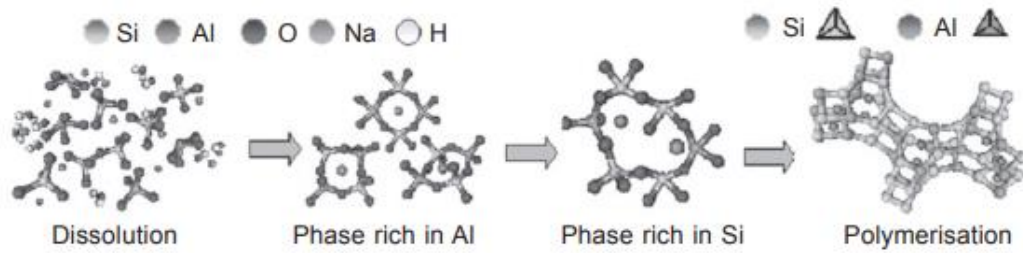


Figure 2.5. Model suggested for the precipitation of geopolymerization product of N-A-S-H gel [47].

In studies within the literature, various precursor materials are used for geopolymerization. Table 2.2 involves details on the precursor materials used and the additives utilized in geopolymers [48]. However, there are some commonly utilized main-stream precursors in geopolymer synthesis, involving BFS, FA, MK, SF and etc. The CaO-SiO₂-Al₂O₃ ternary diagrams illustrated in Figure 2.6 demonstrate the typical composition ranges for these materials.

Table 2.2. Precursors used in geopolymer [48].

| Precursors | |
|--------------------|-----|
| fly ash | FA |
| bottom ash | BA |
| blast furnace slag | BFS |
| metakaolin | MK |

| | |
|---|---------------------|
| natural zeolites | NZ |
| kaolin | KL |
| palm oil fuel ash | POFA |
| granulated lead smelter slag | GLSS |
| rice husk ash | RHA |
| ferrochrome slag | FS |
| ultra-fine kaolite high-performance ash | KHFA |
| biomass fly ash | BFA |
| silico-manganese fume | SMF |
| Additives Used in Geopolymer | |
| calcium aluminate cement | CAC |
| nano-silica | NS |
| calcium hydroxide | Ca(OH) ₂ |
| ordinary Portland cement | OPC |
| silica fume | SF |

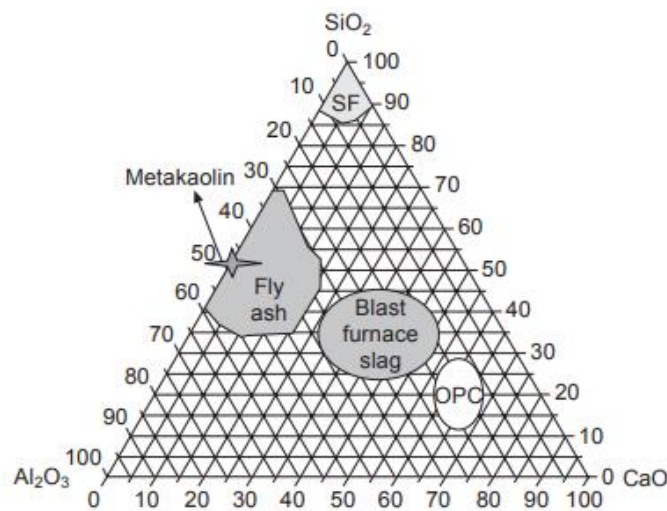


Figure 2.6. Common composition ranges of the raw materials utilized in the manufacturing of alkaline cements [49].

A concise literature review, with a focus on mainstream-precursor-based geopolymer synthesis, is given below.

Chindaprasirt et al. [50] examined the fresh and mechanical properties of geopolymer using coarse lignite high calcium FA. Activation was made with NaOH, Na₂SiO₃, and heating. The workable flow ranged from 110 ± 5% to 135 ± 5%, depending on the Na₂SiO₃ to NaOH mass rate and NaOH concentration. Compressive strength deviated from 10 to 65 MPa, with the optimal Na₂SiO₃ to NaOH ratio noted as 0.67–1.0. NaOH concentration between 10 M and 20 M displayed minimal impact on strength. High-strength geopolymer samples were accomplished with a 1-hour delay after molding before heat treatment, and optimal curing involved a 75 °C temperature in the oven for at least two days.

In the study conducted by Nath and Sarker [51], the results exhibited that geopolymer concrete based on fly ash, cured under ambient conditions, could be formulated to attain the desired engineering performance by including GGBFS as a minor component. The addition of GGBFS were found to be beneficial in attaining setting times and compressive strengths similar to those of OPC. After 28-day curing, the addition of GGBFS, up to 30% of the total binder, yielded concrete achieving a compressive strength of up to 55 MPa, while mortar displayed a compressive strength of up to 63 MPa.

The research by Deb et al. [52] delved into the effectiveness of various rates of GGBFS and activator composition on the engineering features of FA-based geopolymer. The research included GGBFS at 0%, 10%, and 20% of the binder, with diverse activator amount (40% and 35%) and sodium silicate/NaOH rate (1.5–2.5). Geopolymer concretes containing elevated levels of GGBFS and a reduced rate of SS/SH showed a notable enhancement in strength and a slight decrement in workability. The geopolymer concrete, with a binder comprising 20% slag and 80% fly ash, achieved a compressive strength of 51 MPa after 28 day ambient curing, using 40% activator liquid and an SS/SH rate of 1.5.

In a study performed by Saha and Rajasekaran [53], it was aimed to improve the performance of FA-based geopolymer by including GGBFS at various percentage levels. The inclusion of GGBFS yielded a notable decrease in setting time of the geopolymer paste. The elevated CaO amount in GGBFS resulted in forming C–S–H gel, playing a part to the development of a stable silico-aluminate structure through the geopolymerization during the initial stages. Overall, the setting time was notably decreased with elevated dosages of GGBFS. Moreover, the compressive strength enhanced with the percentage rate of GGBFS inclusion. The paste mixture achieved its highest compressive strength, reaching 78.2 MPa, when utilizing a 16 M NaOH and incorporating 50% GGBFS.

In the study carried out by Ismail et al. [54], the microstructural examination of alkali-activated binders containing BFS and FA was investigated. A C–S–H gel replaced with Al and Na (C–N–A–S–H) was recorded as the primary geopolymerization product in geopolymer system when the BFS content is ≥ 50 wt.% of the overall binder. As the fly ash content escalated, the systems appeared to be primarily made of a hybrid binding phase resembling an N–C–A–S–H gel, characterized by water being more tightly bound and an escalated level of crosslinking than noted in C–A–S–H gel precipitating in activated BFS binders.

The study carried out by Rattanasak and Chindaprasirt [55] targeted to examine the leaching behavior of FA mixed with NaOH and the associated mixing protocols for geopolymer preparation. The investigation involved studying the leaching of Al_2O_3 and SiO_2 by combining FA with NaOH for various time intervals, with subsequent analysis of the leachates for silica and alumina contents. The outcomes of study exhibited that the solubility of FA was influenced by the intensity of NaOH and the duration of mixing. The formulation with 10 M NaOH and a sodium silicate/NaOH rate of 1.0 led high-strength geopolymer, reaching up to 70.0 MPa.

The study by Hardjito et al. [56] described the advancement FA-based geopolymer concrete. Low-calcium FA (ASTM C 618 Class F) was activated by a high-alkaline activator. The strength of geopolymer was influenced by various factors: an elevated molarity of NaOH yielded increased strength, and an elevated rate of sodium silicate/NaOH liquid ratio by mass also contributed to increased compressive strength. The study showed that longer curing times, ranging from 6 to 96 hours, resulted in higher strength in geopolymer. Nevertheless, there was not a substantial enhancement in strength after the 48-hour.

In Haq et al.'s research [57], geopolymers were synthesized using FA and bottom ash, and their properties were evaluated. FTIR analysis demonstrated an elevated level of geopolymerization in bottom ash-based geopolymer. Strength examination exhibited that bottom ash-based geopolymers were nearly as feasible as FA-based geopolymers. Thermal conductivity assessment unveiled that FA-based geopolymer showed a less thermal conductivity of 0.58 W/mK relative to bottom ash-based geopolymer at 0.85 W/mK.

In the investigation performed by Chen et al. [58], the successful activation and usage of MK as a precursor was investigated. The findings unveiled that the optimal geopolymer composition consisted of MK, NaOH, Na_2SiO_3 , and H_2O , with a molar rate of $\text{SiO}_2:\text{Al}_2\text{O}_3:\text{Na}_2\text{O}:\text{NaOH}:\text{H}_2\text{O}$ being 3.4:1.1:0.5:1.0:11.8. The most favorable curing condition was recorded as 60 °C for 168 hours, showing peak compressive strength at 52.26 MPa.

The research by Aiken et al. [59] examined the influence of growing BFS amount and dosage of alkaline activator on resistance to sulfuric acid for FA-based geopolymer binders. The findings indicated that an escalated in BFS amount reduced porosity yet caused the

geopolymerization products more vulnerable to sulfuric acid attack. Additionally, it was observed that an increase in activator dosage had minimal influence on sulfuric acid resistance in FA-based geopolymers. Particularly, geopolymer demonstrated greater sulfuric acid resistance compared to their Portland cement counterparts.

The study executed by Albidah et al. [60] involved an extensive experimental study focusing on the impact of varied mix design factors on engineering features of MK-based geopolymer. The findings showed that workability enhances with an escalating of the sodium silicate/NaOH rate up to a specific threshold, noted here as 2.5, and reduced afterward because of increased mix viscosity. Compressive strength mostly showed an upward trend with escalating sodium silicate/NaOH rate and alkaline/MK rate, achieving a maximum at a specific threshold based on the molar rates of the mix, indicative of optimal geopolymerization conditions. Beyond this limit, strength tended to decrease. After 28-day curing period, the best compressive strength obtained was approximately 60 MPa.

In Bing-hui et al. study [61], the effectiveness of various curing temperatures on the dissolution, polymerization, and reprecipitation procedure of the geopolymerization was examined. The results showed that increasing the curing temperature accelerated these processes. The ideal curing condition for geopolymer was decided to be around 60 °C, where the geopolymer specimens demonstrated the best mechanical performance, including a compressive strength of 97.95 MPa after curing for 7 days. However, excessively high curing temperatures (80 and 100 °C) had an adverse influence on physical features, as the overly rapid setting of geopolymer slurries obstructed the transformation into a dense structure for geopolymer specimens.

The research performed by Zhang et al. [62] examined the reaction mechanism, phase development, and mechanical features of MK-based geopolymers. The study investigated variations in Si/Al rates (1.2 to 2.2) and Na/Al rates (0.6 to 1.2). The outcomes of the study expressed that the fraction of geopolymer gels played a significant role in adjusting the mechanical behavior, with both factors increasing as the Si/Al and Na/Al molar rates rise. Meanwhile, the final setting time exhibited an increment with the Si/Al rate yet a decrease with the Na/Al rate. The optimal content for maintaining the highest strength performance was noted as a Si/Al rate of 1.7 and a Na/Al rate of 0.9.

In Wang et al.'s study [63], metakaolinite-based geopolymer was developed by using NaOH and sodium silicate solutions. The resulting material, mainly amorphous with absorbed atmospheric water, maintained the flake-like structure of metakaolinite. Colloid reactions took place primarily at the surface of metakaolinite micro flakes. The mechanical properties of geopolymers were significantly based on the molarity of NaOH. Flexural and compressive strength, and density raised with higher NaOH concentrations (4–12 mol/L), ascribed to increased metakaolinite dissolution and accelerated monomer condensation in higher NaOH concentrations.

The study by Kumar et al. [64] delved into the effectiveness of varied amounts of GBFS (5–50%) on the geopolymerization using isothermal calorimetry. The results revealed that the geopolymerization at 27 °C was primarily affected by GBFS activation, while the geopolymer at 60 °C resulted from the combined interaction of FA and GBFS. The main geopolymerization products observed were A–S–H and C–S–H gels with diverse Si/Al and Ca/Si ratios. The observation of A–S–H and C–S–H gel proposed the interaction between FA and GBFS while geopolymerization.

In Wan et al.'s study [65], MK-based geopolymers were designed with Si/Al rates ranging from 1:1 to 5:1, including SF as a silica corrector to modify Si rates. At a Si/Al rate of 2:1, the dissolution of elevated concentrations of Si and Al components from precursors occurred, yield the creation of advanced amounts of Si-O-T linkages and resulting in geopolymers with high compressive strength. The study revealed that the mechanical performance of geopolymers at different Si/Al rates was depended on the precipitation of the N-A-S-H gel, instead of the presence of zeolitic nuclei or silicate derivatives.

In a study by Cong and Mei [66], the impact of activator type/amount, SF substitution ratio, and curing period on the characteristics of geopolymer was examined. The inclusion of SF was found to be favorable for the strength of calcium carbide residue-activated geopolymer. Thermal gravimetric analysis findings and SEM images demonstrated that the incorporation of SF in CCR-activated system could facilitate the usage of high calcium carbide residue, enable the precipitation of geopolymerization products, and tailor the pore morphology.

The research performed by Duan et al. [67] delved into the effectiveness of SF on the characteristics of FA-based geopolymer under thermal cycles. Research findings showed that the inclusion of SF enhanced strength in geopolymer. SF helped to the refinement of

pores in the geopolymer, optimizing the microstructure and improving thermal resistance. The inclusion of SF resulted in enhanced strength in the geopolymer, and even after exposure to heat cycles, the retained strength remained satisfactory.

Aygörmez et al. [68] carried out research investigating the characteristics of polypropylene fiber-reinforced MK geopolymer mortar exposed to high temperatures reaching 900 °C. The test samples involved substitutions of MK with either SF or colemanite waste. Exposure to high temperatures led to a substantial reduction in mechanical performance. Nevertheless, specimens with substitution of up to 20% and 10% SF or colemanite waste, respectively, showed enhanced mechanical performance.

Liang et al. [69] executed research to examine the impact of replacing MK with RHA on the thermal stability of MK-based geopolymer. The outcomes of the study revealed that the substitution of RHA aided to the improved thermal stability of the geopolymer. The study revealed that the optimal replacement level was 30% RHA by weight of MK, resulting the best performance irrespective of the curing temperature.

2.1.2. CDW-based Geopolymer

In the last decades, urbanization has been increased globally and reached approximately 55% all over the world with the fast population growth [70]. At the same time, the urban transformation has been gaining great importance by countries to ensure the safety of people in case of any disasters and to provide a more livable environment for citizens. Such increment in urbanization and city transformation, therefore, is leading to a tremendous amount of CDW generation because of new building and infrastructure construction activities, rebuilding or renovation, the extension of current structures, roadwork construction, maintenance, and demolition of decrepit buildings [70–72]. According to the advancing sustainable materials management reports published by US Environmental Protection Agency [73], 600 million tons of CDWs were generated in the year of 2018 in the USA. In European Union counties (EU-28), 374 million tons of CDWs (excluding excavated soil), the largest waste stream (by mass), were produced in 2016 [74]. In China, the annual production of CDWs was more than 2.5 billion tons in 2015 [72]. Overall, the amount of generated CDWs worldwide approximately exceeds 10 billion tons annually [8]. Consequently, the landfilled area of CDWs is responsible for approximately 35% of deposition area worldwide [9,10,75]. Such a tremendous amount of generated CDWs

therefore must be managed in an efficient, feasible and innovative way. However, most of the developing countries have been failing to manage high amounts of produced CDWs properly, which causes serious environmental, economic and social problems [76]. In general, CDWs have been used as filler materials for basement/road construction, aggregates in the non-structural concrete or deposited on dumping sites which has increased the demand for new landfilling sites that caused the destruction of vegetation and alteration of the natural environment [10,72,77]. During the deposition process, although most of the building materials are inert, CDWs could cause soil pollution and degradation [71]. Air and water pollution are also the main concerns of the countries, as the dust of CDWs which is inevitable during the demolition of structures, can contaminate air and water during landfilling phase because of different external factors (e.g., wind etc.) [72]. Moreover, demand for new deposition areas and transportation of tremendous amount of produced CDWs are serious economic burdens on the developing and developed countries. Therefore, it is necessary to develop innovative and sustainable ways to handle the produced CDWs by converting them into industrially valuable goods. In that way, developing countries in economic difficulties may turn into a situation that is harmful to the environment, economy, and social aspects to their advantages.

As CDWs are mainly composed of aluminum, silicon, and calcium sources, recent studies have been focused on the utilization of CDWs as precursors to produce environmentally friendly construction materials of geopolymer binders, which is an inorganic polymer originated by interaction of aluminosilicate materials (i.e., precursor) with alkaline activators [26,31]. With the utilization of CDWs in the geopolymer synthesis, in addition to the solving the worldwide CDWs-related problems, the production of energy-, source-, labor-, and carbon-intensive concrete [78,79] can be minimized and a circular economy in the construction sector can be achieved, as produced CDWs can be utilized as raw materials in the development of novel construction materials, in a closed-loop. The current studies prioritizing the development of CDW-based geopolymers [80–82] have proven that CDW-based geopolymer binders can achieve comparable mechanical and durability performance with the conventional cement-based concrete and mainstream (FA, BFS, MK, etc.) geopolymer binders. Nevertheless, the development of CDW-based geopolymer binders requires more effort to improve knowledge about it, as the subjects are less common than studies of geopolymer using mainstream aluminosilicate precursors. The studies focused on the advancement of CDW-based geopolymer showed that the ultimate performance of the

mixtures can be tailored by adjusting the alkaline content, water/binder rate and aggregate/binder rate, chemical composition of the precursor, curing period, and temperature.

In-depth literature analysis emphasizing CDW-based geopolymer is presented below.

In a study performed by Allahverdi and Kani [83], the geopolymerization of CDW materials (waste brick and waste concrete) was examined using various alkali-activators (NaOH and Na₂SiO₃), alongside different water-to-binder ratios, silica modulus, and sodium oxide concentrations. The findings of the study showed that waste bricks showed greater suitability compared to waste concrete, highlighting the potential of construction waste materials for geopolymer production, with a significant achievement of 40 MPa compressive strength at 28 days.

In a separate study carried out by Reig et al. [84], the features and microstructure of alkali-activated mixtures, derived from ceramic waste materials (brick and porcelain), using NaOH and Na₂SiO₃ as alkali activators, were examined. The results revealed the promising potential of alkali-activated ceramic materials.

In a study performed by Komnitsas et al. [85] the researchers thoroughly investigated the geopolymerization potential of CDW (concrete, bricks and tiles) through using NaOH and Na₂SiO₃ and examined the influence molarity of the alkaline activating solution (NaOH molarity of 8–10–12–14) on the compressive strength. The study found that bricks and tiles could be effectively geopolymerized, yielding compressive strengths of 49.5 and 57.8 MPa, respectively. The ease of geopolymerization for bricks and tiles can be ascribed to their elevated SiO₂ and Al₂O₃ and low CaO. The optimal synthesis conditions were determined as 8–10 M NaOH, a curing temperature of 80–90 °C, and a curing period of 7-days.

In another study, Vásquez et al.[86] delved into the development of geopolymers through the activation of concrete waste using NaOH and Na₂SiO₃. The findings revealed that geopolymer systems activated with Na₂SiO₃ accomplished the best compressive strength, even at ambient condition. The geopolymer, composed entirely of concrete waste, showed a highest compressive strength of 25 MPa, while the hybrid geopolymer of concrete waste and 30% OPC exhibited 33 MPa after 28-day ambient curing.

In another study conducted by Khater, H.M. [87], it was also expressed that the alkaline activation of aluminosilicate wastes provides a solution for valorization demolition wastes globally, converting them into valuable materials.

In a separate study performed by Allahverdi and Kani [88], the mixture containing 60% waste brick and 40% waste concrete attained a highest 28-day compressive strength of 50 MPa, suggesting that activation of CDW with a suitable alkali activator can potentially develop geopolymer from these materials.

In the study of Özcelikci et al. [89], it was demonstrated that, based on the specific mix formulating, it is achievable to attain 28-day compressive strengths surpassing 30 and 50 MPa with mortars solely made of CDW and those incorporating a 20% BFS substitution of CDW-based precursors. These Encouraging strength values suggest scalability towards the development of 100% CDW-based structural concretes and components.

Likewise, Vafaei et al. [90] conducted research on the characteristics of geopolymer, utilizing waste bricks and GGBFS, in comparison to two kinds of cement mortars, specifically OPC and high alumina cement, when subjected to acid attack (sulfuric and hydrochloric acids). The findings exhibited that geopolymer mixtures illustrate enhanced durability compared to their cement-based counterparts, displaying fewer noticeable changes, minimal weight loss, and reduced strength loss following exposures.

In studies carried out by Şahin et al. [77] and İlcan et al. [91,92], the engineering features of CDW-based geopolymer systems were thoroughly examined. The investigations focused on varying the alkaline dosage and combinations using different waste materials such as red clay brick (RCB), hollow brick (HB), roof tile (RT), concrete, and glass with activation through NaOH, Na₂SiO₃, and Ca(OH)₂. The outcomes of the studies displayed that the fresh characteristics of CDW-based geopolymer mixture, including static and dynamic yield stress, thixotropic performance and viscosity can be finely adjusted by manipulating the alkaline content, in addition to the water/binder or aggregate/binder ratio. Furthermore, the mechanical performance of the geopolymer was found to be substantially affected by the kind of activators. Additionally, depending on the Si/Al/Ca content of the geopolymer matrix, the precipitated geopolymeric gels can exhibit variations such as C-A-S-H, C-S-H, N-A-S-H, and other similar structures.

The study performed by Ulugöl et al. [81], exhibited that for a CDW-based geopolymer mixture composed of RCB, RT, and HB, the primary precipitated products were N-A-S-H gels with varying zeolitic polytypes extending from amorphous to polycrystalline structure. However, for the geopolymers made of glass waste precursor, the primary geopolymerization product was comparatively less robust and unstable sodium silicate gels. And it was concluded that increasing the NaOH concentration, curing period and temperature, as well as the content of SiO₂ and Al₂O₃ yielded an advancement in the strength up to a specific limit. It was also stated that fineness was influential on the geopolymerization and the compressive strength of CDW-based geopolymer can exceed 45 MPa depending on the given conditions.

In the study of Yıldırım et al. [82], it was expressed that the CDW-based masonry units (RCB, RT, HB) can be successfully utilized to produce geopolymers with a compressive strength of up to 80 MPa at elevated curing temperature, on condition that the mixture design parameters are optimized. Microstructural investigation results revealed that, irrespective of the chemical content of precursors, the primary geopolymerization product was N-A-S-H gels.

Mahmoodi et al. [93] noticed that the maximum compressive strength for CDW-based geopolymers (concrete waste) after 28 days ambient curing and 100 °C heat curing was 20.5 and 37.1 MPa, respectively. The results obtained showed that the engineering features of CDW-based geopolymers are highly hinged on the chemical ratios of Si/Al and Na/Si. Additionally, it was revealed that the inclusion of BFS had a greater impact on the strength characteristics of CDW-based geopolymers compared to FA and MK, as slag led to formation of more C-A-S-H (tobermorite type) and N-A-S-H gels in the CDW-based geopolymer matrix.

In addition to evaluating the engineering properties, the environmental impact of CDW-based geopolymers was examined to establish their viability as a sustainable alternative to OPC, demonstrating a reduced environmental burden.

In this context, Khan et al. [94] conducted a study to explore the ecological sustainability possibility of the CDW-based geopolymer systems. Based on the obtained results, CDW-based geopolymers exhibited less environmental burdens when compared to their equivalent

OPC-based counterparts, with the grinding, crushing, and NaOH identified as having the highest environmental impacts.

In an independent study, Mir et al. [95] performed an analysis aiming to examine and quantify the environmental implications associated with CDW-based geopolymer. The study employed NaOH, $\text{Ca}(\text{OH})_2$, and Na_2SiO_3 , both individually and in binary and ternary combinations, to assess their environmental implications. It was found that the sole usage of NaOH resulted in lower environmental impacts.

In a study carried out by Mahmoodi et al. [96], it was indicated that geopolymer binders exhibited remarkable lessening in embodied energy and embodied CO_2 values in comparison to OPC binders possessing similar strength. Moreover, the utilization of concrete waste as precursors and energy-intensive alkaline activators was found to impose considerable environmental impacts.

Furthermore, different types of industrial waste have been substituted into CDW-based geopolymer mixtures to tailor the engineering properties of the mixtures.

In one of this study, Mahmoodi et al. [97] studied the effects of Class C FA, Class F FA, MK and granulated BFS on engineering features of the ceramic tile waste-based geopolymer. The outcomes of the study exhibited that the inclusion of various types of industrial wastes had a substantial and varied influence on the features of the CDW-based geopolymer by providing extra dissolved Ca^{2+} , Si^{4+} and Al^{3+} in reaction medium, which then produce geopolymerization product, and by forming different physical interactions due to the varied surface texture. Higher compressive strength was achieved for the mixtures cured under ambient condition when calcium sources materials (Class C FA and BFS) were added to the mixtures.

In another study, Hwang et al. [98] analyzed the performance of brick and ceramic waste-based geopolymer mixtures containing varying levels of BFS (0–50%). The findings revealed that the greater substitution of BFS yielded the creation of densified C-S-H and C-A-S-H gels, binding and covering the unreacted particles. Furthermore, the elevated levels of CaO in the BFS led to denser hydrated gels, resulting in better pore refinement. In addition, substitution of BFS was found to be favorable in increasing strength.

In the study of Tan et al. [99], mitigation of efflorescence for CDW (consisting of concrete, mortar, bricks and tiles, glass, aggregate)-based geopolymer mixtures through the inclusion of MK and BFS was investigated. The findings from the research exhibited that substitution of MK and BFS notable decreased the efflorescence problem. Additionally, it was revealed that substitution of MK and BFS increased compressive strength and reduced flowability of the mixtures.

2.2. 3D-AM in Built Environment

Each industrial sector has taken noteworthy steps to integrate rapidly evolving technological applications into manufacturing techniques to address quickly and cost-effectively the increasing needs of the growing population [11,12]. Particularly, the trend towards digitization has further extended with the fast development of technology in recent years, escalating transitions to Industry 4.0. However, despite holding a substantial market share among industrial sectors, the construction industry has fallen behind in keeping pace with emerging technology in the past few decades and has been indecisive in taking required steps in traditional production processes to improve productivity compared to the other sectors [100–103]. The growing demand for housing because of ongoing population growth, disasters, and wars, has resulted in the recognition in recent years by academics and companies that manufacturing processes in the construction sector required to be more efficient, cheap, and fast [104,105]. Given this context, three-dimensional additive manufacturing (3D-AM), whose usage is rapidly gaining popularity due to the numerous advantages it offers in other sectors, has started to be employed in the construction industry [12]. 3D-AM systematically constructs tailored structures through the successive deposition of layers following the digital models, offering a high degree of design freedom [11,102,106]. With the adaptation of 3D-AM in the construction industry, digitalization, automation and individualization in built environments can be acquired [100,107]. The key benefits provided by the 3D-AM technique involve the reduction of production-related errors, shortened production time, decreased occupational safety risks, reduced need for skilled workforce, increased customization, and lowered costs [11,108]. Furthermore, 3D-AM which provides moldless production and the reduced generation of waste materials during the operation process, contributes significantly to mitigating the high environmental burdens caused by the construction sector [104–106].

The rapid adoption of 3D-AM in the construction sector is a direct outcome of the provided advantages. From a numerical point of view, 3D-AM was adopted by 10.0% of construction firms in the EU-27 in 2020, while the adoption rate was 9% in the USA [109] . Although varying market sizes are available, the report published by the European Construction Sector Observatory in 2019 revealed a noticeable growth projection for the 3D printing market in the following years. The market is expected to increase from \$0.04 billion in 2016 to nearly \$40 billion by 2027 [110]. Many countries target to encourage the widespread adoption of 3D printing by providing necessary incentives, with the aim of meeting the growing housing demand in a more affordable, rapid, and aesthetically pleasing manner [111]. For example, the UAE has set a goal for 25% of new constructions to be 3D printed by the end of the year 2030. The digitization demands of countries also foster the adoption of 3D-AM in the construction sectors. Nevertheless, it is crucial to recognize that research regarding the implementation of 3D-AM in the construction is still in its initial stages. The challenges associated with 3D-AM in built environments are outlined in Table 2.3 [112].

Table 2.3. Challenges of 3D printing in built environments (Revised after El-Sayegh et al. [112]).

| Problem Source | Description |
|---------------------------|--|
| Material | Printability, Buildability, Open time |
| 3D-printer | Scalability and Directional dependency |
| Software | Cybersecurity, Interoperability, Suitability of the digital model for printing |
| Architecture and design | Exclusion of building services, Structural integrity, New design principles |
| Construction management | Cost estimation, Construction site setup, Construction scheduling |
| Regulations and liability | Lack of codes regulations, Liability issues |

2.2.1. Test Methods for Performance Assessment of 3D-AM

3D concrete printing (3DCP) represents an advanced technology that involves the construction of structures layer by layer, eliminating need for formwork. The quality of a printed structure relies on several variables, with 3D printable concrete (3DPC) mixes playing a crucial role. As the development of 3DCP transitions from the laboratory to in-situ applications, it becomes vital to comprehend the engineering performance of 3DPC and the elements that affect them. Table 2.4 provides an updated comprehensive analysis of varied testing utilized for characterizing the engineering features of 3DPC.

Table 2.4. Common test methods applied to performance assessment of 3D-AM (Revised after Robayo-Salazar et al. [113] and Kaliyavaradhan et al. [114]).

| | | |
|-----------------------|---|---|
| Fresh State | Flowability | Flow table, slump, v tunnel, rheometer, viscosimeter, vane apparatus. |
| | Extrudability | Modified joint gun, screw pump, visual inspection, ram extruder, thixotropy assessment. |
| | Buildability | Visual analysis, quantifying the layer count and assessing layer deformation, cylinder stability test, green strength, rheological properties, deformation under static load. |
| | Open time | Flow table test, Shear stress test, vicat, V-Funnel and penetration test, interval pumping, visual inspection, rheometer, vane apparatus. |
| Hardened State | Mechanical Properties | Compressive Strength on 3D-printed structure: three different loading directions (perpendicular, lateral, and longitudinal) |
| | | Flexural Strength on 3D-printed structure: three directions of loading (perpendicular, lateral, and longitudinal) |
| | | Interlayer Bond Strength on 3D-printed structure: applying the tensile and compressive load in the different direction. |
| | | Three/Four-Point Bending Test on 3D-printed structure |
| Durability Properties | Shrinkage on both materials and on 3D-printed structure: Visual inspection, drying shrinkage | |
| | Cracks on 3D-printed structure: Visual inspection on layered structure | |
| | Permeability on both materials and on 3D-printed structure: Corrosion caused by chloride exposure and carbonation | |

The fresh characteristics of 3D printable mixture require particular unique specifications. The material must have satisfactory flowability for easy/efficient transportation from the mixer to the nozzle. Conversely, post-deposition, it should own the stiffness need to bear the load applied by subsequent layers. Accomplishing a balance between flowability and extrudability is essential, and while a longer open time improves these properties, a shorter open time is crucial for proper buildability. So, adjusting the optimal open time is of utmost significant. The flowability of printable mix is examined using standardized tests commonly utilized in conventional cementitious system, including the slump and flow table test. While manual tests such as the ram extruder and modified gun have been regarded for extrudability,

some researchers have denied their employment because of variations in applied force on the material. The buildability of 3D printed structures is measured through visual inspection, and some other tests like the cylinder stability and layer settlement test. Additionally, the analysis examines the assessments of buildability by investigating rheological variable such as yield stress. Materials having elevated yield stress demonstrate enhanced buildability performance. Researchers assign the ideal open time by performing flowability tests and correlating the results with the open time. Researchers also extrude the mixtures from the nozzle and monitor the continuity or disruption of the layer, noting that layer disruption happens as the open time passes. Rheometer tests are also used, relating rheology to yield shear strength, beyond which the mixture loses its open time. In examining the fresh characteristics of 3DPC, rheology is crucial. Rheology is examined through various rheometers, and some authors also used soil tests, such as the vane shear test, uniaxial compressive and direct shear test, because of similar behavior of soil and concrete under static conditions. Substantial consideration should be directed towards the creation of materials that address certain distinct needs for flowability, extrudability, and buildability. So, a thorough examination into the influences of printing process-based variables and material-based variables is must. These kinds of research are valuable for any kind of mixture and 3D-printer. A comprehensive investigation of available models and the creation of new ones, such as a buildability model, required to be performed extensively. Additionally, further studies are crucial to establish a standard testing protocols for examining the fresh features of 3D printable mixes [114].

In conventional concrete processes, concrete is poured for any structural element simultaneously. Conversely, 3D printing includes the pouring of building materials layer by layer. This yields 3D printed structures exhibiting an anisotropic behavior. Since 3D printing is a multilayer construction where consolidation/compression is not available, the formation of inter and intra-element pores happens in the printed structures. Consequently, it is essential to examine the density and measure voids in multi-layered structures. As previously stated, the strength properties of 3D printed structures are affected by their anisotropic nature, dependent on the loading and printing directions. Typically, the best compressive strength is noted in the longitudinal direction, ascribed to the greater extrusion pressure in the printing direction. Conversely, the least compressive strength is recorded in the lateral direction, mainly because of layer debonding in that direction. However, it should be emphasized that some studies have claimed that the highest compressive strengths in

directions other than the longitudinal. Given these conflicting findings, further investigation is required in this area to brighten the underlying systems. For flexural strength, the highest scores are noted in the perpendicular direction, ascribed to the superior layer compaction and the occurrence of tensile stress transverse to the loading direction. The examination of tensile bond strength is essential for multilayer objects in 3D. As previously stated, the absence of standardized norms for examining tensile bond strength has results in the use of various shapes (cube, rectangular, and cylindrical) and both direct and indirect methods in its determination. The direct method includes applying direct tension, while the indirect method involves determining the splitting tensile strength. The time gap between two consecutive layers significantly affects the bond strength, where a more printing time interval yield reduced bond strength yet is beneficial for buildability performance. Alterations in the substance of 3D printable mixes have a significant influence on its mechanical performance. While many previous studies have centered on compressive strength, the bond strength of 3DPC is an essential consideration. Therefore, it is crucial to intensively examine the impacts of different factors on bond strength [114].

To ensure the longer service life of a 3D printed structure, a main emphasize should be on its durability. The multilayer structure of 3D printed structure results in interconnected voids between the layers, creating a permeable structure vulnerable to carbonation and chloride-induced corrosion. Additionally, shrinkage and cracking are essential factors affecting the durability of 3D printed structures. Traditional methods used to examine autogenous shrinkage are not proper for 3D. So, a new test method has been developed particularly for examining shrinkage and cracking in printed structures [115]. Additionally, the inclusion of shrinkage-reducing additives, fibers, and adequate curing can help reduce shrinkage and cracking issues.

2.3. Utilization of Geopolymers in 3D-AM

In recent years, there has been limited research investigating the adaption of geopolymer materials with 3D-AM technology, aiming to combine advancements in environmentally friendly material development with innovative production methods. The following summaries highlight key findings from some of these studies.

Chougan et al. [116] carried out a research endeavor to investigate the printability of geopolymer synthesized by the activation of FA, BFS, and SF precursors using NaOH and Na₂SiO₃. The examination concentrated on investigating the rheological, mechanical, and

buildability characteristics of the printable mixtures. The outcomes of the research revealed that the majority of the mixtures showed anisotropic behavior with respect to Young's Modulus, indicating that the mechanical performance was affected by the direction of printing.

In an independent study [117], it was found that accomplishing a geopolymer proper for 3D-AM applications needed a careful balance among factors influencing open time performance, yield stresses, and time-dependent rheological property.

Another research effort [118] investigated the impact of various open time and printing parameters on bond strength, stating that extended open time intervals resulted in a decrease in bond strength. However, low printing speed and a decreased nozzle height were detected as factors contributing to enhanced bond strength.

Panda et al. [119] carried out research to delve into the engineering characteristics of geopolymers, in which FA, BFS, and SF were utilized as precursors. Compressive strength tests were applied in the perpendicular direction to compare results with mold-cast geopolymers. The results revealed that the manufacturing technique had minimal impact on strength, with 3D-printed specimens resulting a compressive strength of 18.4 MPa and mold-cast specimens exhibiting a compressive strength of 16.2 MPa.

In a separate study by Panda et al. [120], it was noted that geopolymers based on fly ash, manufactured through 3D-AM technology, exhibited directional disparities in their mechanical properties. Flexural strength examinations conducted in three distinct loading directions exhibited a maximum difference of approximately 50% in the direction-dependent performances.

In a different investigation performed by Al-Qutaifi et al. [121], the impacts of printing time intervals on geopolymer specimens, printed with 5, 10, and 15-minute time gaps, was investigated through flexural strength testing. The findings exhibited that mitigating the time gaps between consecutive layers considerably affected the improvement of flexural strength in layered objects, as it enhanced the adhesion between additive layers.

The investigation performed by Nematollahi et al. [122] examined the impacts of print-time intervals on the inter-layer strength, as well as the strengths of the printed structure in various orientations. Two distinct print-time intervals, 2 and 15 minutes, were followed during the

printing process. The findings exhibited that the print-time interval substantially influenced the inter-layer strength, while its impact on the strengths of the geopolymer was minimal.

In research undertaken by Panda and Tan [123], an innovative 3D printable geopolymer mortar was designed, enabling the direct printing of building components without needing formwork. Key fresh properties crucial for printable geopolymer, involving extrudability, shape retention, buildability, and open time, were rigorously assessed through experimental methods, resulting to the detection of their viable ranges. Based on the experimental results, a beneficial range for smooth geopolymer mortar extrusion was determined to be 0.6–1.0 KPa yield stress.

The research performed by Muthukrishnan et al. [124] utilized a rheo-chemical approach to examine the early-age strength development ascribed to alkali reactions for formulating a viable geopolymer suitable for 3D-AM. Key outcomes of the study involved: i) the mixing regime considerably affected obtaining a uniform mix. A total mixing time of 15 minutes proved crucial for entire solid activator dissolution, ii) the inclusion of sucrose as a retarder exhibited a significant effect in adjusting the static yield strength's time-dependent growth, iii) geopolymer concrete possessed its proper consistency for 3D printing even after a 90-minute resting period when exposed to re-shearing.

In the research performed by Ma et al. [125], the availability of integrating a continuous micro steel cable (1.2 mm) during the printing process for geopolymer composite material was investigated. The composite exhibited improved flexural bending capacities, suggesting well-bonded and coordinated micro-cable and geopolymer, resulting considerable improvements in mechanical strength, toughness, and post-cracking deformation.

The research performed by Pasupathy et al. [126] examined the use of brick waste for synthesizing printable geopolymer mixtures. The examination emphasized on evaluating the impact of brick waste content on the fresh features. Additionally, the study assessed the hardened properties, regarding varied brick waste amount in the mixture. The findings exhibited that the incorporation of brick waste enhanced the fresh features of mixtures. Mixes incorporating brick waste showed higher yield strength and apparent viscosity at an early age in comparison to the control mix. In contrast, compressive and interlayer strength, exhibited a decrease with higher brick waste amount. Nevertheless, the inclusion of brick wastes up to 10% enhanced the overall strength characteristics.

In Ma et al.'s study [127], a novel printable geopolymer was designed using flue gas desulfurization gypsum (FGD, FA, GBFS, and steel slag (SS)). The influence of SS amount on fresh features, printability, anisotropy performance, and geopolymerization was assessed. Yield stress and plastic viscosity regularly reduced with escalating SS amount. Conversely, 10% SS incorporated geopolymer showed superior performance compared other usage rates. Obtained result was ascribed to the dual effect of SS on reaction kinetics. The OH⁻ generated by SS hydration enhanced the alkaline nature, accelerating the dissolution of SiO₄⁴⁻ and AlO₄⁵⁻, while the minimal reactivity impeded subsequent polymerization. Moreover, the printed specimen exhibited a more dense microstructure and mitigated anisotropy.

The study carried out by Demiral et al. [128] assessed the anisotropy and bonding performance of printed CDW-based geopolymer mortars. The research findings highlighted the significant impact of alkaline activator content on mechanical properties. Compressive and flexural strength tests showed anisotropic behavior in 3D-printed geopolymer mortar specimens, with the bond performance between consecutive layers noted as a key influencing factor. Nevertheless, perpendicular-loaded testing specimens exhibited comparable or modestly superior performance in comparison to mold-casted specimens, suggesting minimal impact of the bond zone on specimens loaded in the perpendicular direction.

In the study performed by Chaiyotha et al. [129], the emphasize was on 3D printing of high-calcium FA-based geopolymer. The mixture proportions were designed based on variables such as a sand/FA rate of 1.55, 1.65, and 1.75, liquid/binder rate of 0.45, 0.50, and 0.55, along with printing rate ranging from 140 to 160 mm/s, printing time interval durations of 10, 20, and 30 minutes, and nozzle heights of 10, 11, and 12 mm for printing. The findings of the research exhibited that, the mixture having a sand/FA rate of 1.65 and a liquid/binder rate of 0.50 was considered the best proper. This mix exhibited a rapid-setting time of 56 mins and ease of extrusion, with a flowability of 103%, particularly when applying a printing rate of 150 mm/s, 3-minute printing time interval between each layer, and a nozzle height of 11 mm. Compressive strength accomplished was 23.9 MPa at the end of 28-day curing, exhibiting the suitability of high-calcium FA for 3D printing.

3. EXPERIMENTAL PROGRAM

3.1. CDW-based Geopolymer Paste Mixture

3.1.1. CDW-based Materials

The CDW-based materials employed in paste mixtures as precursor material (HB, RCB, RT and G) were gathered from the demolition sites. Once the process of selective demolition was completed, since the CDW elements were obtained in large sizes, they were further broken down into smaller pieces. Then, they were subsequently decreased in dimensions with a jaw crusher and milled during one hour in a ball mill to attain powdery materials. Figure 3.1 displays the visual representations of CDW-based materials in raw, crushed, and powder forms and their SEM images. XRF analysis was conducted to find out the oxide compositions of the used precursor materials (Table 3.1). For the CDW-based precursors, the main oxides for the clay-originated precursors were SiO₂, Al₂O₃ and Fe₂O₃, while G contained SiO₂, Na₂O and CaO as the main oxides. Particle size distributions (PSD) of the various precursor materials were also ascertained by conducting laser diffraction analysis (Figure 3.2). While clay-originated wastes including HB, RCB, and RT had similar PSD, G were in coarser grain sizes.



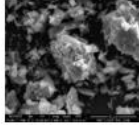


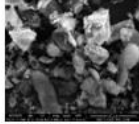


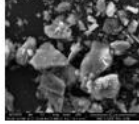


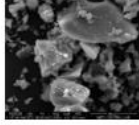
| CDW-based materials | Initial collection | Ball milled | SEM images |
|---------------------|---|--|---|
| HB |  |  |  |
| RCB |  |  |  |
| RT |  |  |  |
| G |  |  |  |

Figure 3.1. Digital and SEM images of precursors.

Table 3.1. Chemical compositions of precursors.

| Oxides, % | HB | RCB | RT | G |
|-----------|----|-----|----|---|
|-----------|----|-----|----|---|

| | | | | |
|------------------------------------|------|------|------|------|
| SiO₂ | 39.7 | 41.7 | 42.6 | 66.5 |
| Al₂O₃ | 13.8 | 17.3 | 15.0 | 0.9 |
| Fe₂O₃ | 11.8 | 11.3 | 11.6 | 0.3 |
| CaO | 11.6 | 7.7 | 10.7 | 10.0 |
| Na₂O | 1.5 | 1.2 | 1.6 | 13.6 |
| MgO | 6.5 | 6.5 | 6.3 | 3.9 |
| SO₃ | 3.4 | 1.4 | 0.7 | 0.2 |
| K₂O | 1.6 | 2.7 | 1.6 | 0.2 |
| TiO₂ | 1.7 | 1.6 | 1.8 | 0.1 |
| P₂O₅ | 0.3 | 0.3 | 0.3 | 0.0 |
| Cr₂O₃ | 0.1 | 0.1 | 0.1 | 0.0 |
| Mn₂O₃ | 0.2 | 0.2 | 0.2 | 0.0 |

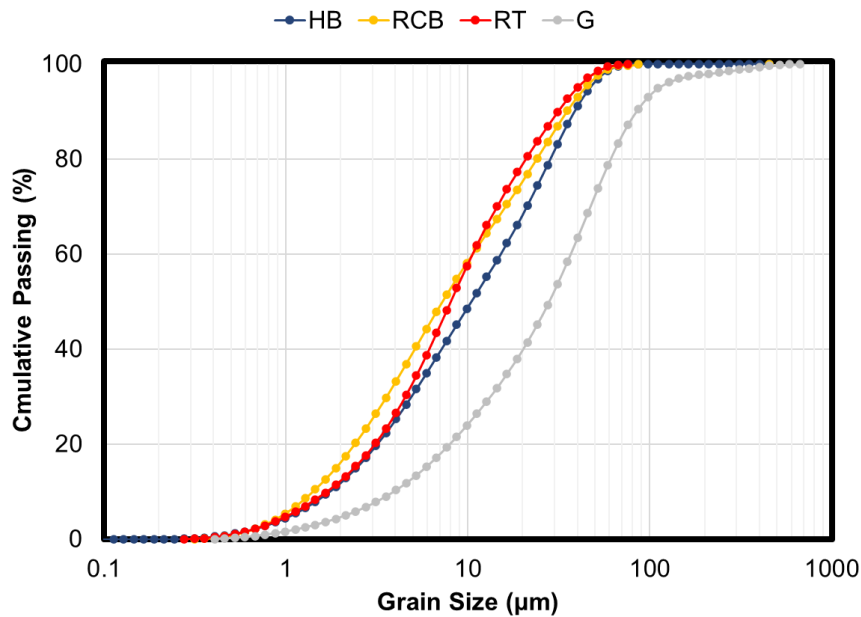


Figure 3.2. PSD curves of CDW-based precursors.

3.2. CDW-based Geopolymer Mortar Mixture

3.2.1. CDW-based Materials

In the powder design of CDW-based mortar mixtures, bricks waste (BW) and concrete waste (CW) obtained from demolition sites were used as CDW-based precursors, after undergoing a thorough process of crushing and milling. Figure 3.3 demonstrates the physical appearance and SEM images of the powdered form of the utilized precursors, offering insights into their surface texture and morphological characteristics. Besides, Table 3.2 presents the oxide composition of the precursors obtained through XRF analysis, providing information on the available species within the precursors. According to the results, BW primarily consist of SiO₂ and Al₂O₃, while CW is primarily made of SiO₂ and CaO. The identification of these species through XRF analysis in CDW-based precursors strongly suggests their

compatibility with geopolymerization in an alkaline environment. Figure 3.4 illustrates the PSD of the precursors, which was analyzed using laser diffraction analysis. Based on the findings, the maximum particle size of BW was determined to be 70 μm , whereas CW had a coarser particle distribution, with 75% of particles below 100 μm .

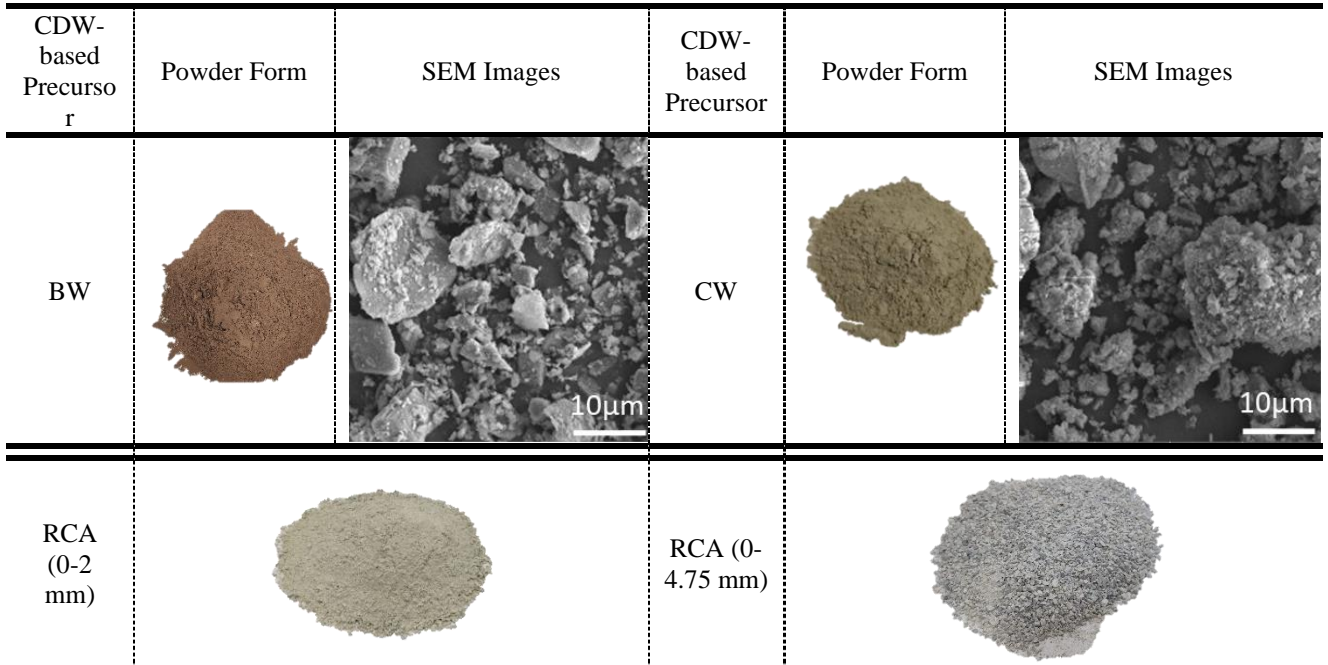


Figure 3.3. Digital and SEM images of precursors and aggregates.

Table 3.2. Chemical composition of precursors.

| Oxides, % | BW | CW |
|------------------------------------|------|------|
| SiO₂ | 50.0 | 37.4 |
| Al₂O₃ | 21.8 | 5.1 |
| Fe₂O₃ | 7.9 | 2.4 |
| CaO | 4.3 | 26.0 |
| Na₂O | 0.7 | 0.2 |
| MgO | 2.2 | 3.8 |
| SO₃ | 1.0 | 0.5 |
| K₂O | 4.0 | 0.9 |
| TiO₂ | 1.0 | 0.2 |
| P₂O₅ | 0.2 | 0.0 |
| Cr₂O₃ | 0.0 | 0.1 |
| Mn₂O₃ | 0.1 | 0.1 |

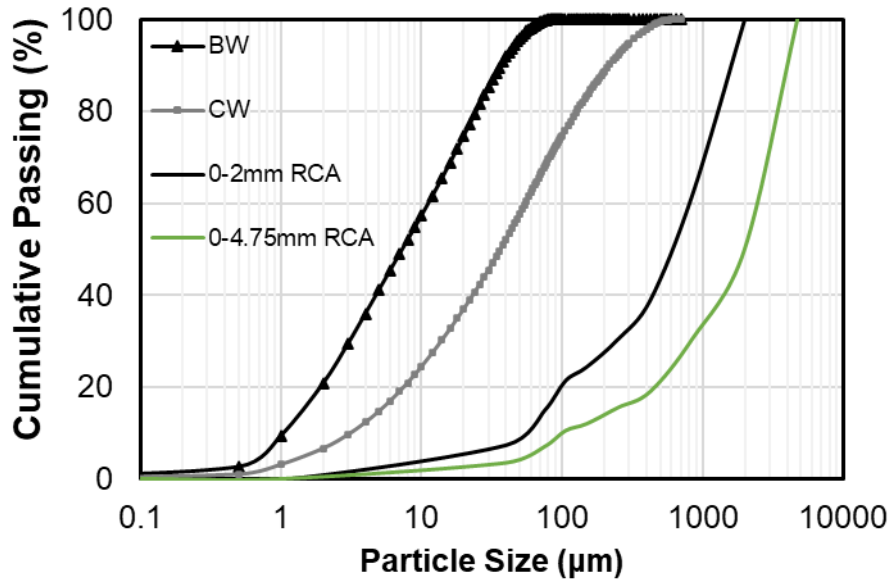


Figure 3.4. PSD of precursors and RCAs.

Recycled concrete was employed as an aggregate obtained by crushing concrete rubble fragments sourced from demolition sites. The aim was to enhance the recycling rate of CDW by incorporating concrete waste as filler materials in addition to the precursor. RCAs were generated in two size fractions, namely 0-2 mm and 0-4.75 mm, by sieving the crushed concrete waste, as depicted in Figure 3.3. The RCAs were used without undergoing any form of treatment prior to their incorporation in the mixture.

3.3. Industrial Waste-based Materials

To optimize the engineering features of the CDW-based geopolymer and promote the formation of additional geopolymeric gels, industrial waste materials such as BFS, FA and SF were included in the geopolymer precursor blends, thereby providing supplementary sources of Si, Al and Ca to the matrix. Figure 3.5 demonstrates the physical appearance and SEM images of the utilized precursors, offering insights into their surface texture and morphological characteristics. Besides, Table 3.3 tabulates the oxide composition of the precursors obtained through X-ray fluorescence (XRF) analysis, providing information on the available species within the precursors. The main oxides available in the chemical composition of BFS were SiO_2 , Al_2O_3 and CaO , while FA contained SiO_2 , Al_2O_3 and Fe_2O_3 and SF contained high amount of SiO_2 as the main oxides. Figure 3.6 illustrates the PSD of the precursors, which was analyzed using laser diffraction analysis. Based on the findings, SF had a maximum particle size of 20 μm , whereas the BFS used had a recorded maximum particle size of approximately 40 μm . FA were in coarser grain sizes.

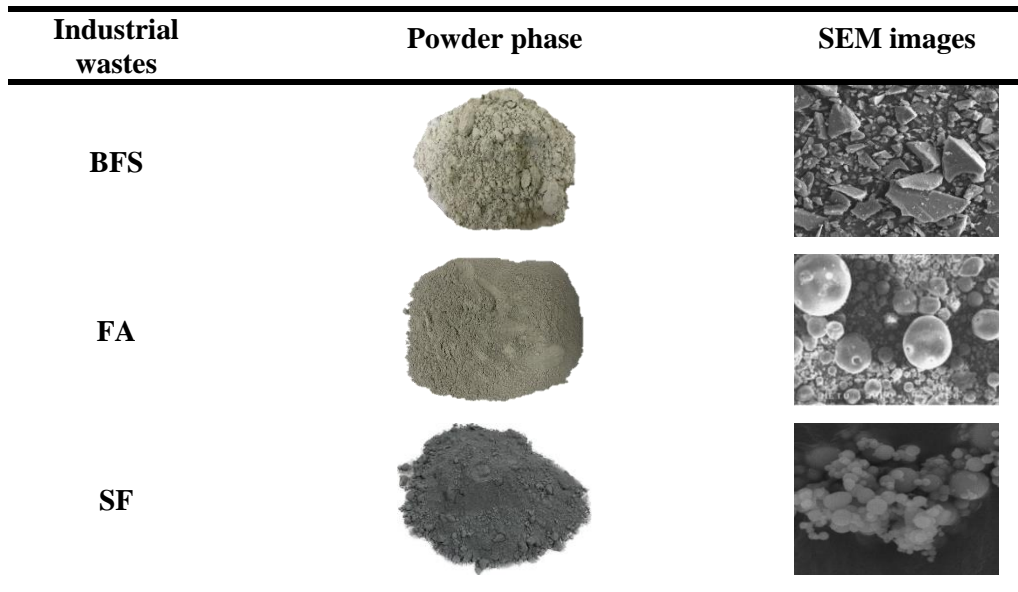


Figure 3.5. Digital and SEM images of industrial waste-based precursors.

Table 3.3. Chemical composition of precursors.

| Oxides, % | BFS | FA | SF |
|------------------------------------|------|------|------|
| SiO₂ | 38.2 | 60.1 | 81.2 |
| Al₂O₃ | 13.0 | 21.4 | 0.5 |
| Fe₂O₃ | 0.7 | 7.4 | 1.3 |
| CaO | 35.3 | 1.0 | 0.4 |
| Na₂O | 0.1 | 1.0 | 0.6 |
| MgO | 6.5 | 1.8 | 5.8 |
| SO₃ | 0.5 | 0.2 | 0.5 |
| K₂O | 0.9 | 2.9 | 2.6 |
| TiO₂ | 1.0 | 0.9 | 0.1 |
| P₂O₅ | 0.0 | 0.2 | 0.0 |
| Cr₂O₃ | 0.0 | 0.0 | 2.5 |
| Mn₂O₃ | 1.4 | 0.1 | 0.1 |

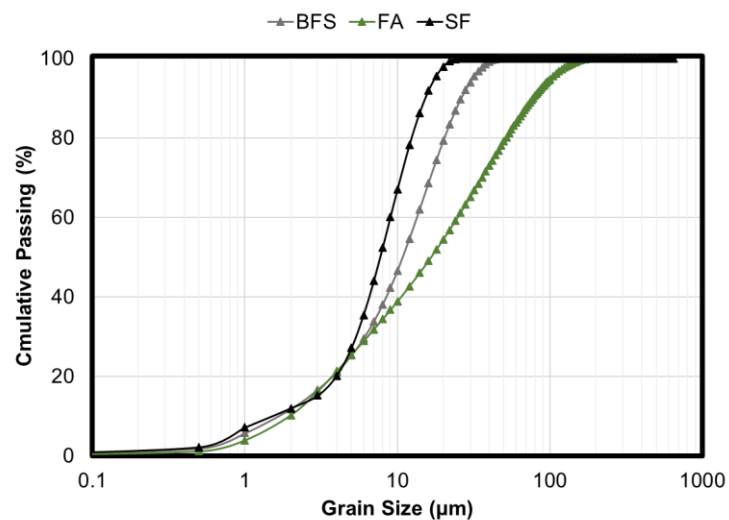



Figure 3.6. PSD of industrial waste-based precursors.

3.4. Alkaline Activators

3.4.1. NaOH

In the scope of thesis study, the alkaline activation of waste-based precursors relied on sodium hydroxide in flake form. The sodium hydroxide utilized boasted a minimum purity of 98%, with sodium carbonate not surpassing 0.4%, sodium chloride at 0.1%, and iron content limited to 15 ppm. Comprehensive information and digital representations of the specific sodium hydroxide used can be found in Table 3.4 of the thesis.


Table 3.4. Characteristics of NaOH.

| Features | | Digital Image |
|-------------------------|-----------|--|
| Sodium hydroxide | 98.27 % |  |
| Sodium chlorite | 0.02 % | |
| Sodium carbonate | 0.35 % | |
| Iron (Fe) | 13.17 ppm | |

3.4.2. Ca(OH)₂

In the thesis studies, the used calcium hydroxide was in powder form with 87% purity. The Ca(OH)₂ utilized was procured from "Tekkim Kimya". The properties and physical characteristics of the Ca(OH)₂ are detailed in Table 3.5.


Table 3.5. Characteristics of Ca(OH)₂.

| Features | | Digital Image |
|-----------------------------------|-------------|--|
| Molecular Weight | 74.09 g/mol |  |
| Melting Points | 550 °C | |
| Purity (%) | min. 87 | |
| MgO (%) | max. 1 | |
| Acid-insoluble (%) | max. 1 | |
| Loss on ignition (%) | max. 3 | |
| Grain Size (<90 mm) (%) | min. 90 | |

3.4.3. Na₂SiO₃

Na₂SiO₃ typically exists in a liquid state and is colorless. The Na₂SiO₃ employed in this dissertation study was obtained from "Emir Kimya." Detailed properties of the Na₂SiO₃ are provided in Table 3.6.

Table 3.6. Characteristics of Na₂SiO₃.

| Features | | Digital Image |
|--|------|---|
| SiO ₂ | 23 % |  |
| Na ₂ O | 11% | |
| Module (SiO ₂ /Na ₂ O) | 1.9 | |
| Baume (20 °C, Be ¹) | 40 | |
| Density (20°C, gr/cm ³) | 1.4 | |
| H ₂ O | 66% | |

3.5. Mixture Preparation Procedure

3.5.1. Small-scale production

The production procedure of geopolymer paste mixtures began with preparing alkaline solutions. The required quantities of NaOH in the form of solid flakes were dissolved in water, after that left to cool since the dissolution reaction of NaOH is exothermic. A mortar mixer was employed to combine each material into a homogeneous mixture. The mixing process involved following steps: (i) all of the solid components were softly mixed [precursors, and Ca(OH)₂] for a minute at a low speed; (ii) the NaOH was then included and the mixture was allowed to stir for another 60 seconds; (iii) mixing was continued for a further 90 seconds at low speed; (iv) finally, the mixture was blended at a medium speed for the last 60 seconds, and that concluded the mixing procedure.



Figure 3.7. The mixer used for small-scale production.

3.5.2. Large-scale production

The process of preparing the mixture commenced by preparing the NaOH solution, considering the exothermic nature of the reaction. Following this, all solid ingredients were placed into the mixing container and mixed for 2 min to ensure a uniform distribution. Then, the NaOH was included to the mixing container within a minute. Afterward, the mixture was

further mixed for 2 min. For systems having liquid components, liquids were included into the pre-mixed slurry and the mixing was continued for additional 1 min. After the mixing process was finalized, specimens were prepared following the relevant test standards.



Figure 3.8. The mixer used for large-scale production.

3.6. Curing Condition

After completing the mixing procedure, specimens were prepared in accordance with the corresponding test standards. Specimens stayed in their molds for 24 hours at the laboratory environment ($23 \pm 2 \text{ }^\circ\text{C}$ and $50 \pm 5\%$ relative humidity). Subsequently, they were cured in ambient condition in laboratory until they reached the required testing ages.



Figure 3.9. Digital images of samples cured under ambient conditions.

4. RESULTS AND DISCUSSIONS

4.1. Effect of Industrial Waste-Based Precursors on Performance of CDW-Based Geopolymer Paste

The research was initiated on the basis of paste phase, investigating the effects of different industrial waste-based precursors. Additionally, the environmental burdens of CDW-based geopolymer systems were examined. The findings will be applied during the mortar mixture design phase to formulate blends that are not only more cost-effective and high-performing but also environmentally sustainable.

4.1.1. Introduction

Although several studies have been performed on the effectiveness of industrial waste addition on the features of CDW-based geopolymer mixtures, these studies are much fewer in comparison to those conducted on mainstream precursor-based geopolymers and tend to focus on specific topics. The novelty of this study lies in its comprehensive and comparative experimental and environmental impact analysis on CDW-based geopolymer mixtures containing industrial wastes. Additionally, special attention was given to tests conducted in the scope of this study to explore the possibility of using these materials in advanced manufacturing technologies. Experimental studies evaluated in detail the effects of industrial waste-based precursors on the fresh characteristics of the geopolymer mixtures, by conducting flow table, buildability, vane shear, ram extruder test methods. Additionally, compressive strength test was performed to figure out the impacts of industrial wastes on the mechanical performance of mixes. To assess the environmental burden of the developed geopolymer mixtures and substitution of industrial wastes, a LCA was conducted in the scope of this study. CDW-based HB, RCB, RT, and G and industrial waste-based BFS, FA, and SF were used as precursors in geopolymer mortar mixture designs. To activate precursors, NaOH, and Ca(OH)₂ were utilized. The findings of this research will support to the available literature by demonstrating the effects of industrial waste-based precursors on the features of the CDW-based geopolymer systems. Besides that, the outcomes of this study are believed to make a significant contribution to the current state-of-the-art, as the findings provide comprehensive insights and knowledge about tailoring the engineering features of the CDW-based geopolymer mixtures considering environmental burdens. In addition to that, developed products will be further considered and optimized for novel sources to provide requirements for advanced manufacturing processes.

4.1.2. Experimental Studies

4.1.2.1. Materials and mixture design

In total, seven different geopolymer paste mixture designs were set in this study. First, a dry base paste mixture design containing entirely (100%) CDW was devised, and the precursors content of these mixtures was made of 30% RCB, 30% HB, 30% RT, 10% G, by the total weight of precursor materials according to the preliminary study published by the authors [77]. Then, in addition to the 100% CDW-based system, different industrial waste-incorporated paste mixtures were designed. To do this, clay-originated waste powders of HB, RCB, RT were substituted by BFS, FA and SF separately at two replacement rates of 10% and 20%. All paste mixtures were produced with NaOH molarity of 6.25M and the Ca(OH)₂ usage rate of 10% and the water/binder rate was constant at 0.33. Table 4.1 presents the mix details.

Table 4.1. Details of mixes.

| Mixture Code | Alkali activators | | | | Precursor materials (1000 g) | | | | | | |
|--------------|-------------------|------------|---------------------|------------|------------------------------|-------|-------|-----|-----|-----|-----|
| | NaOH | | Ca(OH) ₂ | | HB | RCB | RT | G | BFS | FA | SF |
| | Molarity (M) | Amount (g) | Rate (%) | Amount (g) | | | | | | | |
| 100CDW | 6.25 | 82.5 | 10 | 100 | 300 | 300 | 300 | 100 | - | - | - |
| 90CDW-10BFS | | | 10 | 100 | 266.7 | 266.7 | 266.7 | 100 | 100 | - | - |
| 80CDW-20BFS | | | 10 | 100 | 233.3 | 233.3 | 233.3 | 100 | 200 | - | - |
| 90CDW-10FA | | | 10 | 100 | 266.7 | 266.7 | 266.7 | 100 | - | 100 | - |
| 80CDW-20FA | | | 10 | 100 | 233.3 | 233.3 | 233.3 | 100 | - | 200 | - |
| 90CDW-10SF | | | 10 | 100 | 266.7 | 266.7 | 266.7 | 100 | - | - | 100 |
| 80CDW-20SF | | | 10 | 100 | 233.3 | 233.3 | 233.3 | 100 | - | - | 200 |

4.1.2.2. Testing methods

Flow table test

To examine the workability of geopolymer pasts, the flow table was conducted by following the ASTM C1437-15 standard. Kazemian et al. [130] found a robust interrelation among flow diameter and yield stress. Therefore, it can be possible to state that this test assesses the yield stress which is crucial for fresh state property assessment. To examine the yield stress of the mixture, the flowability index (Γ) was determined by using Eq.1 [131] considering the flow diameters of the paste.

$$\Gamma = \frac{d_1 d_2 - d_0^2}{d_0^2} \quad (1)$$

where the inner diameter of the mold is d_0 (100 mm) while d_1 is the highest flow value and d_2 is the flow value orthogonal to d_1 .

Buildability test

A modified version of mini-slump test proposed by Nematollahi et al. [132] was performed to assess the buildability characteristics of geopolymer mortar within the purpose of investigating the response of fresh state mixtures under static load. This test involved placing the mixture in the mini-slump cone followed by a one-minute waiting period. After that, a plate was positioned on the mixture, with a static load of 600 g for a minute. The deformation of the paste was then measured in two directions and the average height was noted. The results were evaluated by considering that lower deformation or higher final height indicates higher yield stress of the mixture.

Vane shear test

Vane shear test was also conducted to assess the fresh characteristics of prepared geopolymer paste mixtures. The pocket-type vane shear tool was employed to assess the flow features of fresh-state geopolymer mixes. The test was performed to determine the resistance of the material to shear forces and to evaluate the rheological properties of the geopolymer. This test procedure was utilized to evaluate the yield stresses of geopolymer mixtures comparatively, as yield stress values could change according to the test methods employed [133]. The vane shear test was also performed on the mixtures after 30, 60, and 120 minutes from the end of mixing to give insight into how the shear yield stress changes over time and determine the workable time of the geopolymer mixtures.

Ram extruder

This study used a ram extrusion test to evaluate the shear yield stress of geopolymer paste mixtures. The extruder utilized in this research was developed based on literature studies [134–136], and comprised of four parts: piston, chamber, nozzle, and stands (Figure 4.1). Ram extruder was established on a testing device as seen from the Figure 4.1. Although the diameter of the chamber was 4 cm, mixtures extruded from nozzle having a diameter of 1.5 cm. The piston speed was adjusted to 2.25 mm/s by considering this difference. This piston speed resulted in an extrusion rate of 16 mm/s for the extruded material.

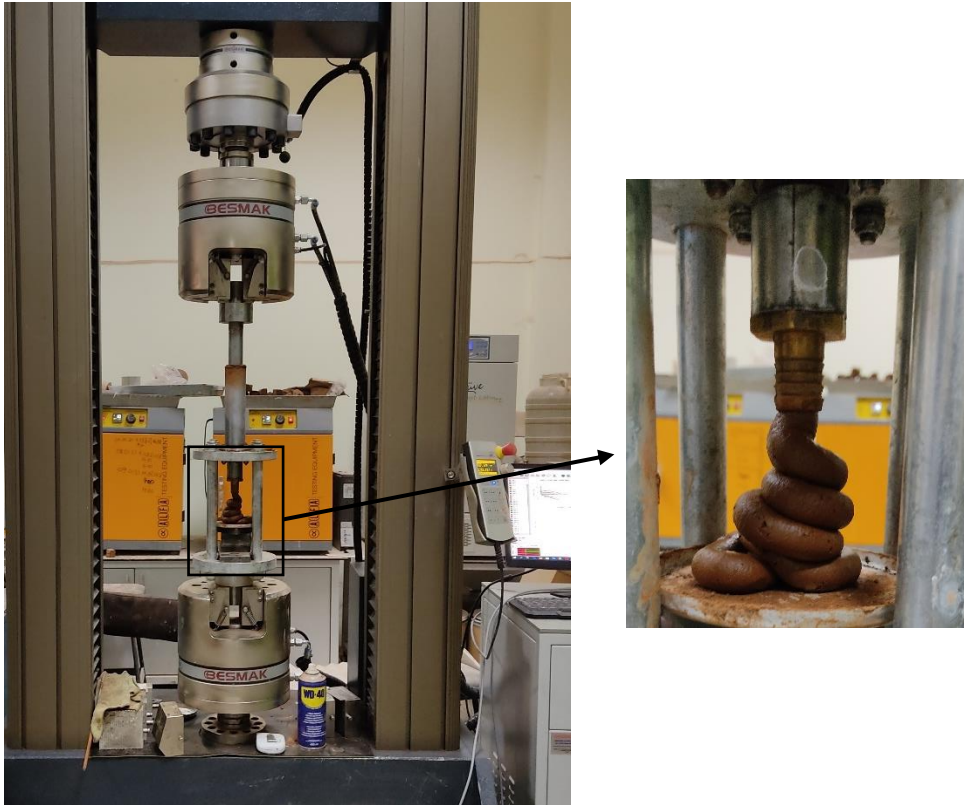


Figure 4.1. View of the ram extruder setup.

Extrusion pressure was determined using the equation proposed by Chen et al. [134] (Eq.2). The measured extrusion pressure or yield stress during the mix is flowed through the chamber was represented by σ_0 , and the average extrusion force used to attain the predetermined piston speed was denoted by F.

$$\sigma_0 = 4F/\pi \times D_0^2 \quad (2)$$

Extrusion pressures were used to find out the shear yield stress, in accordance with Von Mises criterion [137], by using the Eq.3.

$$\tau_0 = \sigma_0/\sqrt{3} \quad (3)$$

The open time performance was also examined with this test. This was at 0, 30, 60, and 120 minutes, similar to the vane shear test. This was done because geopolymerization reactions might cause these mixtures to lose their consistency.

Compressive strength test

The test was carried out by following ASTM C109 standard at a loading rate of 0.9 kN/s, to delve into the strength characteristics of the 50×50×50 mm (cubic) geopolymer. Compressive strength tests were applied on three replicates of the cubic samples for each mixture at curing ages of 7- and 28-day. The mean of the results obtained from the three replicates were reported as compressive strength.

Life cycle assessment

System description

LCAs were performed following thoroughly International Organization for Standards (ISO) 14040 and 14044 criteria for the methodology of this study. LCA studies were prepared in four phases involving goal and scope definition, inventory analysis, impact assessment, and interpretation in ISO guidelines as given in Figure 4.2.

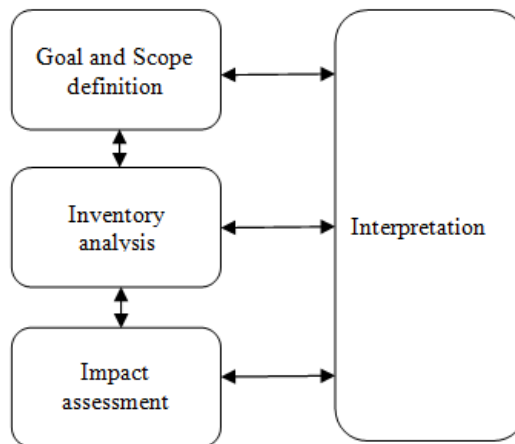


Figure 4.2. LCA framework based on ISO standards.

Goal and scope

The target of this research was to examine the environmental burdens and sustainability performance of manufacturing geopolymer pastes for using CDWs with industrial waste-based materials including BFS, FA and SF at different rates (90% CDW-10% industrial waste-based material, 80% CDW-20% industrial waste-based material) with the suitable blend (6.25M-NaOH and 10% Ca(OH)₂) of activators. The LCAs were performed with Simapro software in an iterative manner.

Life cycle inventory

The system's inventory data composed of the material and energy inputs at the system boundary were gathered and presented in this part. Material procurement processes were carried out in different cities. CDW-based materials were gathered from various demolition

sites and alkaline activators were taken from the chemical manufacturer in Ankara, Turkey. While FA was provided from İSKEN Sugözü Thermal Power Plant, BFS was obtained from İskenderun Iron and Steel Inc., and SF was brought from Antalya-Etibank Ferro-Krom Factory. The information regarding the distances and vehicles required for the transportation of each material is given in Table 4.2.

Table 4.2. Transportation details of the precursors and alkaline activators.

| Transportation of CDW | | Transportation of BFS | | Transportation of FA | | Transportation of SF | | Transportation of Alkali Activators | |
|-----------------------|----|-----------------------|-----|----------------------|-----|----------------------|-----|-------------------------------------|----|
| ton | km | ton | km | ton | km | ton | km | Ton | km |
| 10 | 20 | 10 | 620 | 10 | 560 | 10 | 480 | 0.5 | 15 |

To prepare geopolymer mixture, CDWs were subjected to the crusher and milling processes to obtain powdery form. Then, geopolymer pastes were obtained through mixing process with the mixer. During analysis, crusher, ball mill and mixer devices were selected as large-scale devices used in the sector. The information regarding to the equipments used and the electrical energy consumptions are also presented in Table 4.3. The energy consumption values were calculated by multiplying the number of kg of material entered into each mixture at these stages by the consumption values per kg.

Table 4.3. Consumed electrical energies of machines.

| # | Jaw Crusher | | Ball Mill | | Mixer | |
|-------------|-------------|--------|-----------|--------|--------|--------|
| | Amount | Unit | Amount | Unit | Amount | Unit |
| Capacity | 20000 | kg | 20000 | kg | 600 | kg |
| Duration | 1 | h | 1 | h | 1 | h |
| Consumption | 15 | kwh | 280 | kwh | 7.5 | kwh |
| | 0.00075 | kwh/kg | 0.014 | kwh/kg | 0.01 | kwh/kg |

Life cycle impact assessment (LCIA)

The impact assessment results were obtained by using CML IA method [138] on Simapro software [139], and the Ecoinvent 3.0 database. The main impact categories used in this study are global warming (kg CO₂ eq.), ozone depletion (kg CFC-11 eq.), acidification (kg SO₂ eq.), eutrophication (kg PO₄ eq.) and photochemical oxidation (kg C₂H₄ eq.).

Assumptions & limitations

The assumptions made for the LCA were as in followings:

- The LCA was a cradle-to-gate analysis.

- The functional unit was set to be 1 m³ of pastes.
- The process was determined to be located in Turkey, however, due to the lack of available data in the software, RoW geography was chosen for the LCA. Nevertheless, electricity data were modeled based on the Turkey electricity country mix.
- The energy input of large-scale devices used in the sector, such as a jaw crusher, ball mill, and mixer, was considered for the production of geopolymers and calculated based on their corresponding hourly power consumption to accurately represent the energy consumption induced by the material's life cycle. The energy consumption calculations were according to the production capacity and power consumption of the industrial-grade crusher, ball mill, and mixer, which had respective power consumption values of 15 kW, 280 kW, and 7.5 kW.
- A production process for CDWs was not included. The Ecoinvent database was only used for treatment process for these wastes. This treatment process involved energy for dismantling, particulate matter emissions caused by dismantling and handling.
- BFS, FA and SF were waste of the iron industry, coal thermal power plants and silicon alloy plants, respectively and do not require a separate process for production [140]. FA and SF, for example, were waste materials and had no bearing on the environmental impact of the end product, as determined by [141]. Their environmental impact was limited to the specific processing required for their use in concrete (grinding, drying and stock). The LCA data for these materials were taken directly from the Ecoinvent database for waste and emissions to treatment.

4.1.3. Experimental Results and Discussion

4.1.3.1. Fresh properties

Rheological findings of 100% CDW-based and BFS-, FA- and SF-incorporated geopolymer paste mixes are given in Figure 4.3.

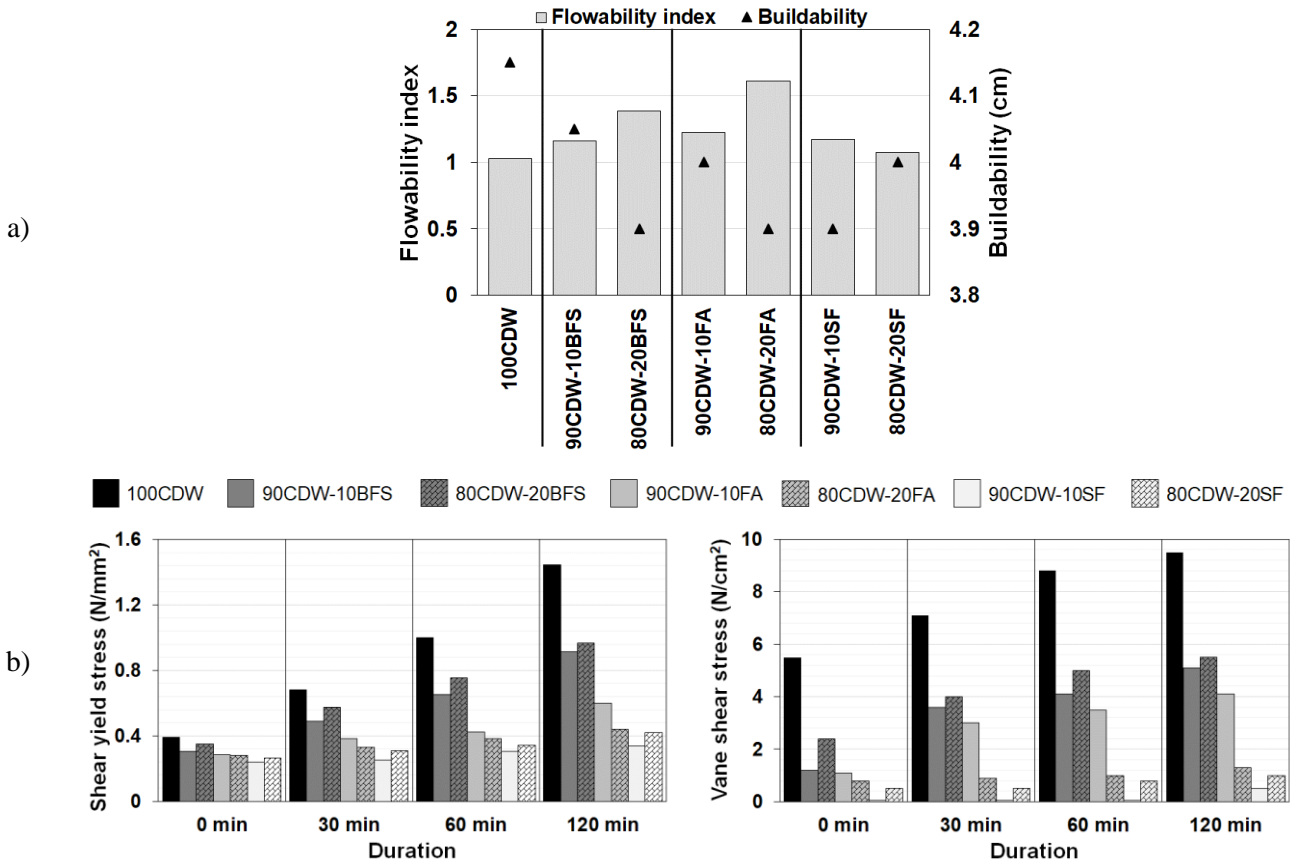


Figure 4.3. Rheological test results of (a) flowability and buildability, (b) yield stresses.

Effects of BFS

According to findings, BFS incorporation enhanced the workability of the mixes while decreasing buildability. This behavior was recorded for each replacement rate. This notification can be ascribed to diversity in the chemical and physical characteristic features of the BFS and CDW-based precursors and might be linked to the relatively lower water need of BFS due to the reduced number of plate-shaped powders [142–145]. These reasons also yielded mitigation in the vane shear stress and shear yield stress results of the mixes by declining the viscosity of the mixes, and less rapid setting and hardening behavior (extended open time which means a longer duration during which a substance remains workable or usable) as can be followed from and Figure 4.3.b. The vane shear stress and shear yield stress of the mixes continuously elevated with each elapsed testing time. This can be ascribed to the progressive geopolymerization that leads to the reinforcement of the matrix over time [77,91]. As mentioned before, the results showed that, at the end of 120 minutes, BFS substitution resulted in lower vane shear stress values (compared to 100% CDW-based mixture), in agreement with previous studies [146–149]. On the other hand, contrary to expectations, the results showed that the substitution of BFS did not yield rapid

hardening response (Figure 4.3.b), even though an excess of calcium ions in BFS leads to rapid gel formation in an alkaline environment, as reported in the current literature [145,150–152]. This opposite result might be ascribed to the rapid precipitation of calcium-based gels in the alkaline medium, which covers the precursor materials and slows down the dissolution rate for the initial hours, thus delaying the hardening of the matrix [153]. Additionally, the elevated workability of the BFS-incorporated mixes may also be contributed to the extended open time. When the incorporation rates of BFS within the mixes was raised from 10% to 20%, the vane shear stress and shear yield stress of the mixes enhanced. Possible reasons observing this behavior could be attributed to the elevated surface areas with the rise in BFS amount and thus elevated water need for wetting the surface of the particles [154] and excessive increase in calcium content.

Effects of FA

When the test results of geopolymer pastes are evaluated from Figure 4.3.a, FA-incorporated mixes exhibited relatively greater flowability in comparison to 100% CDW-based pastes. Also, the buildability reduced with the replacement of FA. As the substitution rate increased, the increase in the flowability (increase in flowability index and decrease in buildability) continued to increase. These results were also observable from the shear yield stress and vane shear stress results. The enhancement in workability of the geopolymer paste mixes with the incorporation of FA can be also related to the variation in the physical and chemical features of used precursors, for example, less porosity and comparatively smoother surface and spherical structure of the FA particles. These may result in lower water need to lubricate the particle surface, less water absorption and less particle-to-particle interaction [142,155–159]. When evaluating the test results in terms of the time-dependent variability in the fresh features of the paste mixes, it can be seen that shear yield stress and vane shear stress values of the FA-substituted mixes raised over time. This was an expected result considering the ongoing geopolymerization reactions with time. At the end of 120 minutes, it was noticed that FA-incorporated paste mixes had considerably less vane shear stress and shear yield stress values in comparison to those of 100% CDW-based mix. This finding might be attributed to the fact that greater workability of the FA-incorporated mixes arising from the shape of the FA particles preventing trapping of free water in agglomeration [160]. In literature, there are parallel results which indicate that incorporation of the FA escalates the setting time of the geopolymer mixtures [161]. So, this finding means that the substitution

of FA increased the setting time of the mixtures and positively influenced the long-term workability characteristics of the mixes.

Effects of SF

To clarify the effectiveness of SF on the fresh features of CDW-based geopolymer mixtures, obtained results were examined by comparing the fresh features of the geopolymer mixture composed of 100% CDW-based precursor. Flowability test results illustrated in the Figure 4.3.a showed that 10% substitution of SF yielded an increment in the flowability of CDW-based geopolymer paste. However, 20% substitution of SF caused a decrement in flowability index and showed slightly higher flowability performance than the 100CDW coded mixture. Considering the results, the buildability of mixes decreased with the substitution of SF, irrespective of usage rate. Although 10% SF substitution negatively affected the buildability, increment of SF usage rate showed an increment in buildability performance, yet 100% CDW-based geopolymer mixture showed higher buildability performance compared to the mixtures containing SF. Similar trends were obtained from both ram extruder and vane shear test results. According to results, 10% substitution of SF considerable decreased the shear yield and vane shear stress values, but 20% SF containing mixture showed increment in both shear yield and vane shear stresses. However, 100% CDW-based geopolymer mixtures showed higher shear stress values than the mixtures containing SF. These trends were similar for each testing duration of 0-, 30-, 60-, and 120-min. Open time test results exhibited that the inclusion of SF retarded the geopolymerization as can be followed from Figure 4.3.b. There has not been observed considerable changes in shear stresses of mixtures containing SF until 120 min, although 100% CDW-based geopolymer mixtures showed an increment in shear stresses with elapsed time until 120 min.

Although it was expected SF to decrease flowability and increase shear stresses because of very fine particle size, high surface area and high-water absorption capacity, substitution of 10% SF caused increment in flowability, and therefore decrement in buildability performance and shear stresses. This could be attributed that the fine SF may densify the inner structure and reduce the amount of water filled in the voids and may show lubricating effect by preventing particles to sticking each other due fine spherical shape (as CDW-based precursors have rough surface) [77,162,163]. In addition, lower amount of OH⁻ ion existence on the surface of CDW-based precursor with the presence of SF particles in medium may cause retardation of dissolution and reaction [164]. Therefore, due to lower dissolution and

reaction, weak bonding in medium may yield higher flowability. Besides that, the formation of silica-based complexes, because of the dissolution of SF at the beginning of mixing, may act as a superplasticizer by sterical repulsion and adsorption on the surface of CDW-based precursor, which can be another reason for the increment in the flowability [77,165]. However, substitution of 20% SF caused decrement in flowability and thereby enhancement of buildability and shear stresses compared to 10% SF substitution. So, the above-mentioned positive effects of SF on fluidity were replaced by the negative effects with the increase in the amount of use. This phenomenon can be attributed to increase in the number of fine particles, resulting in a larger surface area, an increased water absorption, and a denser pore structure [66,166]. In addition, as observed in the study of Memon et al. [162], containing higher amount of SF yielded more cohesiveness and stickiness, which can also be reason of decrement in flowability for the 20% substitution.

In addition to the initial fresh properties, open time performance of mixtures was enhanced with the substitution of SF irrespective of usage rate. Such finding could be explained in a way of that the inclusion of SF may lower the OH^- ion presence on the surface of CDW-based precursor due to fineness, which may lead retardation of dissolution and geopolymerization [164]. Besides that, undissolved SF particles may be adsorbed on the surface of CDW-based precursors because of electrostatic interaction, which may also retard the rate of dissolution and geopolymerization [167].

4.1.3.2. Compressive strength

Compressive strength test results of 100% CDW-based and BFS-, FA- and SF-incorporated geopolymer paste mixes are demonstrated in Figure 4.4.

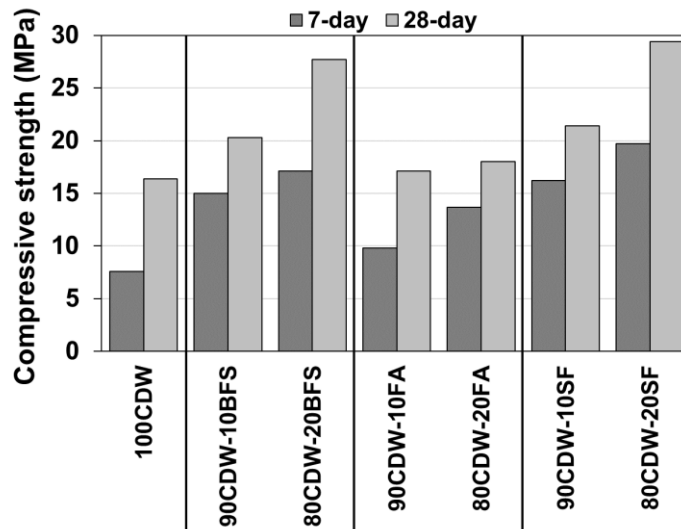


Figure 4.4. Compressive strength test results.

Effect of BFS

Inclusion of BFS yielded improvement in strength performance of the geopolymer pastes. The research findings revealed a consistent upward trend as the proportion of BFS augmented across all tested mixes at both 7- and 28-day curing periods. BFS substitution by 10% provided 23.8% increment in the 28-day average compressive strength of geopolymer mixtures, while the increment level was 69% for 28-day-old 20% BFS-substituted mixes. This notification can be ascribed to the improvement of the geopolymer matrix's microstructure as the reactivity of the precursor content increases with the addition of BFS [51,52,168,169]. Another potential factor could be the rise in the calcium amount, which provides greater amount of Ca^{2+} in the reaction medium. These ions can participate in geopolymerization and partial hydration, yielding to the further precipitation of strength-contributing products [170,171]. By considering this, it is possible to state that BFS incorporation provided the formation of calcium-based gel structures (calcium silicate hydrate (C-S-H) and calcium alumino-silicate hydrate (C-A-S-H)) and also an intertwined gel ([C-(N)-A-S-H]) alongside with the sodium alumino-silicate hydrate (N-A-S-H) gels (main reaction product of CDW-based geopolymers) in favor of obtaining geopolymer paste mixtures with a denser and more compact microstructure [89,172,173].

Effect of FA

According to the obtained results, there was not a noticeable impact of FA inclusion on the 28-day strength of the paste mixes, irrespective of substitution rate. Although there were significant increases in the compressive strength of 7-day-old FA-substituted geopolymer

mixtures, lower levels of strength increases were observed in those of 28-day-old geopolymer mixes. As in the BFS-substituted mixtures, increases in the FA substitution rate was more beneficial for increasing compressive strength results. FA substitution by 10% provided 4.26% increment in the 28-day average compressive strength of geopolymer, while the increment level was 9.76% for 28-day-old 20% BFS-substituted mixtures. Although, increases in compressive strength with the incorporation of FA can be ascribed to greater proportion of amorphous phase present in the FA [174] and the increased presence of Si and Al in the reaction medium [172,175], the main rationale for the limited enhancement in 28-day compressive strength of the geopolymer pastes with the inclusion of FA can be related to the decreased calcium amount in the reaction medium because of the replacement of FA with masonry-originated waste materials (HB, RCB and RT) [161].

Effect of SF

Compressive strength test results exhibited that incorporation of SF into the CDW-based geopolymer system increased compressive strength test results, regardless of SF usage rates. At 28-day, the compressive strength increased by ~30.5% and 79.3% and reached 21.4 and 29.4 MPa for 10% and 20% SF substituted CDW-based geopolymer mixtures, respectively. Increment in compressive strength with the inclusion of SF into alkali activated medium can be attributed to (i) increment in the quantity of reactive Si in reaction medium to form strength giving geopolymer products [77,91,162,176], (ii) high pozzolanic reactivity of SF with the available Ca(OH)_2 , resulting in more C-(A)-S-H production [22,66,164,177,178], (iii) densified micro pores and more compact matrix because of both more geopolymer product formation and the behaving of SF as a micro-aggregate [66,67,162] .

4.1.3.3. Environmental impacts - LCIA results

Seven different geopolymer paste mixtures produced in this study were evaluated by considering five impact assessments and the main components affecting each category including NaOH, Ca(OH)_2 , transportation, electrical energy, water consumption, CDW treatment and the industrial wastes such as BFS, FA, SF were also investigated. The results obtained were exhibited in the Figure 4.5.

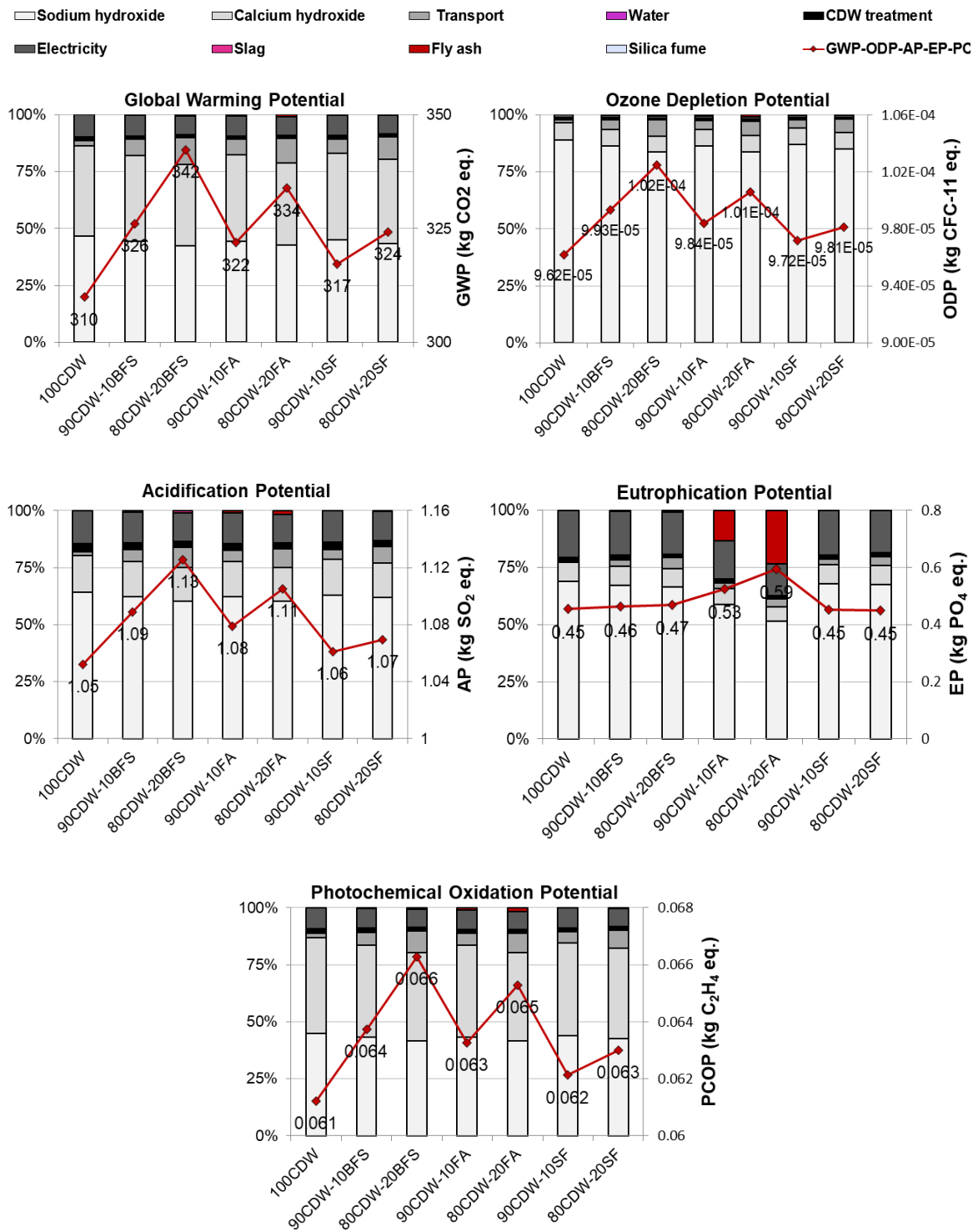


Figure 4.5. Distribution of the input variables for the various impact categories.

In accordance with the global warming impact category, which is related to CO₂ equivalent emission results, it can be stated that the industrial waste incorporation resulted in increment of global warming potential (GWP) values of CDW-based geopolymer mixtures. The geopolymer paste mixture containing 100% CDW had the smallest value of 310 kg CO₂ eq.

It was followed by the 90CDW-10SF coded mixture with the value of 317 kg CO₂ eq. The highest impact was observed in the mixtures containing BFS. When the most important influencing components including NaOH, Ca(OH)₂, and electricity were evaluated, it can be seen that their shares were between of 42-47%, 36-40%, and 8-10%, respectively. The main reason for differences between the GWP of the industrial waste-based precursor included and non-included mixtures was the transportation-related environmental burden. By taking the GWP impact of transportation into account, it can be seen that while 7.3 kg CO₂ eq. recorded for the mixture made of 100 % CDW, this value ranged between 19-40 kg CO₂ eq. levels for mixtures containing industrial wastes. In all geopolymers paste mixtures, the main contributor to the ozone depletion impact category was NaOH with values ranged from 85% to 89%. The primary factor contributing to ozone depletion potential (ODP) of the mixtures can be related to the use of carbon tetrachloride to recover chlorine from gas streams in the chlor-alkali process to produce NaOH [179]. It was followed by Ca(OH)₂ with values of approximately 7% for all mixtures. Electricity values ranged from 0.9-1.0%. As in the GWP, the effect of transportation on ODP values were seen as the determining factor, which resulted in the differences between the mixtures (e.g., 1% for 100CDW, 7% for 80CDW20BFS). Similar trend with GWP were recorded for the industrial waste incorporation on the ODP results. In the acidification category, NaOH has the highest impact with values between 60-64%. Ca(OH)₂ followed with values between 14-15%, while the electrical energy consumed by the devices was also an important factor with values between 12-14%. The eutrophication impact category is related to the potential for excessive nutrient loads, such as nitrogen and phosphorus, to cause environmental problems like harmful algal blooms in bodies of water. In this category, NaOH has the highest impact with values in the range of 51-68%, followed by electricity with values in the range of 14-20%. Although in the other impact categories, the influences of industrial wastes on the paste mixtures were negligible and very close to each other, this difference was greater in the eutrophication category as FA showed high influences on eutrophication potential. The higher eutrophication impact of FA compared to SF and BFS could be due to its higher content of phosphorus and/or nitrogen as it is produced from the combustion of coal. In the photochemical oxidation impact category, NaOH and Ca(OH)₂ were noticed to have almost similar levels of impact, with values in the range of 38-45%. Electricity is the third most impacting category with values ranging between 7-9%, followed by transportation with values between 2-9%.

In general, NaOH, Ca(OH)₂, transportation and electricity are the components that have the greatest effect on the impact categories, while water, CDW treatment and industrial wastes (BFS, FA and SF) are almost negligible. It was observed that alkaline activators, especially NaOH, had the greatest effect, while transportation was the most decisive factor on the results of BFS, FA and SF included mixtures compared to 100CDW coded mixture. Depending on the locations where these industrial wastes were obtained, as the transportation values increased, the impact values increased accordingly. Although the best mixture in terms of environmental performance was 100% CDW-based paste (except eutrophication), industrial waste-incorporated mixtures were very close with it, and if the transportation values can be reduced, even better results may be obtained compared to the mixture containing entirely CDW-based materials. For all impact categories, the mixture made of 100% CDW containing higher levels of CDW-based materials, had higher emissions in terms of electricity values compared to the mixtures containing BFS, SF and FA. This result can be attributed to that more electricity was consumed in the crusher and grinder devices used for precursor preparation with CDW-based materials including HB, RCB and RT. According to the outcomes of the research, 100% CDW-based geopolymer paste demonstrated lower environmental impacts, except for eutrophication. These findings indicated that the geopolymer system containing entirely CDW was more beneficial with regard to environmental burden, but the utilization of FA, BFS and SF followed very closely behind.

Inclusion of industrial waste-based precursors resulted in the enhancement of engineering features of geopolymer mixes. However, the environmental burden of developed geopolymer mixes was increased at the same time with the inclusion of those wastes because of mainly procurement-related (transportation) energy consumption. But in this point, it should be considered that if those mixtures have similar engineering properties compared to 100% CDW-based geopolymer mixture, it is believed to observe similar environmental burden. The utilization of industrial waste-based precursors allows for a reduction in water usage within the matrix. This is because the inclusion of these waste materials has been found to enhance the workability performance. As a result, an enhancement in the mechanical properties of the mixture becomes apparent since the presence of excess free water, which contributes to weakness, can be effectively minimized. Besides that, the compressive strengths of industrial waste included mixtures (especially for BFS and SF included) were already higher compared to the non-included one. Therefore, the use alkaline

activators can be mitigated to adjust the mechanical performance of the mixture similar to the 100 %CDW-based geopolymer. In this way, the environmental burden of industrial waste-based geopolymer can be reduced and be similar to the 100% CDW-based geopolymer mixture. When considering environmental impact per MPa (in terms of compressive strength), the addition of industrial wastes was very beneficial as the strength of the mixtures enhanced remarkably while the environmental impacts depended on mainly transportation and were not significant. However, the wider availability of CDWs compared to industrial wastes bring environmental advantages considering the transportation-related impacts. Overall, results obtained suggest that industrial waste-based precursors can be efficiently utilized in CDW-based geopolymer matrix to adjust engineering properties without endangering the environmental burden of the mixture.

4.2. Low-Alkaline Activated CDW-Based Geopolymer Mortars

Based on the information obtained from the paste phase, studies have been conducted to develop CDW-based mortars that are more environmentally friendly, economical, and high-performance.

4.2.1. Introduction

Upon reviewing the studies conducted on CDW-based geopolymers, it becomes evident that they possess the potential to replace cement-based systems due to their low environmental impact and comparable engineering performance. However, a closer examination of the literature reveals the undeniable need to enhance grinding efficiency and minimize the environmental impact associated with the activators used in CDW-based geopolymers [180]. In particular, optimizing the alkaline content is crucial from economic, environmental, and work safety perspectives. Excessive alkaline content not only increases costs and environmental burdens but also poses potential health risks to workers in the absence of adequate safety measures. Therefore, achieving the optimal balance in alkaline content is essential to ensure cost-effectiveness, minimize environmental impacts, and maintain a safe working environment. Therefore, despite the existence of various studies, there is a clear imperative for a more comprehensive investigation to address these considerations effectively. In this context, the target of this research is to design a CDW-based geopolymer mixture with reduced alkaline content with solely NaOH usage, while increasing the utilization of RCA to enhance both the environmental and economic aspects of the mixture through higher upcycling rates. To achieve this, industrial waste-based precursors including

BFS and SF were used in addition to the low-activity brick waste (BW) and concrete waste (CW) in CDW-based geopolymer mixtures which were activated with different molarities of NaOH (4M-5M-6M-7M and 8M), drawing inspiration from previous studies by the authors [77,91,181]. Additionally, efforts were made to reduce the environmental burden by incorporating higher proportions of RCAs with two different fractions (0-2.00 mm and 0-4.75 mm) into the mixtures, exceeding the proportions used in previous studies [89,91,92,128]. The study utilized a comprehensive testing approach, encompassing a range of assessments such as flow table, setting time, flow curve, three-interval thixotropy, compressive and flexural strength, water absorption, sorptivity, efflorescence, drying shrinkage, wet-dry and freeze-thaw cycling tests. This comprehensive methodology facilitated a thorough exploration of the characteristic features of the geopolymer mixtures, effectively fulfilling the research objectives, developing an eco-friendly construction material that minimizes the use of alkaline activators and maximizes waste materials, contributing significantly to the current body of knowledge by offering comprehensive insights into the high-value valorization of CDW.

4.2.2. Experimental Studies

4.2.2.1. Materials and mixture design

A total of thirteen different CDW-based geopolymer mortar mixes were designed, and the details of each mixture are presented in Table 4.4. The parameters that varied in the mixture designs included the dry blend content, NaOH molarity, RCA dosages and sizes, and water to binder ratio. The first five blends, coded as GxM (where x represents the used molarity), utilized 100% CDW-based precursors with NaOH molarity ranging from 4M to 8M. In the next five blends, coded as GxM/S, 25% of BFS was substituted with brick wastes (BW), while maintaining the same NaOH molarity as the completely CDW-based mixtures. For these mixtures, RCAs with a size fraction of 0-2 mm were used. Additionally, a mixture coded as G5M/S-CA was designed to examine the influence of using RCAs with a size fraction of 0-4.75 mm. Furthermore, to increase the recycling ratio of CDW, the RCAs content was increased in the G5M/S-HA and G5M/S/SF-HA mixtures, as indicated in Table 2. In the G5M/S/SF-HA mixtures, 5% SF was included to enhance the geopolymer matrix by providing additional reactive species in favor of geopolymerization gels. The content of CW was kept constant at 15% of the total weight of precursors, based on the findings of previous studies [91,105,128]. The water-to-binder ratio for the GxM and GxM/S mixtures was determined as 0.38 and remained constant to examine the effects of alkaline molarity.

For the G5M/S-CA, G5M/S-HA, and G5M/S/SF-HA mixtures, the NaOH molarity was determined as 5M, considering the obtained results as well as the environmental and economic burdens associated with the alkaline activator. The water/binder ratio of these mixes was determined based on the obtained constant flow value of 15.5 cm to design workable mixtures.

Table 4.4. Mixtures proportion details.

| No | Mixture Code | Precursors (1000g) | | | | Aggregate RCA | Activator NaOH | Water to binder ratio |
|----|--------------|--------------------|-----|-----|----|------------------|-------------------|--------------------------|
| | | BW | CW | S | SF | | | |
| 1 | G4M | 850 | 150 | 0 | 0 | 500 (0-2 mm) | 4M | 0.38 |
| 2 | G5M | 850 | 150 | 0 | 0 | 500 (0-2 mm) | 5M | 0.38 |
| 3 | G6M | 850 | 150 | 0 | 0 | 500 (0-2 mm) | 6M | 0.38 |
| 4 | G7M | 850 | 150 | 0 | 0 | 500 (0-2 mm) | 7M | 0.38 |
| 5 | G8M | 850 | 150 | 0 | 0 | 500 (0-2 mm) | 8M | 0.38 |
| 6 | G4M/S | 600 | 150 | 250 | 0 | 500 (0-2 mm) | 4M | 0.38 |
| 7 | G5M/S | 600 | 150 | 250 | 0 | 500 (0-2 mm) | 5M | 0.38 |
| 8 | G6M/S | 600 | 150 | 250 | 0 | 500 (0-2 mm) | 6M | 0.38 |
| 9 | G7M/S | 600 | 150 | 250 | 0 | 500 (0-2 mm) | 7M | 0.38 |
| 10 | G8M/S | 600 | 150 | 250 | 0 | 500 (0-2 mm) | 8M | 0.38 |
| 11 | G5M/S-CA | 600 | 150 | 250 | 0 | 500 (0-4.75mm) | 5M | 0.36 |
| 12 | G5M/S-HA | 600 | 150 | 250 | 0 | 1000 (0-2mm) | 5M | 0.42 |
| 13 | G5M/S/SF-HA | 550 | 150 | 250 | 50 | 1000 (0-2mm) | 5M | 0.41 |

G: Geopolymer, M: Molarity, S: blast furnace slag, CA: Coarser Aggregate, SF: Silica Fume, HA: Higher Amount of Aggregate

4.2.2.2. Testing methods

To assess the workability performance of the mixture, flow table test was performed immediately after mixing procedure in accordance with ASTM C1437-15. After agitation process, flow diameters of mixture perpendicular to each other were measured and recorded. In addition to the empirical flow table test, advanced rheometer was employed to investigate

static and dynamic yield stresses, viscosity and thixotropy performance of the mixtures. The flow curve and three interval thixotropy test (3ITT) methods were performed using MCR 102 Anton Paar branded rotational rheometer to evaluate the rheological properties of the samples. For the flow curve test method, mixtures underwent a shearing force with a linearly augmenting shear rate, starting from 0.1 s^{-1} and reaching up to 100 s^{-1} over a duration of 200 seconds. Subsequently, a 30-second resting period was observed, followed by the application of shear load with a linearly reducing shear rate, decreasing from 100 s^{-1} to 0.1 s^{-1} within 200 seconds. For the 3ITT, test protocol was applied in three stages: i) a low shear rate of 0.1 s^{-1} was employed for 60 seconds, ii) Subsequently, the mixture underwent a constant high shear rate of 10 s^{-1} for 10 seconds, iii) Then, the mixture was sheared with a low shear rate of 0.1 s^{-1} for 40 seconds. More details of the given tests can be found in the study of Ilcan et al. [92]. In addition, the Vicat test was performed by following ASTM C807 to find out the initial setting time, which indicates the elapsed time for the mixture to lose its plasticity (workability loss).

The cubic samples ($50 \times 50 \times 50 \text{ mm}$) were employed for compressive strength by following ASTM C109 standard using a hydraulic testing equipment with a loading rate of 0.9 kN/s . Additionally, prismatic samples ($40 \times 40 \times 160 \text{ mm}$) were tested for flexural strength according to the ASTM C78 standard using a loading rate of 0.05 kN/s and a support span of 100 mm to examine the mechanical features of the developed CDW-based geopolymers. Three replicates were tested for each mixture, and the average strength results were noted.

Water absorption and sorptivity (capillary water absorption) tests were performed on cylindrical specimens with a thickness of 50 mm and a diameter of 100 mm in accordance with ASTM C642 and ASTM C1585 standards, respectively. Tests were conducted at the end of 28-day ambient curing. For the sorptivity test results, the following equation was used:

$$I = \frac{m_t}{a * d} \tag{1}$$

where I represents the water absorbed by capillarity, m_t is the change in specimen weight, a is the contact area of the specimen with water, and d is the density of water. Then initial and secondary sorptivity coefficients were calculated.

The efflorescence performance of the mixtures was assessed using 50×50×50 mm cubic specimens aged for 28 days. Cubic samples were placed in a container with water, ensuring that they were in contact with the water up to a depth of 1-1.5 cm, to accelerate the efflorescence phenomenon. The test for efflorescence was then continued up to 90 days. Finally, visual inspection and compressive strength testing were performed to assess the efflorescence performance.

Drying shrinkage test was performed by following ASTM C596 standard. Three prismatic specimens (25×25×285 mm) were manufactured for each mortar mixture, and their size assessments were conducted at the end of 7 days, 28 days, and 120 days in addition to initial measurement. Microstrain was calculated by using taken measurement in the following equation,

$$\text{Microstrain} = \frac{L_x - L_i}{L_i} \times 10^6 \quad (2)$$

In the formula, L_i denotes the initial length, which includes the length of the specimen and the pins positioned to both ends, while L_x represents the length of the specimen at the specific age of testing.

The resistance of the CDW-based mixture against to the freeze-thaw cycling were measured by following the ASTM C666 standard (Procedure A). 28-day aged specimens were subjected to the 300th cycling and after completion of cycling, strength and weight loss of CDW-based geopolymer mixtures were calculated. In addition, wet-dry cycling was implemented to the 28-day mixtures up to 90 days. Specimens were kept in water for 16 hours and in laboratory conditions for 8 hours. Similarly, after completion of wet-dry cycling, strength and weight loss were measured.

To assess the means and standard deviation values, statistical analysis was performed using the results from samples. A comparison between the results obtained was conducted through one-way ANOVA analysis.

4.2.3. Experimental Results and Discussion

4.2.3.1. Fresh Properties of Mixtures

Flow Table

The results of the flow table tests for CDW-based geopolymer mortars are presented in Figure 4.6. For the mixtures using solely CDW-based precursors, the flow diameters were similar for NaOH concentrations ranging from 4M to 6M ($p>0.05$). However, an increase in workability was observed for the mixture activated with 7M NaOH ($p<0.001$). Subsequently, a decrease in workability was observed in the transition from 7M to 8M NaOH concentrations ($p<0.001$). This trend can be explained by the dissolution, mobility and reaction mechanisms of the precursors under different alkaline content and the viscosity of NaOH solutions [77]. Up to a 6M NaOH concentration, it was expected that workability decreased due to the increased viscosity associated with higher NaOH concentrations. However, no significant changes in workability were observed. This could be attributed to the improved dissolution of the precursors with increased alkalinity, which reduces friction between particles because of changes in geometrical of particles and promotes the formation of a less flocculated structure. This effect may suppress the negative impact of increased viscosity [182]. Furthermore, the increased NaOH concentration may lead to a higher zeta potential of the geopolymer, improving dispersion ability by preventing flocculation and resulting in better workability [182,183]. The observed improvement in workability for the 7M NaOH activated mixture can be attributed to a notable enhancement in the dissolution rate of the precursors compared to the 4M, 5M, and 6M NaOH concentrations. The subsequent decrease in workability could be due to limited ion mobility, increased stickiness, and viscosity associated with higher NaOH molarity, which counteract the positive effects of increased NaOH concentration [77,91,92].

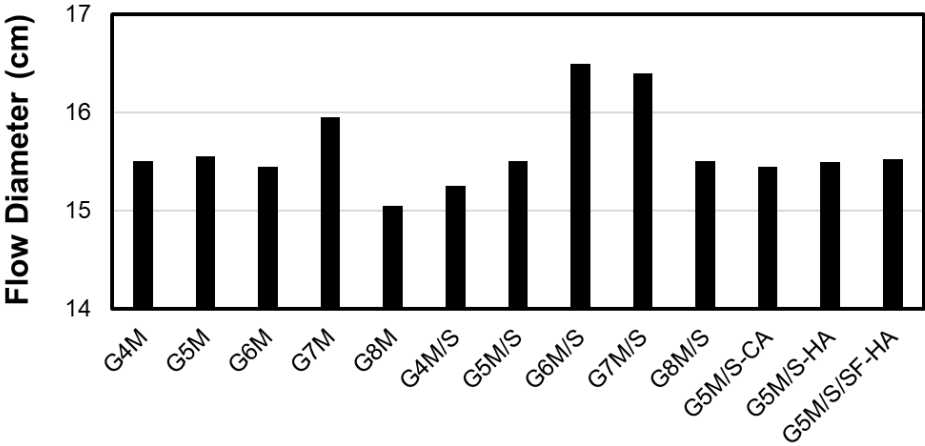


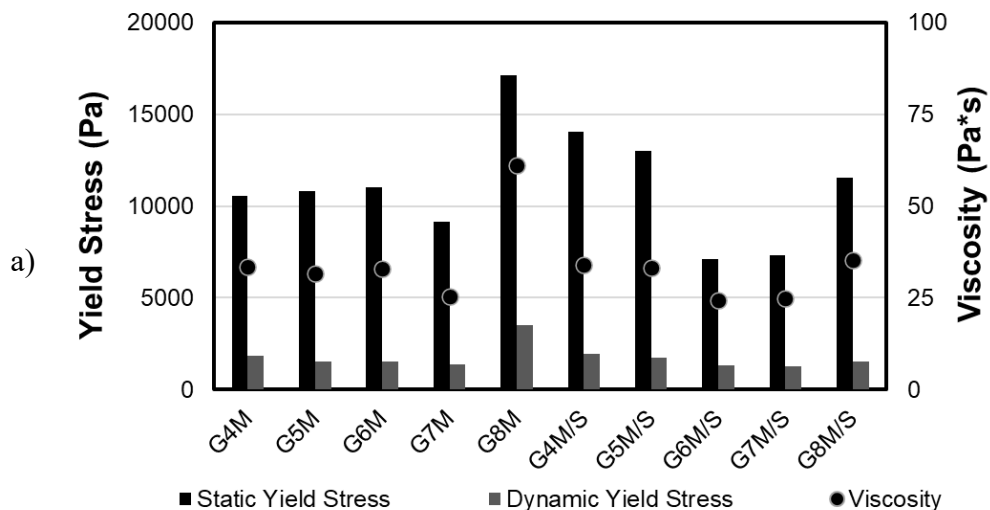
Figure 4.6. Flow table test results.

Similar trends were observed for the mixtures containing slag, with an increase in NaOH molarity leading to a higher flow diameter followed by a decrease. The underlying factors, including dissolution, mobility, reaction mechanisms, and viscosity, associated with varying NaOH concentrations, are also applicable to these results. Notably, the peak in flowability occurred at a lower NaOH molarity of 6M for the mixtures containing BFS compared to the solely CDW-based mixtures. This can be ascribed to the greater reactivity of BFS, requiring lower NaOH concentrations for dissolution [181]. Overall, the inclusion of BFS improved the flowability of the mixtures activated with 6M, 7M, and 8M by providing better dissolution in the matrix, hence the formation of favorable geometrical shapes in terms of internal frictions. Also, reducing the presence of plate-shaped masonry-originated waste powders, thereby reducing the water requirement in the matrix may be the reason for improved flowability in high alkalinity environment [142,145]. Furthermore, slag inclusion may result in increase for zeta potential, providing better particle dispersion and flowability [184]. The absence of positive effects in mixtures activated with 4M and 5M NaOH could be attributed to the presence of more flocculated structures, which hindered the beneficial effects of slag on the mixtures. Moreover, the finer particle size of BFS compared to BW could have led to higher water demand in cases of low alkalinity, as the finer particles may have remained undissolved in the matrix because of low alkalinity [185,186].

To achieve a flow diameter of approximately 15.5 cm, the water-to-binder ratio was adjusted for the G5M/S-CA, G5M/S-HA, and G5M/S/SF-HA mixtures. As can be followed from the Table 4.4, the inclusion of coarse aggregates (0-4.75 mm) in G5M/S-CA yielded a lower water/binder rate in comparison to G5M/S, indicating that coarser RCAs contributed to better workability. This can be ascribed to the greater water absorption capacity of finer RCAs, which required more water to achieve similar workability. Furthermore, increase in the amount of finer RCAs led to a greater water/binder rate due to the increased solid content, internal friction, and water absorption by the RCAs [91,187,188]. Additionally, the results showed that the inclusion of SF improved workability as water/binder ratio decreased from 0.42 to 0.41, which could be attributed to the (i) less internal friction because of rounded shape (ii) provided lubrication effect due to smooths surface texture [162,163], (iii) ability to retard the dissolution and polycondensation processes of CDWs, resulted reducing hydration product formation in the early stages [164]. SF may also act as a superplasticizer due to the presence of silica-based complexes [165].

Rheometer

Figure 4.7 presents the flow curve and 3ITT results, which evaluate the effect of NaOH molarity and BFS inclusion on the rheological features of the CDW-based geopolymer mixture. Tests for the G5M/S-CA, G5M/S-HA, and G5M/S/SF-HA mixtures were not conducted due to limitations of the rheometer used. The obtained test results were consistent with the findings from the flow table test results. The static yield stresses of the geopolymers were higher than the dynamic yield stresses, indicating a decrease in yield stress under agitation load. The turning points in the yield stresses and viscosity results were observed at 7M NaOH for the 100% CDW-based mixture and at 6M NaOH for the mixture with 25% BFS incorporation. The results showed that while an increase in NaOH molarity was beneficial up to a certain point, it turned negative afterward due to increased viscosity of the solution, stickiness, and limited ion mobility [91]. The inclusion of BFS was found to be beneficial in reducing the yield stresses of the mixtures activated with 6M, 7M, and 8M NaOH concentrations, due to enhanced dissolution of the precursors. The results from the 3ITT test highlighted the superior viscosity recovery performance of the CDW-based geopolymer mixtures, implying a higher rate of thixotropic behavior. However, similar to the findings in the study by İlcan et al. [92], no linear correlation between NaOH molarity and thixotropy performance was observed. Additionally, the inclusion of BFS resulted in a slight decrement in thixotropic behavior with some deviations.



b)

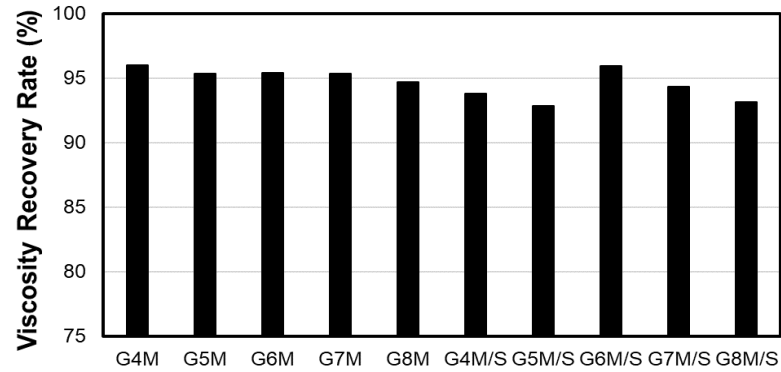


Figure 4.7. Rheometer tests results a) Flow curve, b) 3ITT.

Initial Setting

The initial setting time of CDW-based geopolymer mixtures was presented in Figure 4.8. Mixtures activated with 4M NaOH did not exhibit initial setting within 10 hours and did not harden even after 24 hours, regardless of the precursor content. Therefore, the results for G4M and G4M/S were not included in the graph. This could be ascribed to the lower alkaline content required to dissolve the precursors in early ages, resulting in slower geopolymerization reactions. As shown in the figure, as the alkaline molarity increases, the initial setting time decreases due to faster geopolymerization resulting from increased precursor dissolution and gel condensation. The inclusion of BFS led to a faster initial setting time, irrespective of the NaOH concentration. This can be attributed to the enhanced "Ca" species in the matrix, which can react with the available dissolved species to form strength-giving products such as C-(A)-S-H gels [145,150]. Coarser RCA incorporation yielded shortened initial setting time. Furthermore, inclusion of high amount of finer RCAs also shortened the initial setting time. This could be because of the increased water absorption capacity of RCAs, providing increased local alkalinity, enhanced dissolution, and greater condensation [91]. Additionally, finer RCAs may also act as precursors as they are made of concrete waste, providing extra sources for participation in geopolymerization. The results also indicated that the inclusion of SF resulted in a longer initial setting time. The addition of SF may reduce the presence of OH⁻ ions on the surface of CDW-based precursors, possibly due to its fineness, resulting in the retardation of dissolution and geopolymerization processes [164]. Additionally, undissolved SF particles may be adsorbed onto the surface of CDW-based precursors through electrostatic interaction, further contributing to the retardation of dissolution and geopolymerization rates [167].

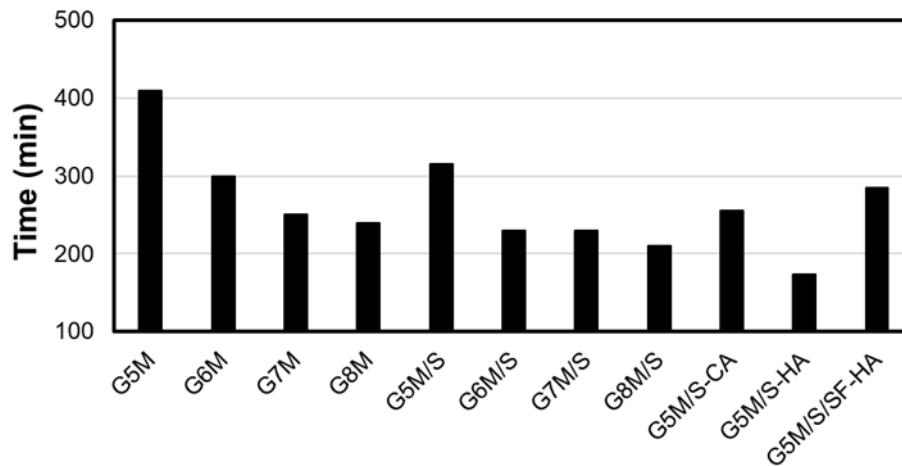


Figure 4.8. Setting time (Vicat test) results.

4.2.3.2. Mechanical Performance

Compressive Strength

The results of the compressive strength tests conducted on CDW-based geopolymer mixtures are demonstrated in Figure 4.9. Compressive strength values increased from 7 days to 28 days, indicating ongoing geopolymerization. The compressive strength of the 100% CDW-based geopolymer mortar and the mixture with 25% BFS substitution gradually increased with increasing NaOH molarity up to 8M, although there were some deviations. This is expected as higher alkalinity enhances the dissolution of precursors and improves geopolymerization [189,190]. Despite the mixture activated with 4M not hardening even after 24 hours, it exhibited a compressive strength value of 7.2 MPa at the end of 28-day ambient curing, indicating that 4M was sufficient for the activation of CDW-based precursors, albeit with a delayed hardening process. The 100% CDW-based geopolymer mixture showed the greatest compressive strength value of 10.5 MPa, while the 25% BFS substituted CDW-based mixture exhibited a compressive strength of 23.4 MPa. The increase in compressive strength with the inclusion of BFS can be ascribed to several factors, including the enhancement of the microstructure of the geopolymer matrix through increased reactivity of the precursor content, the higher calcium content of the mixtures, which provides more available Ca^{2+} ions for geopolymerization, and the self-cementitious properties of BFS[51,52,89,181]. Overall, the inclusion of BFS promotes the formation of calcium-based gel structures, resulting in geopolymer mixtures with a denser and more compact microstructure [172].

The replacement of finer RCAs with coarser RCAs in CDW-based geopolymer mortar yielded a slight decrement in compressive strength ($p < 0.05$). This could be attributed to several factors. Firstly, finer RCAs may provide additional precursors compared to the coarser RCAs as they contain more concrete wastes and unhydrated cement particles, leading to the precipitation of more strength-giving hydration products. Additionally, coarser RCAs may contribute to the creation of extra interfacial transition zone (ITZ) between geopolymer paste and RCA surfaces, which can introduce additional weaknesses in the matrix. Moreover, finer RCAs may promote the development of a more compact and homogeneous structure compared to coarser RCAs. All these positive effects of finer RCAs, therefore, compensate for the negative effects of the higher water-to-binder ratio [191] in matrices containing finer RCAs, resulting higher compressive strength compared to the coarser RCAs. Furthermore, the results indicated that an increase in the amount of finer RCAs led to a reduction in strength. This can be explained by the greater water-to-binder ratio associated with increased RCA content, which results in the formation of more porous structures. Moreover, the binder phase per filler materials decreases with increased RCA content, leading to weaker bonding between particles. Findings also demonstrate that the inclusion of SF significantly enhanced the compressive strength. This can be ascribed to two main factors: (i) the increment in the amount of reactive Si in the reaction environment contributes to the formation of geopolymer products that provide strength [162], (ii) the presence of SF leads to the densification of microstructure and a more compact matrix, as it promotes the formation of additional geopolymer products and behaves as a micro-aggregate [66,67,162]. The G5M/S/SF-HA coded mixtures exhibited the best compressive strength in comparison to other designed mixtures, suggesting that by carefully adjusting the precursor content, it is feasible to achieve enhanced compressive strength while maintaining lower alkalinity and incorporating a higher proportion of RCAs.

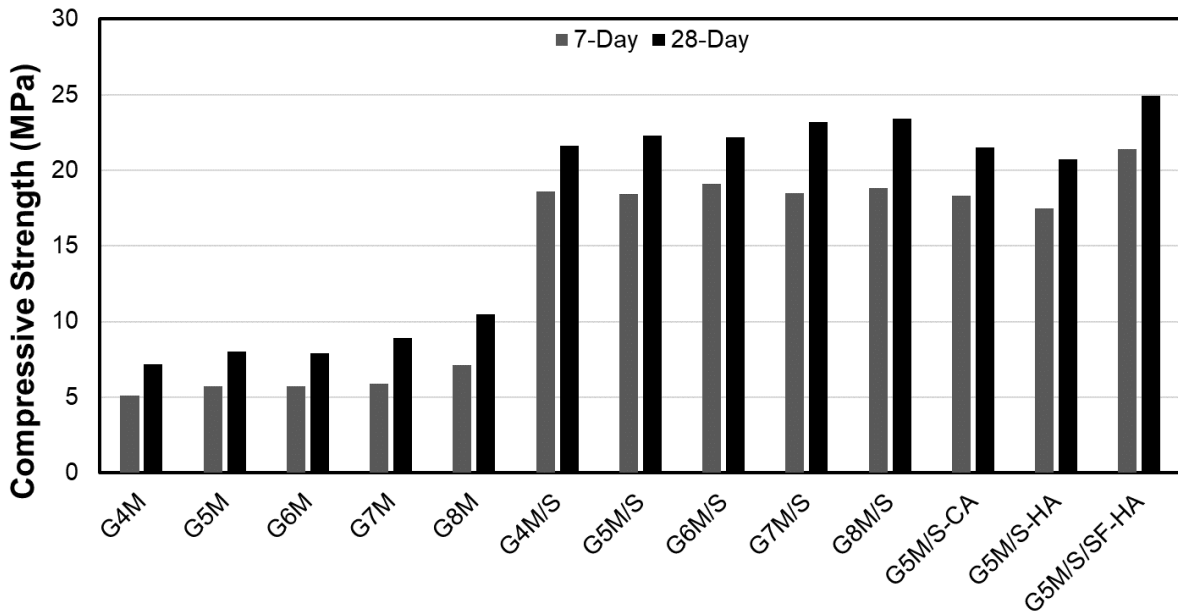


Figure 4.9. Compressive strength of mixtures.

Flexural Strength

The flexural strength test results of geopolymers are given in Figure 4.10. Flexural strength specimens could not be obtained from the mixtures activated with 4M NaOH due to cracking during hardening and breakage while demolding. This can be attributed to the presence of immature geopolymerization products in the matrix, which have lower tensile strength and are unable to withstand drying shrinkage effectively in the early ages (discussed in drying shrinkage section). Results showed that the strength values increased from 7-day to 28-day ambient curing due to ongoing geopolymerization. The 28-day flexural strength test results showed similar trends as in the compressive strength results regarding the NaOH molarity. The 100% CDW-based geopolymer mortars reached a maximum flexural strength of 2.3 MPa, while the 25% BFS incorporated mixtures showed 4.1 MPa at the end of 28-day ambient curing. Coarser RCA resulted a reduction in flexural strength, while an increment in finer RCA content also led to a reduction in strength. The inclusion of BFS was found beneficial for the flexural strength. The possible reasons explaining these results were discussed in more detailed in the context of compressive strength. Similarly, G5M/S/SF-HA exhibited highest flexural strength indicating that precise manipulation of the precursor content enables the attainment of improved flexural strength.

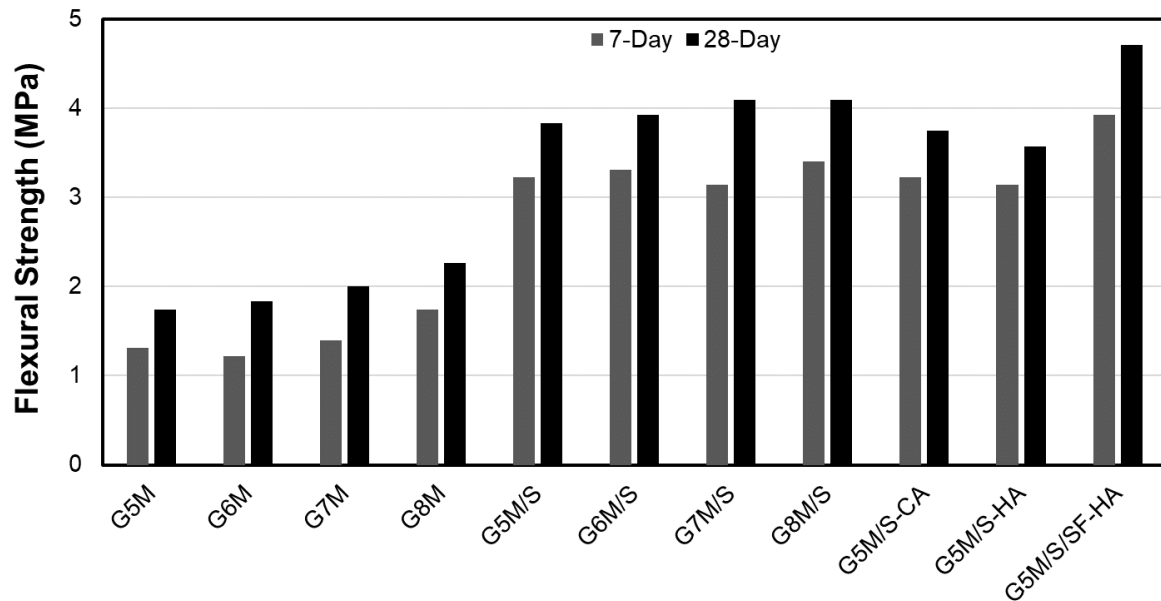


Figure 4.10. Flexural strength test results.

Based on the results of the mechanical tests, a NaOH concentration of 5M was identified as the possible lowest molarity for achieving proper geopolymerization, resulting in both compressive and flexural strength at early ages. In comparison, 100% CDW-based geopolymers exhibited compressive strengths ranging from 7.2 to 10.5 mPa and flexural strengths of 1.7 to 2.3 mPa, whereas the CDW-based geopolymer mortars incorporating industrial waste achieved significantly higher compressive strengths, ranging from 20.7 to 24.9 mPa, and flexural strengths between 3.6 and 4.7 mPa. The results demonstrated that the mechanical features of the geopolymer can be tailored by adjusting the composition of the mixture, as it primarily relies on the dissolution of precursors, the reaction of dissolved species, and the polycondensation of phases. According to the findings, the mechanical performance of geopolymers appears to be more influenced by precursor content when compared to the alkaline content. Once a sufficient level of alkalinity is ensured to facilitate precursor dissolution, the increase in NaOH molarity, while contributing to improved mechanical performance, does not exhibit a significant rate of increment. Similarly, the water/binder ratio and aggregate content have an impact on mechanical performance, as they are linked to the inner structure, porosity, and so on, although their effects are not as pronounced as those of the precursor content.

4.2.3.3. Transport Properties of Geopolymer

Water absorption

Figure 4.11 illustrates the water absorption test results. The findings indicated that increasing the molarity of NaOH led to reduced water absorption in CDW-based geopolymer mixtures, regardless of the precursor content. The higher NaOH concentrations facilitated enhanced dissolution of precursors, resulting in increased geopolymerization products within the matrix. This led to the formation of denser and more homogeneous structures, ultimately leading to lower water absorption [189,190]. This can be ascribed to the reduced presence of void spaces in the matrix due to the higher quantity of geopolymer gels. Additionally, lower alkalinity levels can result in unreacted particles remaining within the matrix, leading to higher water absorption [192]. CDW-based precursors and BFS tend to have higher water demand, further contributing to increased water absorption. Moreover, inadequate geopolymerization due to lower alkalinity can result in the formation of a heterogeneous inner structure, which in turn can cause an increase in water absorption [193].

The test results indicate that the inclusion of BFS has a beneficial effect on reducing water absorption in geopolymer mixes. This can be ascribed to several factors. Firstly, the presence of BFS increases the chemical activity of the precursor content, leading to the formation of more geopolymer products [51,52]. Additionally, BFS contains a higher calcium content, which provides more available Ca^{2+} ions for the formation of Ca-based geopolymer products [181]. Moreover, the self-cementitious properties of BFS contribute to the generation of additional gels within the matrix. Overall, the inclusion of BFS promotes the development of more compact and homogeneous structures, thereby reducing water absorption in CDW-based geopolymer mixtures [64]. Furthermore, the denser structure of C-A-S-H (calcium-aluminosilicate hydrate) compared to other types of geopolymer gels, such as sodium-aluminosilicate gel, can be maintained by incorporating BFS, as it contributes to the formation of more Ca-based geopolymer gels [193,194]. The enhanced pore-filling capacity of C-A-S-H compared to other gels results in a more compact structure within the CDW-based geopolymer matrix [195].

Although the compressive strength test results of mixtures containing BFS were higher than those of 100% CDW-based geopolymer mixes for each NaOH concentration, the water absorption of 100% CDW-based mixes activated with 7M and 8M NaOH solutions was lower than that of BFS-incorporated mixtures activated at lower alkalinity levels. This can be attributed to the slower dissolution of BFS and CDWs in lower alkalinity environments, causing the presence of unreacted particles within the matrix. As these particles have higher

water demand, the water absorption of BFS-incorporated geopolymer mixes activated at lower alkalinity levels may show slightly higher water absorption compared to the high alkalinity activated 100% CDW-based geopolymer mixtures, as the presence of unreacted CDW particles is limited in mixtures activated with high alkaline solutions [186,196].

The inclusion of coarser RCAs led to an increase in water absorption capacity, despite the lower water-to-binder ratio that was expected to reduce the porous structure by reducing the volume of capillary pores. One possible reason for this observation could be the presence of larger open-sized cracks, microcracks, fissures, and old ITZ within the coarser RCAs [194,197,198]. Such defects can be observed in Figure 4.12, which offers a close-up view of the coarse RCAs captured through the digital manual microscope. As the fracture size increases, the detrimental effects of RCAs become more apparent, particularly as larger deficiencies become more prominent. Additionally, finer RCAs may act as precursors, providing more gels to fill the pores. The finer RCAs can also enhance dispersion and refine the pores, thereby contributing to decreased water absorption capacity. The results also revealed that the inclusion of higher amounts of finer RCAs led to a higher water absorption rate. However, increment was not significant, although the amount of finer RCAs were doubled. This can be attributed to the positive effects of the finer RCAs mitigating the negative effects of the higher water demand associated with RCAs. Furthermore, the results demonstrated that mixtures incorporating SF exhibited lower water absorption capacity compared to both G5M/S and G5M/S-HA mixtures. This can be attributed to several factors: (i) SF may refine the pore structure due to its finer particle sizes [66], (ii) SF provides additional silicon ions that promote the formation of extra gels, which occupy the pores [162], and (iii) the inclusion of low amount of SF improves the workability, allowing for a lower water-to-binder ratio and consequently resulting in a less porous structure.

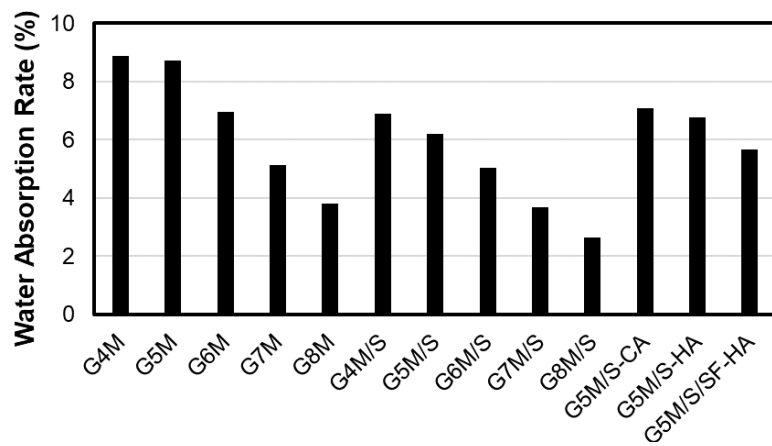


Figure 4.11. Water absorption test results of 28-day aged mixtures.

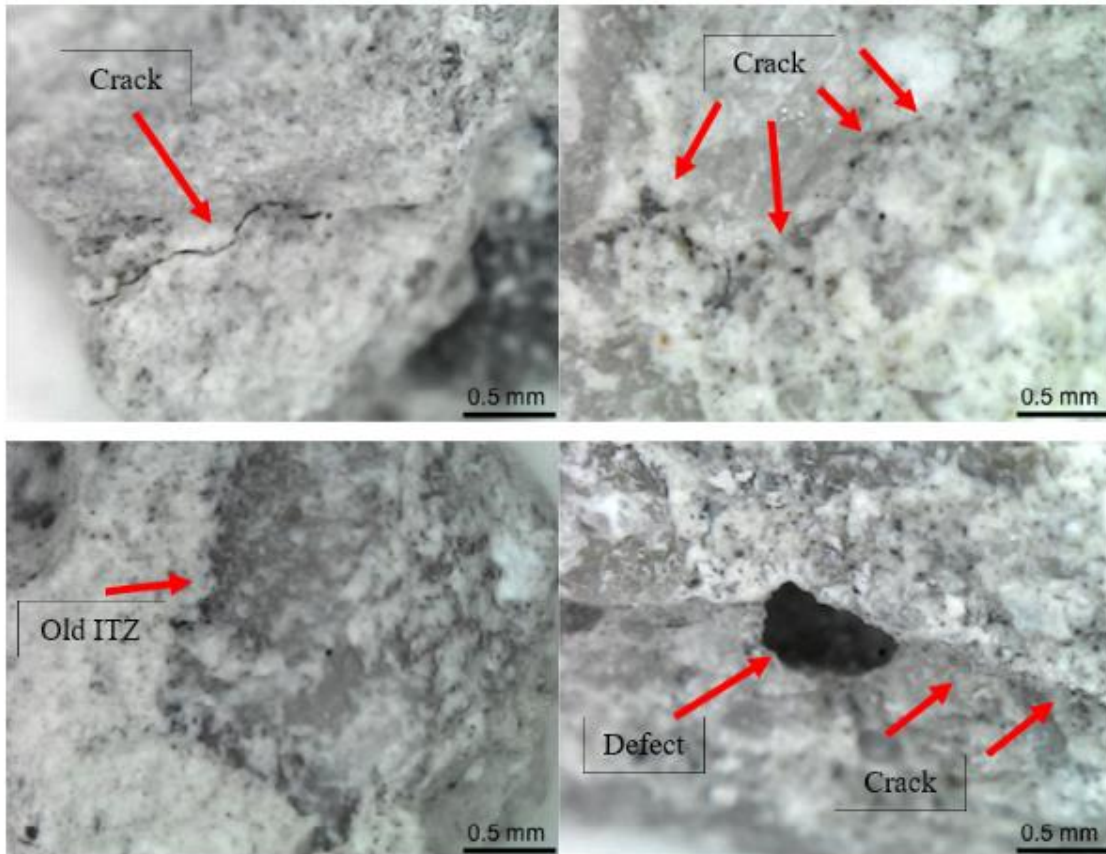


Figure 4.12. Representative close-up views of coarse RCAs.

Water Sorptivity

Figure 4.13 presents the capillary water absorption performance of the CDW-based geopolymer mixes. Similar to the water absorption results, an increase in NaOH molarity led to a lower absorption capacity due to the enhanced geopolymerization process, regardless of the precursor content [189]. The inclusion of BFS in the mixtures resulted in reduced sorptivity performance. This can be ascribed to the additional precipitation of C-A-S-H gels provided by BFS, which are denser and possess pore-filling abilities compared to other geopolymer gels [193–195]. Moreover, literature studies have indicated that, besides the volume of permeable voids, the tortuosity of pore structures also plays a crucial role in the water sorptivity performance of mixtures [194]. The presence of BFS has been found to contribute to an increase in pore network tortuosity, primarily because of the precipitation of C-A-S-H, which has a high tortuosity characteristic [193]. The results also revealed that the addition of coarser RCAs and a higher amount of finer RCAs led to an increase in sorptivity of the mixtures, consistent with the observations made for water absorption. This can be attributed to the same reasons mentioned earlier regarding water absorption, such as

the presence of larger open-sized cracks, fissures, old ITZ, and the potential role of finer RCAs as precursors providing more gels to fill the pores. Additionally, the incorporation of SF resulted in enhanced sorptivity performance. This can be attributed to SF occupying the pores and providing a denser and more compact matrix structure, thus reducing the capillary water absorption capacity.

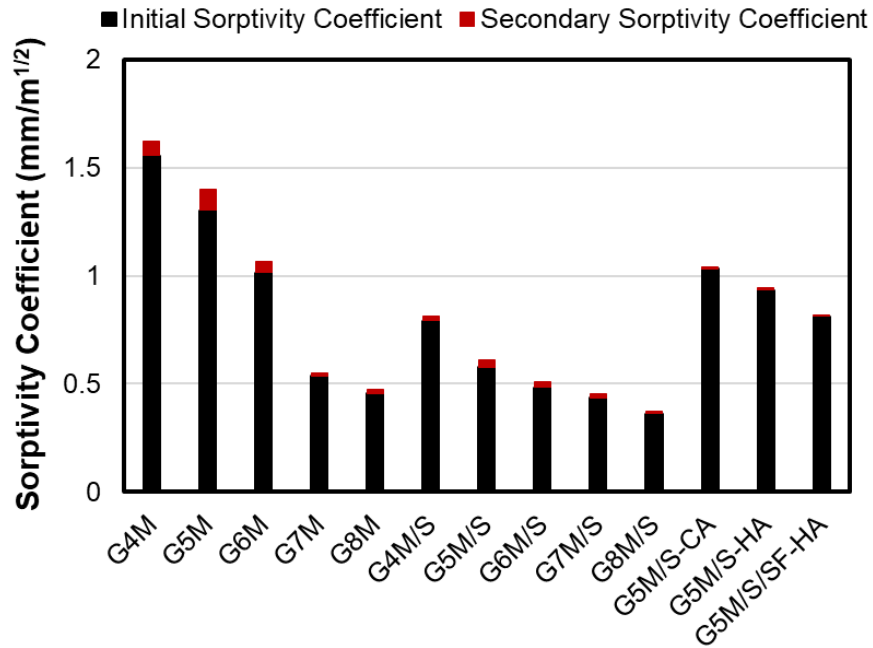


Figure 4.13. Sorptivity coefficient of mixtures.

4.2.3.4. Efflorescence

While an increase in alkaline content promotes a favorable environment for geopolymerization reactions, excessive unreacted alkali ions can migrate through the pores and react with atmospheric CO₂, resulting in the creation of white salt deposits (in a form of natrite, Na₂CO₃·7H₂O) on the surface, known as efflorescence. The detailed reactions involved in the generation of efflorescence products due to the interaction with atmospheric CO₂ are described in the study conducted by Özçelikçi et al. [89]. To examine the influence of alkaline content on the extent of efflorescence and its impact on compressive strength, rigorous conditions were applied to CDW-based geopolymer mortars for the purpose of efflorescence evaluation. Strength loss after the efflorescence were given in Figure 4.14.a. 100% CDW-based geopolymer mixture were significantly affected by efflorescence procedure (p<0.001). The observed reductions in strength can be attributed to the decay of the geopolymer structure, which occurs due to internal pressure generated by the crystallization process and capillary suction [99,199]. After 90 days, significant cracks with

wider openings were observed in the mixtures that underwent efflorescence (Figure 4.14.b). This can be explained by the insufficient strength of the mixtures to withstand the resulting stresses. Furthermore, the presence of water during testing may cause leaching of alkalis and the gels formed within the matrix, resulting in a decrease in strength. The mixtures having compressive strength values greater than 20 MPa at the end of 28-day ambient curing were not affected from the efflorescence by showing strength loss in a range of 3.2-7.1% ($p>0.05$). The decline in strength following efflorescence can be attributed to alkali loss and the internal pressure generated during the crystallization process. The impact of NaOH molarity was not distinctly observed in terms of its effect on strength reduction. However, the inclusion of coarser RCAs and higher amounts of finer RCAs led to slight increased strength loss. This can be attributed to the higher water absorption and sorptivity capacity of these mixtures. Additionally, coarser RCA (2-4.75 mm) is more prone to be carbonated which may results formation of more inner stress while efflorescence testing, causing more strength reduction [200]. On the other hand, the incorporation of SF did not yield significant advantages in terms of reducing the strength reduction.

Figure 4.14.c provides representative images of the reference specimen and the specimen after efflorescence for visual observation. Despite the significant reduction in the effectiveness of efflorescence on compressive strength because of the inclusion of BFS, the specimens still exhibited whitish crystalline deposits on the surface, indicating the formation of efflorescence. Therefore, the results suggest that lower alkalinity (even at 4M) and the inclusion of Ca- and Si-based precursors do not completely solve the issue of efflorescence in geopolymer mixtures. It is still necessary to increase the activity of the precursor content in a medium with lower alkalinity to achieve a more homogeneous and compact internal structure with limited alkali leaching.

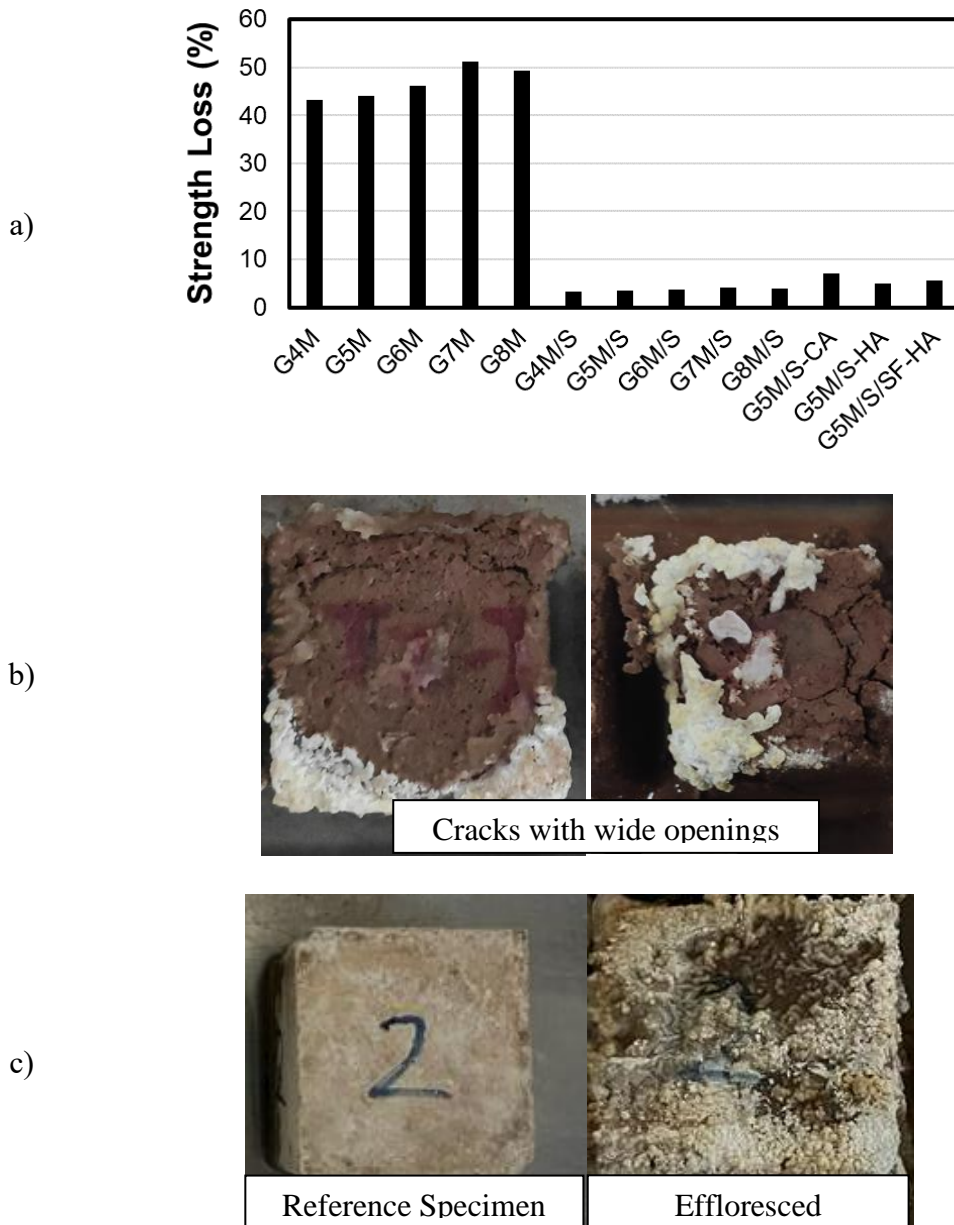


Figure 4.14. Efflorescence test results: a) strength loss comparison among developed mixtures, b) visual representation of cracks observed in the 100% CDW-based mixture, c) representative images showing effloresced specimens with emphasis on the extent of efflorescence and its appearance.

4.2.3.5. Drying Shrinkage

The drying shrinkage test results of CDW-based geopolymer mixes are illustrated in Figure 4.15. The drying shrinkage tests could not be performed on the mixtures coded as G4M, G4M/S, and G5M/S-HA due to crack formation during the early stages of geopolymerization. For the mixtures containing 100% CDW, a notable increase in drying shrinkage was observed from 7 days to 28 days, followed by stabilization at later ages. This

behavior can be attributed to the slow reaction of CDW-based precursors at early ages, where unreacted precursors do not contribute notably to shrinkage [201]. The higher formation of gels at later stages may have led to increased shrinkage in these mixtures. Furthermore, an increase in NaOH molarity resulted in higher shrinkage for these mixtures. This could be due to the enhanced dissolution and increased product formation caused by higher NaOH molarity, leading to an abundance of shrinkage-prone products [202]. Despite the higher amount of gel formation, which has been shown to improve strength in the compressive strength section, the low tensile strength of mixtures containing 100% CDW may have promoted to their inability to resist shrinkage and resulted in the observed shrinkage behavior. However, the opposite trend was observed for mixtures containing slag. As the NaOH molarity increased, these mixtures formed a more compact structure and exhibited higher strength, which, despite the potential increase in shrinkage due to the higher gel formation, resulted in reduced drying shrinkage.

Mixtures with BFS showed higher shrinkage at the end of 7 days but remained stable at later ages. This can be ascribed to the enhanced reactivity of the system with the inclusion of BFS, leading to more gel formation and higher shrinkage potential at early ages since powdery materials do not shrink [201,203]. Additionally, the exothermic hydration reaction of calcium silicate in BFS contributed to the higher drying shrinkage of the geopolymer [203]. Furthermore, the increased formation of gel products may contribute to the rise in chemical shrinkage [203]. However, these effects were overcome with higher NaOH molarity, where the following effects became dominant in reducing shrinkage: i) more BFS particles were activated, resulting in a denser paste with lower porosity [204], ii) improved bulk modulus and resistance of the slurry to drying shrinkage and deformation, or in other words, higher strength development of geopolymers [205–207], and iii) increased precipitation of C-(A)-S-H gel, reducing the free water content and significantly reducing drying shrinkage strain [203].

The results at 28 and 120 days demonstrated that mixtures incorporating BFS exhibited lower drying shrinkage compared to the 100% CDW-based mixtures. This improvement in drying shrinkage performance can be attributed to several factors: i) the self-cementing and hydration capability of BFS, which reduced the total amount of evaporated water in the mixture, ii) the reduced interconnected capillary networks with the presence of BFS [89], iii) the increased reactivity of precursor content with BFS, resulting in a lower amount of

uncombined water and less water loss [208], iv) the promotion of more C-A-S-H gels formation by BFS, leading to a denser matrix with an enhanced bulk modulus and improved resistance to drying shrinkage and deformation [205], and v) the potential contribution of BFS to refining the pore structure, reducing pore size, and increasing capillary tension in the mixture [205].

The results also indicated that the increase in aggregate size led to a higher drying shrinkage ($p < 0.001$), which can be attributed to the formation of a less compact structure compared to the mixture containing 0-2 mm RCAs, and the lower stiffness of the used RCAs in contrast to natural coarse aggregates [207]. The presence of defects, old ITZ, cracks and large proportion of hardened old mortar in coarser RCAs, along with the relatively low hardness, might not effectively restrain the development of drying shrinkage [209].

As the RCA content increased for the G5M/S/SF-HA, the water/binder ratio also augmented to maintain flowability, which in turn led to a higher potential for drying shrinkage. However, the mixture with SF substitution exhibited a drying shrinkage performance similar to that of the G5M/S-coded mixture, indicating that SF mitigates drying shrinkage. This can be attributed to several reasons. Firstly, the increased SF content facilitated the conversion of free water into bound water, reducing the available free water for shrinkage [203]. Secondly, SF's pore-filling effect and its ability to create a denser structure contributed to the mitigation of drying shrinkage [203,204].

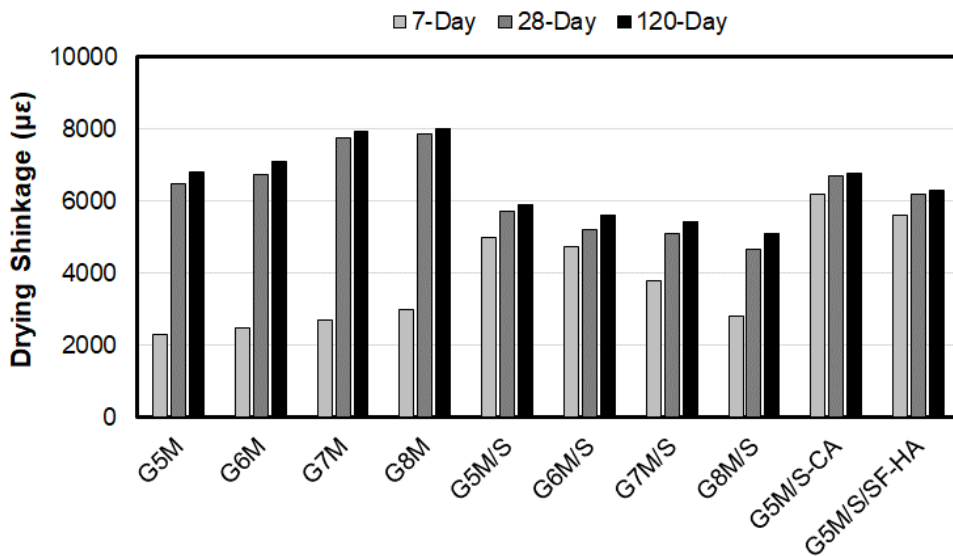


Figure 4.15. Drying shrinkage test results.

4.2.3.6. Wet-Dry Cycling Resistance

The wet-dry cycling performance of the CDW-based geopolymer mixes was evaluated and presented in Figure 4.16 to assess their resistance against the effects of weather conditions. Since, repetitive crystallization through repeated cycles of hydration and evaporation can cause expansion and subsequent contraction, resulting in the formation of internal stresses within the pores [68,210]. These stresses may, in turn, reduce the overall strength of the matrix. The results indicated that as the NaOH molarity increased for the 100% CDW-based geopolymer mixture, there was a slight decrease in strength loss, while weight loss remained similar. In general, the detrimental effects on strength reduction caused by wet-dry cycles can be attributed to the expansion-contraction, which may lead to the development of internal crystallization stresses in the pores, and the leaching of soluble compounds [211]. In this context, it can be inferred that higher strength, along with increased NaOH molarity, may provide better resistance to internal stresses, thereby mitigating the negative effects of wet-dry cycling. Additionally, the lower permeability observed with increased NaOH molarity may limit the leaching of soluble compounds, contributing to better overall resistance against the damaging effects of wet-dry cycles [212].

The results further demonstrated that the inclusion of BFS significantly enhanced the wet-dry resistance of CDW-based geopolymer mixtures, attributed to its positive impact on both higher strength and lower permeability. Additionally, the inclusion of BFS may lead to the maturity of polymerization, ensuring volumetric stability. In the absence of this maturity, the geopolymer structure is susceptible to complete destruction when exposed to water [211]. Interestingly, the effect of NaOH molarity was not apparent for mixtures containing S. Moreover, the inclusion of coarser RCA and a higher amount of finer RCA did not cause substantial changes in the resistance performance against wet-dry cycling. Additionally, the inclusion of SF showed a slight improvement, as it resulted in lower strength loss during the wet-dry cycling tests. This can be attributed to the lower permeability and improved strength capacity provided by the inclusion of SF.

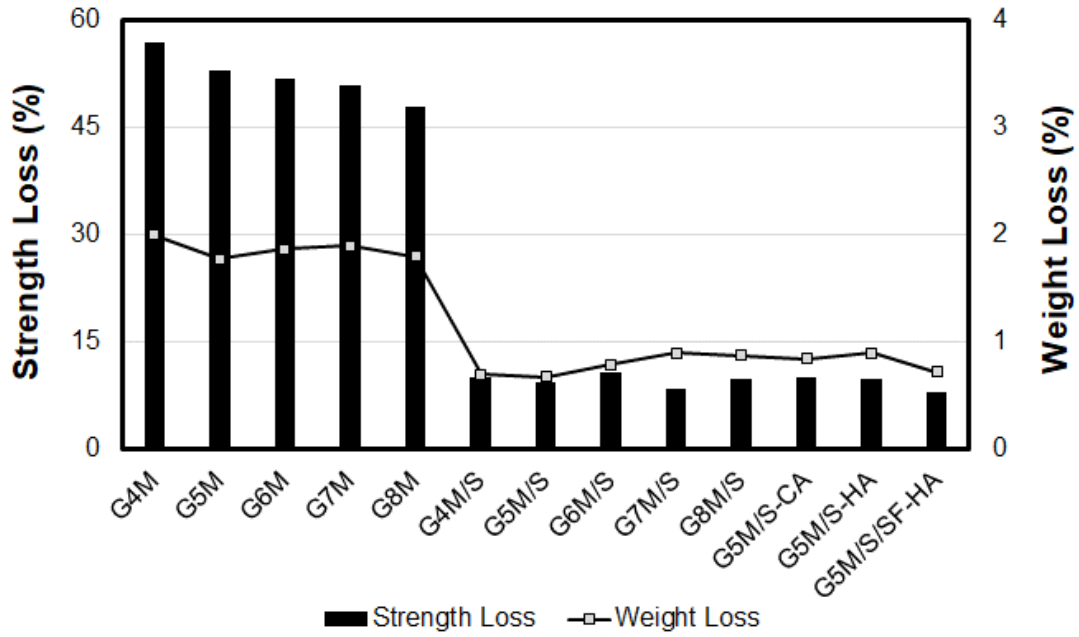
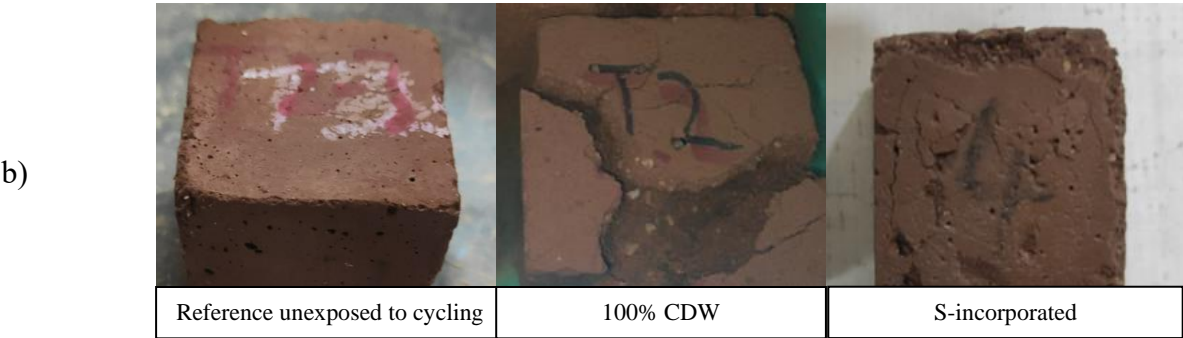
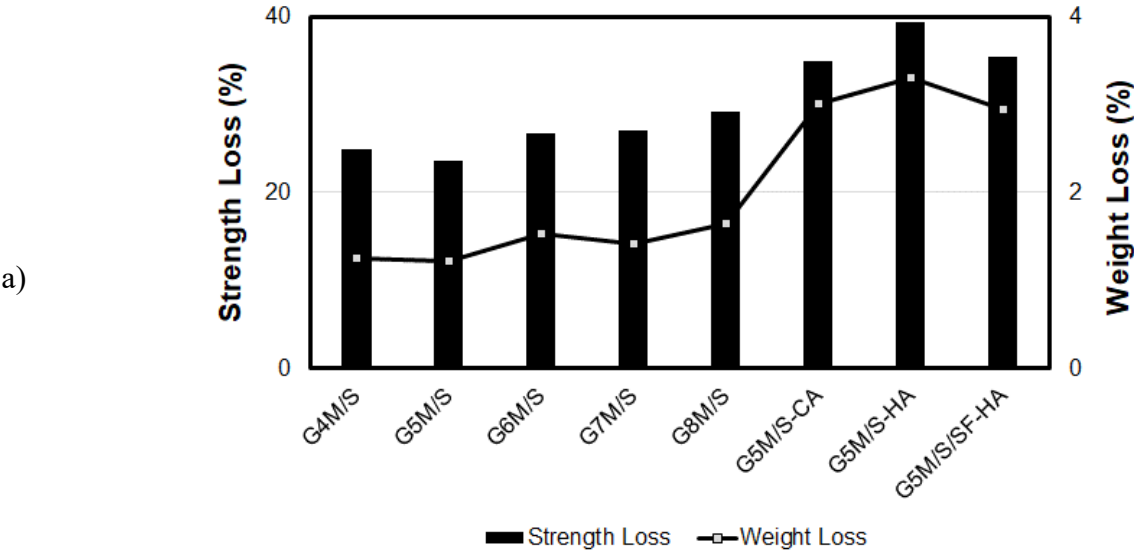


Figure 4.16. Wet-Dry resistance of CDW-based geopolymer mixture.

4.2.3.7. Freeze-Thaw Cycling Resistance

The freeze-thaw cycling performance of the CDW-based geopolymer mixes was evaluated, and the strength and weight loss after cycling were presented in Figure 4.17 to examine their resistance against harsh conditions. Specimens prepared with 100% CDW-based geopolymer mixtures were completely decomposed after 300 cycles, irrespective of the NaOH molarity, and therefore not shown in Figure 4.17. This significant degradation could be attributed to the lower strength capacity of these mixtures, which could not withstand the internal stress generated during the cycling process. In contrast, the inclusion of BFS resulted in better performance against freeze-thaw cycling. This improvement can be attributed to the enhanced mechanical performance of mixtures with BFS inclusion. During cycling, the internal stress in pores gradually increases, and as the stresses formed exceed the strength of the surface, cracks begin to form. With continued cycling, the cracks propagate, eventually leading to the destruction of the samples. Therefore, the enhanced resistance observed in mixtures containing BFS is likely due to its positive effect on the mechanical features of the geopolymer. By enhancing the mechanical performance, BFS incorporation helps the geopolymer matrix withstand the stresses induced during freeze-thaw cycling, leading to reduced crack formation and better resistance to deterioration. However, the effectiveness of NaOH concentration on the performance of the mixture against cycling was not clear. While the strength loss was in a range of 23.6 -29.1%, the weight loss was in a range of 1.22-1.65%. On one hand, mixtures activated with lower molarities may exhibit a more porous

structure due to a lower amount of gels, which can provide an advantage against freeze-thaw cycles. On the other hand, mixtures activated with higher alkalinity may form more and stronger gels, which can help counteract the internal stresses caused by cycling. Therefore, the impact of freeze-thaw cycling on the geopolymer's performance may not significantly vary with different NaOH molarities. The inclusion of coarser RCA resulted in a slight increment in both strength loss and weight loss. This can be attributed to the reduction in mechanical performance associated with the coarser RCA. Additionally, the inclusion of a higher amount of fine RCA led to an increment in both strength and weight loss. This could be due to the combination of lower mechanical performance and increased water absorption, which may accelerate the deterioration process, leading to higher formation of internal stress within the matrix [213]. The incorporation of SF provided better resistance to freeze-thaw cycling due to the higher mechanical performance and lower permeability it offered. These characteristics helped the geopolymer matrix withstand the stresses and strains induced by the cycling, resulting in improved durability and performance during harsh freeze-thaw conditions.



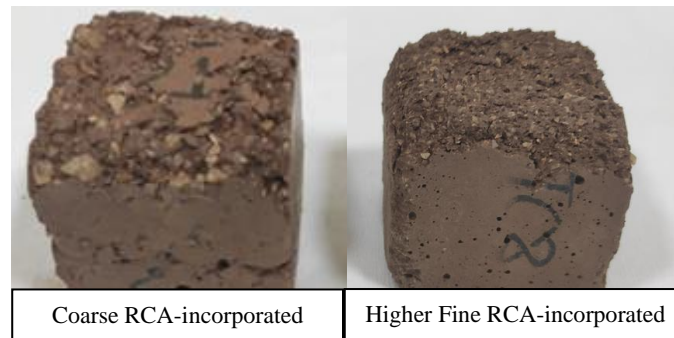


Figure 4.17. Freeze-Thaw resistance of CDW-based geopolymer mixture, a) test results, b) representative images of tested specimen.

The results obtained from the comprehensive test program highlight the potential to customize the properties of CDW-based geopolymers by adjusting key factors, including NaOH molarity, precursor and aggregate content, and the water-to-binder ratio. These parameters were identified as significantly influential in the geopolymerization process and the internal structure of the matrix. Improved geopolymerization led to enhanced mechanical performance and superior transport properties, as the geopolymerization products effectively occupied the available pores in the matrix, reducing water ingress rates. Similarly, enhanced geopolymerization resulted in improved durability performance for CDW-based geopolymer mortars by reducing permeability and reinforcing matrix strength, which contributes to the prevention of potential durability issues. In this context, the obtained findings were found to corroborate and reinforce each other. While designing mixtures with low alkali content, it is evident that the strength criterion plays a significant role. However, it is also apparent from the test results obtained under harsh conditions that strength alone can be misleading, and attention must also be paid to transport properties.

While the literature commonly suggests optimal geopolymer performance within the NaOH molarity range of 8 to 12 M, this study's findings propose that 5 M NaOH is sufficient to activate CDW-based precursors [16,91]. Moreover, through the substitution of mainstream precursors, the study illustrates the achievement of low-alkaline activated geopolymer with satisfactory engineering properties, even when incorporating a high volume of RCAs.

4.3. 3D-Printable CDW-based Geopolymer: Investigating the Effects of Additives on Engineering Properties

Studies have been conducted on improving the engineering properties of 3D-printable CDW-based geopolymer through the usage of various additives in mixture design.

4.3.1. Introduction

While there are already several studies aiming to address the limitations of CDW-based geopolymer mixtures, it is obvious that different additives should be tested to mitigate the efflorescence problem encountered in geopolymer and to mitigate/prevent possible cracks that may occur because of the higher shrinkage performance of CDW-based geopolymer. In this regard, different additives were used in this study to modify the feature of CDW-based geopolymer mixtures. In this regard, calcite, polypropylene fiber, nano SiO_2 , Al_2O_3 , and TiO_2 , carbon nano tubes (CNTs), graphene nanoplatelet (GNP), methyl cellulose (MC), Na_2SiO_3 , calcium oxide (CaO), calcium aluminate cement (CAC), and $\text{Ca}(\text{OH})_2$ were included to 3D-printable CDW-based geopolymer mixtures, considering the methodologies used in previous literature to address efflorescence issues and potential cracks formation [214]. Overall, it was aimed to examine the alterations of the fresh, mechanical, and transport features of 3D-printable CDW-based geopolymer mixtures by incorporating additives, while exploring the connections between these properties, efflorescence performance, and the potential occurrence of cracks in printed products. In pursuit of this objective, a series of tests and analyses were performed, including flow table tests, compressive strength tests, flexural strength tests, water absorption tests, sorptivity tests, efflorescence tests, and visual observations of 3D-printed filaments to assess crack formation.

Although the impact of different additives on the engineering properties of mainstream precursor-based geopolymer systems has been explored in the literature, this is limited for CDW-based geopolymers. Given that, in the scope of this study, the effects of different additives found to be successful in literature reviews have been thoroughly investigated on CDW-based geopolymer systems. In this regard, the study has deviated from the existing literature and this research is expected to enrich the existing literature by shedding light on how various additives impact the engineering properties of 3D-printable CDW-based geopolymer mixtures. Furthermore, the study's outcomes are anticipated to make a substantial contribution to the current state-of-the-art, as they provide comprehensive

insights and knowledge regarding the mitigation of shrinkage-related crack formation in 3D-printed filaments and efflorescence issues in CDW-based geopolymer mixtures.

4.3.2. Experimental Studies

4.3.2.1. Materials and mixture design

In order to enhance the transport, mechanical, and durability properties of the CDW-based geopolymer mixture, several types of additives were incorporated into the base mixture design considering the available literature findings [214]. In this context, nano SiO₂, Al₂O₃, and TiO₂ were introduced into the mixture to improve the pore structure and facilitate seeding/nucleation effects, promoting the precipitation of additional geopolymeric gels [215–217]. Likewise, carbon nanotubes (CNTs) and graphene nanoplatelets (GNP) were integrated into the matrix to regulate the permeability of the geopolymer matrix [218,219]. Furthermore, methyl cellulose derivatives (MC) and CaO were added to the matrix to alter the inner structure, reducing the occurrence of efflorescence and crack formation. Additionally, calcium aluminate cement (CAC) was introduced to provide early strength to the CDW-based geopolymer and absorb excess water in the reaction medium, thus helping to minimize crack formation [220]. For enhancing the tensile capacity of the CDW-based geopolymer and reduce the likelihood of crack formation, polypropylene (PP) fibers were also incorporated. To enhance mechanical performance and reduce the permeability, Ca[OH]₂ and Na₂SiO₃ were also employed as activators in addition to the NaOH [77,91]. Calcite was also incorporated as an aggregate/filler material in the CDW-based geopolymer mixture in favor of more dense structure [221]. Specific details regarding the additives employed have been tabulated in Table 4.5.

Table 4.5. Detailed information regarding the additives.

| Additives | Abbreviation | Informative Details |
|--------------------------|-------------------------------------|---|
| Nano Silicon | Nano SiO ₂ | <20nm, purity of 99.5%, powder form |
| Nano Aluminum | Nano Al ₂ O ₃ | <28nm, purity of 22%, liquid form |
| Nano Titanium | Nano TiO ₂ | 10-20nm, purity of 99%, powder form |
| Carbon Nanotubes | CNTs | 8-18nm, purity of 96%, powder form |
| Graphene Nanoplatelets | GNP | <5nm, purity of 99%, powder form |
| Methyl Cellulose | MC | <100µm, purity of 92%, powder form |
| Calcium Oxide | CaO | <150µm, powder form |
| Calcium Aluminate Cement | CAC | <40µm, powder form |
| Polypropylene fiber | PP fiber | 6mm±0.25mm, 250 aspect ratio, 100% polypropylene, 0.88-0.94g/cm ³ |
| Calcium Hydroxide | Ca(OH) ₂ | Purity of 87%, powder form |
| Sodium Silicate | Na ₂ SiO ₃ | Water content of 45%, silicate modulus of 1.9, density of 1.39 gr/cm ³ |
| Calcite | - | <200µm, powder form |

In this study, range of additives were introduced into the 3D-printable CDW-based geopolymer mixture to address efflorescence and crack formation while simultaneously examining their potential impacts on both engineering features. Total of fourteen different 3D-printable CDW-based geopolymer mortar mixtures were formulated, and the details of each mixture are given in Table 4.6. The water-to-binder (W/B) ratio for the mixtures was established using a flow value of 16.0-16.5 cm, drawing from previous experience with the pumpability of CDW-based mixtures, to design 3D-printable formulations. The mixtures were coded as 'CDW-x,' with 'x' denoting the sequence of the mixture code. Details of the mixtures are as follows: (i) CDW-1, reference mixture without additive, (ii) CDW-2, 50% calcite replacement with RCA, (iii) CDW-3, addition of fiber at 0.5% of the total weight of the precursor materials, (iv) CDW-4, addition of nano SiO₂ at 2.5% of the total weight of the precursor materials, (v) CDW-5, addition of nano Al₂O₃ at 2.5% of the total weight of the precursor materials, (vi) CDW-6, addition of nano TiO₂ at 2.5% of the total weight of the precursor materials, (vii) CDW-7, addition of CNTs at 0.5% of the total weight of the precursor materials, (viii) CDW-8, addition of GNP at 0.5% of the total weight of the precursor materials, (ix) CDW-9, addition of MC at 0.5% of the total weight of the precursor materials, (x) CDW-10, addition of Na₂SiO₃ at 0.5 of the weight of the NaOH, (Na₂SiO₃/NaOH=0.5), (xi) CDW-11, replacing 100% of CW with CaO (equivalent to 15% of the total precursor content), (xii) CDW-12, replacing 100% of CW with CAC (equivalent to 15% of the total precursor content), (xiii) replacing 100% of CW with BW, (xiv) replacing 100% of CW with BW and addition of Ca(OH)₂ at 5% precursor weight.

Table 4.6. Mixtures proportion details for 1000g.

| Mixture Code | BW (g) | CW (g) | BFS (g) | SF (g) | RCA (g) | W/B (ratio) | Additive |
|--------------|--------|--------|---------|--------|---------|-------------|---|
| CDW-1 | 550 | 150 | 250 | 50 | 1000 | 0.44 | N/A |
| CDW-2 | 550 | 150 | 250 | 50 | 500 | 0.475 | 500g -Calcite |
| CDW-3 | 550 | 150 | 250 | 50 | 1000 | 0.455 | 5g-PP Fiber |
| CDW-4 | 550 | 150 | 250 | 50 | 1000 | 0.460 | 25g-Nano SiO ₂ |
| CDW-5 | 550 | 150 | 250 | 50 | 1000 | 0.450 | 25g-Nano Al ₂ O ₃ |
| CDW-6 | 550 | 150 | 250 | 50 | 1000 | 0.450 | 25g-Nano TiO ₂ |
| CDW-7 | 550 | 150 | 250 | 50 | 1000 | 0.520 | 5g-CNTs |
| CDW-8 | 550 | 150 | 250 | 50 | 1000 | 0.460 | 5g-GNP |
| CDW-9 | 550 | 150 | 250 | 50 | 1000 | 0.475 | 5g-MC |
| CDW-10 | 550 | 150 | 250 | 50 | 1000 | 0.440 | 44g-Na ₂ SiO ₃ |
| CDW-11 | 550 | 0 | 250 | 50 | 1000 | 0.445 | 150g-CaO |
| CDW-12 | 550 | 0 | 250 | 50 | 1000 | 0.470 | 150g-CAC |
| CDW-13 | 700 | 0 | 250 | 50 | 1000 | 0.445 | N/A |
| CDW-14 | 700 | 0 | 250 | 50 | 1000 | 0.470 | 50g-Ca(OH) ₂ |

4.3.2.3. Testing methods

To adjust the water-to-binder ratio, flow table test was performed by following the ASTM C1437-15 standard. After following the standard agitation process, the flow diameters of the mixture, measured at perpendicular to each other, were documented. Based on the results, the water/binder ratio was adjusted.

Cubic samples measuring 50×50×50 mm were subjected to compressive strength by following the ASTM C109 standard, utilizing hydraulic testing equipment operating at a loading rate of 0.9 kN/s to evaluate the mechanical performance of the developed CDW-based geopolymers. Furthermore, prismatic specimens measuring 40×40×160 mm were subjected to flexural strength testing in accordance with ASTM C78 standards, employing a loading rate of 0.05 kN/s. Three replicates were tested for each mixture, and the average strength results were recorded.

To assess transport properties, water absorption and sorptivity (capillary water absorption) tests were performed on cylindrical specimens measuring 50 mm in thickness and 100 mm in diameter, following the guidelines outlined in ASTM C642 and ASTM C1585 standards, respectively. The tests were carried out upon the completion of 28-day ambient curing. For the sorptivity test results, the following equation was applied:

$$I = \frac{m_t}{a * d} \quad (1)$$

In this equation, “I” signifies the water absorbed by capillarity, “m_t” denotes the change in specimen weight, “a” represents the contact area of the specimen with water, and “d” stands for the density of water. Subsequently, both initial and secondary sorptivity coefficients were computed.

To evaluate the efflorescence performance of the mixtures, cylindrical specimens measuring 100 mm in diameter and 200 mm in thickness, aged for 28 days, were employed. Cylindrical samples were submerged in a container of water, ensuring that they were immersed to a depth of 1-1.5 cm, in order to expedite the efflorescence process. The efflorescence test was extended for a total duration of 28 days, after which visual inspections were conducted to evaluate the extent of efflorescence.

To examine the crack characteristics of 3D-printed filaments, two-layered specimens, measuring 800 mm in length, 40 mm in width, and 32 mm in height, were fabricated using a laboratory-scale 3D printer (100×100×40 cm [width × length × height] effective printing area). The details regarding the 3D-printer used were illustrated in Figure 4.18. The 3D printer system is composed of several key components, including a CNC router, a nozzle, a printing platform, transmission pipe, a mortar pump, and a control panel with a computer. While printing, the printer speed was set to 50mm/s, and a 19mm circular nozzle was employed. The specimens were exposed to ambient conditions for a period of 90 days, and visual inspections were carried out at intervals of 1, 7, 28, 56, and 90 days.

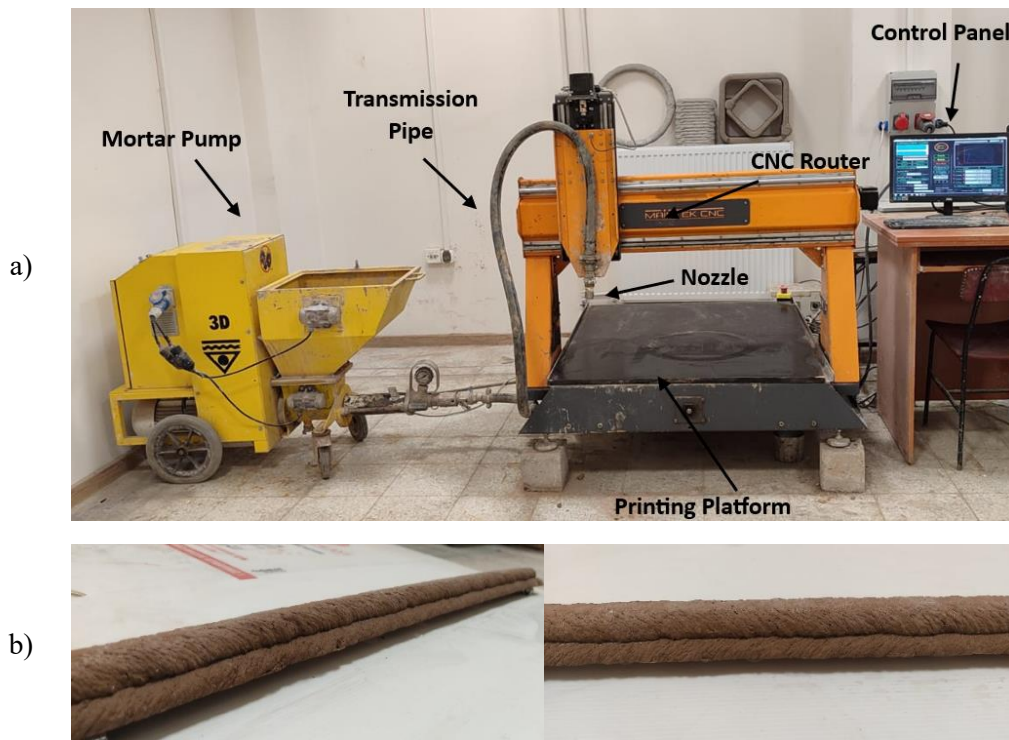


Figure 4.18. Details of a) the gantry type 3D printer and b) two-layered specimen.

4.3.3. Experimental Results and Discussion

4.3.3.1. Fresh Property

To achieve a flow table spread value of 16.0-16.5 cm, efforts were made to adjust the water-to-binder ratios for the respective mixtures as represented in the Table 4.6. Considering variations in water content resulting from the addition of additives, general approaches regarding to influence of additives on the fresh features of CDW-based geopolymer mixture were developed. In this context, it was observed that calcite led to a significant reduction in flowability, although calcite was expected to increase flowability because of smooth surface

texture [222]. Observed decrement can be attributed to the increased fineness of the solid content ($<200\ \mu\text{m}$) which requires more water to maintain flowability [223]. Inclusion of PP fiber also resulted in a slight decrement in flowability. The inclusion of fibers may hinder the flow of cement paste, leading to a decrease in flowability [224]. While nano SiO_2 produced a more viscous geopolymer mixture, nano Al_2O_3 and TiO_2 resulted in a slight increase in fluidity. The incorporation of CNTs, MC, and GNP was observed to have a negative effect on the workability of CDW-based geopolymer, even when added in small amounts. Particularly, CNTs incorporated geopolymer mixture required high amount of water (water/binder rate of 0.52) to maintain flow value of 16.0-16.5 cm. Although the inclusion of Na_2SiO_3 was anticipated to improve workability due to its plasticizing and deflocculating properties, no significant improvement in flowability was observed [91]. According to the results, the substitution of CaO did not have a considerable impact on workability. Results also showed that the inclusion of CAC yielded in a significant reduction in fluidity. This can be ascribed to the fine particle size and rapid reaction kinetics of CAC. The results also demonstrated that replacing CW with BW led to an increase in water requirements, indicating reduced workability. This observation suggests that BW has an adverse effect on the workability of CDW-based geopolymer mixtures compared to CW. This could be attributed to diversity in fineness, water absorption capacity and reaction kinetics of precursors. The inclusion of $\text{Ca}(\text{OH})_2$ led to a decrease in flowability, which can be attributed to several factors [77,91,92]: (i) enhanced rigidity with increased geopolymeric gels, (ii) provision of additional nucleation sites for the further development of geopolymerization products, (iii) An increase in surface cohesiveness, (iv) enhanced electrostatic attraction and charge neutralization (charge-balancing).

4.3.3.2. Mechanical Performance

Compressive Strength

The average compressive strength test results of 28-day aged CDW-based geopolymer mixes were illustrated in Figure 4.19. According to the results, the incorporation of calcite was observed to lead to a slight decrease in compressive strength. This can be attributed to the elevated water content within the matrix, which in turn increases the pore volume and defects of the geopolymer [225,226]. Additionally, under higher alkaline conditions, there is limited dissolution of calcite, which does not contribute to the expected additional gel formation [227]. Furthermore, since RCA contain a powdered form of calcium-rich material (e.g., unreacted cement particles, hydrated gels etc.), which can facilitate extra gel formation

through geopolymerization, replacing RCA may lead to a reduction in the available “Ca” sources in the medium, resulting reduction in formation of strength giving geopolymerization products. Similarly, the introduction of PP fibers led to a decrease, which can be attributed to the elevated water content within the matrix. However, the addition of nano SiO₂ and Al₂O₃ resulted in a slight improvement in the compressive strength performance of CDW-based geopolymer mortars, despite the elevated water-to-binder ratio. This can be ascribed to the increment of the available “Si” and “Al” sources in the medium, which, in turn, promotes the formation of strength-contributing products such as CASH, NASH, and CSH [217]. Furthermore, the seeding or nucleation effect of nanoparticles can encourage the formation of additional gels within the medium [228]. The incorporation of nanoparticles may also contribute to the improvement of the matrix by promoting more compact structures [228,229]. The inclusion of nano TiO₂ also contributed to an increase in compressive strength, potentially attributable to its seeding or nucleation effect and the development of a more compact inner structure [216]. The incorporation of CNTs led to a decrement in compressive strength, which might be ascribed to the excessive presence of residual free water in the matrix, as indicated by a high water/binder ratio of 0.520. The inclusion of GNP also yield to a slight decrement in compressive strength, which can be attributed to the increased presence of free water within the matrix, despite the material's potential for seeding or nucleation effects. The inclusion of MC to the CDW-based geopolymer mixture resulted in a notable decrease in compressive strength, which could potentially be attributed to alterations in the microstructure of the geopolymer composite [230]. The incorporation of Na₂SiO₃ at a Na₂SiO₃/NaOH ratio of 0.5 led to an improvement in compressive strength, although the increase was not as substantial as anticipated. The increase can be attributed to several following factors: (i) enhancing the SiO₂/Al₂O₃ ratio promotes the creation of shorter and stronger Si-O-Si bonds instead of Si-O-Al and Al-O-Al bonds, consequently strengthening the geopolymer bonds and establishing a denser and more rigid microstructure marked by the prevalence of Si-rich aluminosilicate gel [46,231], (ii) an elevated precipitation of geopolymerization products facilitated by the presence of highly soluble reactive silica [232,233]. Substituting CW with CaO resulted in a significant decrease in compressive strength test results, contrary to the expected enhancement, as CaO was anticipated to react with available silica and form C-A-S-H hydrates [234]. The absence of the anticipated positive effects can potentially be attributed to the formation of a greater quantity of C-S-H gels characterized by a lower degree of polymerization, rather than the desired N-A-S-H and C,N-A-S-H gels [234–236]. Furthermore, an excessive presence of

CaO might disrupt the ideal gel binder structure and hinder the timely precipitation of extra products, as it has the potential to locally disturb the Si/Al ratio, leading to a less uniform microstructure [87]. Moreover, any surplus CaO may not participate in the geopolymerization process and could remain unreacted (agglomeration) [237], thereby contributing to the creation of defects within the microstructure [91]. The results also demonstrated a substantial improvement in the compressive strength performance of CDW-based geopolymer mortars when CW was replaced with CAC, as it introduced extra “Al” and “Ca” sources into the geopolymeric system, promoting the precipitation of aluminosilicate gel. As documented by Vafaei and Allahverdi, CAC is identified as a favorable source of reactive aluminum in the alkali-activation process, where both the “Al” and “Ca” present in CAC can be incorporated into the precipitation of C-A-S-H and N-A-S-H gels [238,239]. Furthermore, the findings of test results indicated that substituting CW with BW led to an increase in compressive strength. This improvement can be attributed to two factors: the finer particle size of BW, which enhances reactivity and solubility in the reaction medium, and the chemical composition of BW, which contains a higher concentration of Si and Al species. Considering these results, it can be concluded that, for designing CDW-based geopolymer mixtures with a focus on strength development, BW is the preferred choice. Despite the anticipated strength improvement in CDW-based geopolymer [77,91,128] due to the promotion of CASH and CSH gels with the additional “Ca” sources from Ca(OH)_2 , the addition of Ca(OH)_2 resulted in a reduction in the compressive strength of the geopolymer mortar [240]. This can be attributed to the fact that the available slag in precursor content might already supply a sufficient amount of “Ca” in the reaction environment, and any excess “Ca” from Ca(OH)_2 beyond that may not effectively participate in the reaction and remains unreacted. In a comprehensive overview, the CDW-based geopolymer mixtures, cured under ambient conditions, demonstrated a compressive strength value spanning from 16.5 MPa to 29.8 MPa. Notably, the CDW-12 coded mixture (CAC incorporated) exhibited the highest compressive strength, while the CDW-11 coded mixture (CaO incorporated) recorded the lowest.

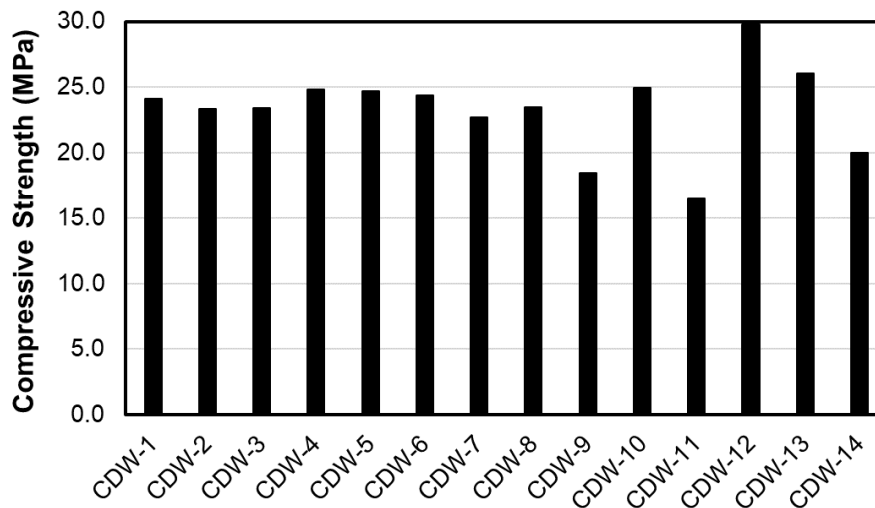


Figure 4.19. Compressive strength test results.

Flexural Strength

The average flexural strength test results of 28-day aged CDW-based geopolymer mortars were presented in Figure 4.20. The findings showed parallel trends to those observed in the compressive strength results, as flexural strength is also influenced by the overall matrix strength. The explanations provided for changes in compressive strength due to the inclusion or substitution of additives are equally applicable to flexural strength. Nonetheless, it was observed that the inclusion of PP fibers yielded a slight improvement in the flexural strength of CDW-based geopolymer. This increment can be because of the role of fibers as inter-discontinuity sutures and ability of inhibiting the crack growth by bridging the cracks [224]. Since the fibers used had a length of 6mm and were incorporated at a low rate of 0.5% of the binder, the increase in flexural strength was relatively modest. In summary, it was observed that the water/binder rate is the primary factor influencing the strength of the matrix. Moreover, increasing the “Si” and “Al” content leads to improved mechanical performance in low-alkaline activated geopolymer mixtures derived from CDW. It's worth noting that enhancing the “Ca” sources in the medium, to a certain extent, did not contribute to the development of strength in this context. Furthermore, the inclusion of fibers demonstrated promising outcomes, particularly in terms of enhancing flexural strength.

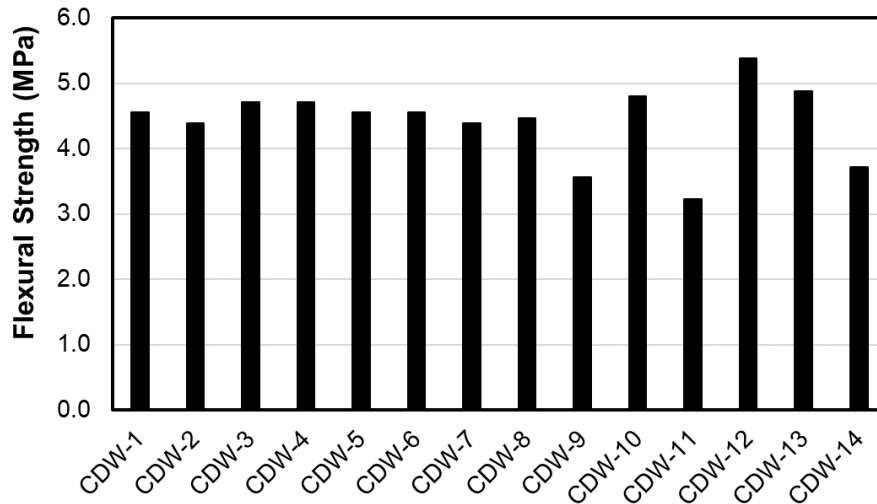


Figure 4.20. Flexural strength test results.

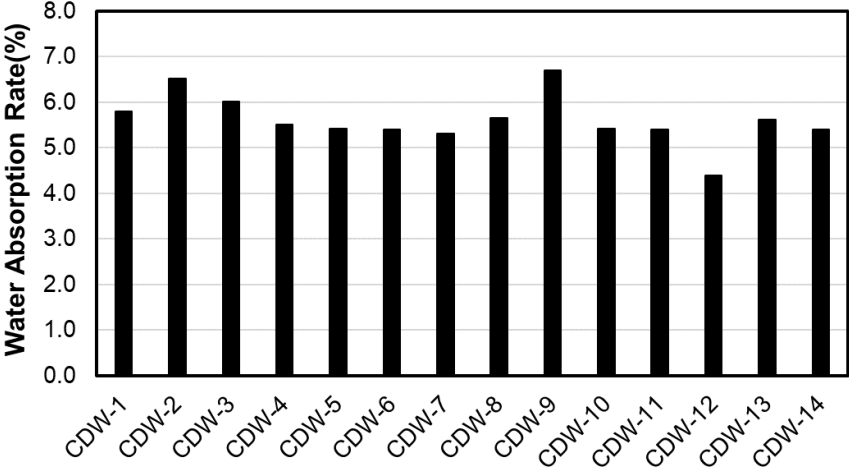
4.3.3.3. Transport Properties

Sorptivity test is employed to assess a geopolymers' capacity for transporting and absorbing water through capillary suction, while water absorption is used to measure amount of water that geopolymer can absorb. A decrease in sorptivity and water absorption serves as a robust indicator of enhanced durability. Water absorption and sorptivity test results were illustrated in the Figure 4.21 to examine the effectiveness of additives on the transport features of geopolymer mixes. While water absorption rate of mixtures varied in a range of 4.4% to 6.7%, sorptivity coefficient values were in between 0.50 to 0.94 mm/m^{1/2}. In comparison to the cement-based mixture, the water absorption values are consistent, ensuring adequate durability as they fall within the range of 4% to 6% [241,242]. Nevertheless, the sorptivity values of CDW-based geopolymer are slightly elevated compared to those of the cement-based mixture, falling within the range of 0.18 mm/m^{1/2} to 0.42 mm/m^{1/2} [243]. Also, according to the Cement Concrete & Aggregates Australia, the recommended sorptivity index is below 0.21 mm/m^{1/2} (for class C exposure) [244,245].

According to findings, incorporation of calcite yielded rise in water absorption rate and sorptivity index of mixture. Although it was expected improve inner structure with calcite behaving as a filler material [246], increased water-to-binder ratio to maintain 3D-printability may cause formation of voids in matrix. Besides dilution effect caused by replacement of RCA which contains powder form of CW may also cause more porous inner structure. Inclusion of fiber also resulted slight increase in transport properties possibly because of increased water content which may cause existence of voids after hardening process. Nano sized additives including SiO₂, Al₂O₃, TiO₂, CNTs and GNP resulted

enhancement in absorption rate and sorptivity, possibly because of pore refinement ability of nano particles. Inclusion of MC cause significant increase in water absorption rate and sorptivity coefficient which could be attributed to alterations in the microstructure of the geopolymer composite as observed in the compressive strength results. Na_2SiO_3 inclusion was found favorable for the transport properties of CDW-based geopolymer as it provides extra gel formation yielding more dense and compact structures in matrix. CaO was also found favorable for the transport properties although it causes notable strength reduction in geopolymer mortars. This could be attributed to its ability to fill voids because of its fineness which may provide more dense structure and lower the permeability of matrix [237]. Additionally, during curing period, CaO may consume the free water in pores and fill the voids with the $\text{Ca}(\text{OH})_2$ precipitation [247]. Results also indicate that CAC incorporation significantly lower the water absorption rate and sorptivity coefficient of CDW-based geopolymer as it provides more compact inner structure with fewer unreacted particles because of enhanced geopolymerization [248]. Results also showed that substitution of CW with BW resulted in slight better transport properties which could be attributed to increased geopolymerization with more BW, providing more dense structure. Similarly with the CaO , although the inclusion of $\text{Ca}(\text{OH})_2$ resulted decrement in strength performance of CDW-based geopolymer, it provided lower permeability, attributed to ability to fill void by its fineness.

a)



b)

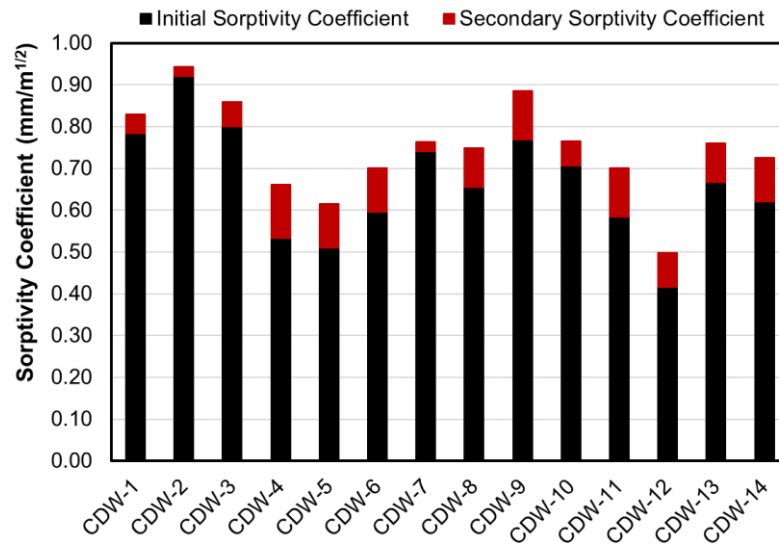


Figure 4.21. Test results of a) water absorption and b) sorptivity for CDW-based geopolymer mortars.

4.3.3.4. Efflorescence

Digital images of specimen after efflorescence test were illustrated in Figure 4.22 to examine the effect of additives on efflorescence characteristics. It was noticed that for the mixtures coded as CDW-4, -5, -8, -9, -10, -11, -12, -14, the efflorescence products formed on the surface of the specimen after exposure to the accelerated testing were mitigated compared to the CDW-1 coded reference mixture. Considering these observations with the strength and transport property examination, it could be concluded that by improving the strength and lowering permeability of the mixture it is possible to mitigate the efflorescence properties of geopolymer mixture but there are also results that contradict this finding (e.g., CDW-9 and -13 coded mixtures). By consuming excessive alkali ions in the matrix and preventing the way they leak, efflorescence mitigation can be succeeded. Because, excess ions tend to leak through the pores and interact with the CO₂ in the atmosphere, resulting in efflorescence on the surface of the specimen [89]. Results showed that nano SiO₂ and Al₂O₃ had a positive effect on efflorescence as they have an ability to bind extra alkali ions available in matrix and provide more dense structure to prevent leakage of free alkalis to outer surface of the specimen. More compact structure provided by extra geopolymerization also provided mitigation for efflorescence for the mixtures containing Na₂SiO₃ and CAC [248,249]. Furthermore, GNP, CaO, Ca(OH)₂ inclusion resulted mitigation in efflorescence by providing less permeability for the specimen. Although inclusion of MC cause strength reduction and more permeable structure, it reduces slightly the occurrence of efflorescence

products on the surface of specimen. Similarly, while substitution of CW with BW provided better strength and permeability performance, mitigation in efflorescence were not recorded. Therefore, in addition to strength and permeability properties, characteristics properties (e.g., chemical content) of ingredients are also effective on the efflorescence performance of CDW-based geopolymer.

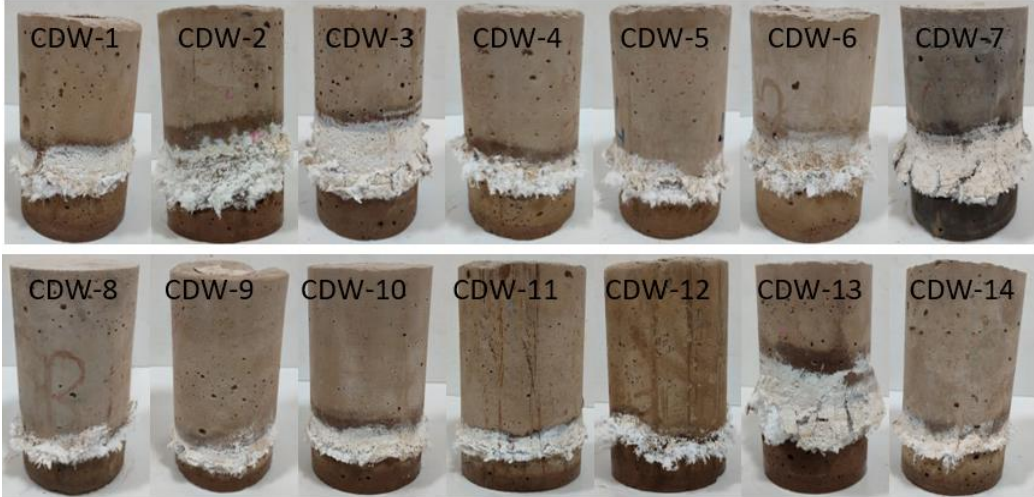


Figure 4.22. Visual inspection of efflorescence in CDW-based geopolymer mortars.

4.3.3.5. Characterization and Analysis of Cracks in 3D-Printed Filaments

Crack formation in the 3D-printed filament is more prone to occur due to the absence of a mold, which typically serves to mitigate water loss during the hardening phase. Hence, conducting a thorough investigation into the cracks in 3D-printed filaments is imperative for accurately assessing the performance of 3D-printed structures. The examination results pertaining to crack formation, observed through visual inspection of 3D-printed filaments over a span of 90 days, have been systematically organized in Table 4.7. As can be followed from the table, at end of 1-day of curing, there are no observation of cracks on the 3D-printed filaments. The absence of cracks indicates the absence of plastic shrinkage in CDW-based geopolymer mortars. This finding showed that tensile strain capacity of the CDW-based geopolymer mortar exceeds the tensile strain developed during plastic phase. Nevertheless, as the curing duration progressed, microcracks began to emerge on the surfaces of certain filaments. The formed microcracks on CDW-based printed filaments had an identical shape of thin and in parallel to each other as can be seen from the Figure 4.23. The results revealed that inclusion of calcite, nano SiO₂, Al₂O₃, and TiO₂, did not yield favorable outcomes in terms of crack mitigation. Similarly, substituting CW with BW also did not show favorable effects on the mitigation of cracks. While the inclusion of fibers was anticipated to mitigate

crack formation, at the end of the 28-day ambient curing, a few microcracks were observed on the surface of the filament. However, as evident in Fig. 4.23.b and 4.23.c, the crack opening sizes were reduced, and in certain sections, the fibers effectively hindered the propagation of cracks. So, it can be interpreted that the fibers can be an alternative solution to mitigate crack formation yet the amount of it should be arranged properly. Additionally, the reason behind the observing cracks while with the fibers can be ascribed to augmented water/binder ratio, since the extra water to maintain flowability tend to escape from the pores causing formation of cracks. Results also indicated that the mixtures incorporating CNTs, and GNP exhibited an earlier onset of crack formation compared to the other geopolymer formulations. For the CNTs, the extremely increased water-to-binder ratio may cause more severe shrinkage in early age as free water (non-bound) tend to evaporate [250]. For the GNP the detecting early microcracks can be attributed to both increased amount of water in matrix and the acceleration of reaction mechanism with the GNP, resulting chemical shrinkage, as observed in the study of Zhu et al. [251]. The results demonstrated that the inclusion of MC, Na_2SiO_3 , CaO, CAC, and $\text{Ca}(\text{OH})_2$ was beneficial for mitigating crack formation in CDW-based geopolymer mortar. At the end of the 90-day ambient curing period, no cracks were observed on the 3D-printed filaments for CDW-9, -10, -11, -12, and -14 coded mixtures. Provided relatively accelerated reaction with Na_2SiO_3 inclusion with enhanced geopolymerization can result reduction in shrinkage, yielding no crack observation in 3D-printed filament [91,235,252]. Enhancement of mechanical performance of CDW-based geopolymer with the inclusion of CAC can provided adequate strength that can withstand formed strain stress during shrinking, mitigating formation of cracks on the surface of 3D-printed filaments. For the MC, the water retention ability may provide favorable condition for mitigation of shrinkage, resulting in prevention of crack formation [253]. For the CaO incorporated mixture, available CaO in matrix may consume the free water in pores and fill the voids with the $\text{Ca}(\text{OH})_2$ precipitation and corresponding volume expansion (approximately 2.5 times) may compensate the shrinkage nature of geopolymerization, resulting no crack formation [254]. The reduction in mesopores and the rise in the Ca/Si ratio of C-S-H gels, attributed to the incorporation of $\text{Ca}(\text{OH})_2$, contribute to the mitigation of shrinkage, as elucidated in the study by Zhu et al. [255]. Furthermore, the residual $\text{Ca}(\text{OH})_2$ plays a role as an obstruction during the deformation process.

Table 4.7. Visual inspection of cracks in 3D-printed filaments.

| Mixture Code | Crack Characterization | | | | |
|--------------|------------------------|----------------------|----------------------|----------------------|----------------------|
| | 1-Day | 7-Day | 28-Day | 56-Day | 90-Day |
| CDW-1 | No Crack | No Crack | Few Microcracks | Multiple Microcracks | Multiple Microcracks |
| CDW-2 | No Crack | No Crack | Few Microcracks | Multiple Microcracks | Multiple Microcracks |
| CDW-3 | No Crack | No Crack | Few Microcracks | Multiple Microcracks | Multiple Microcracks |
| CDW-4 | No Crack | No Crack | Few Microcracks | Multiple Microcracks | Multiple Microcracks |
| CDW-5 | No Crack | No Crack | Few Microcracks | Multiple Microcracks | Multiple Microcracks |
| CDW-6 | No Crack | No Crack | Multiple Microcracks | Multiple Microcracks | Multiple Microcracks |
| CDW-7 | No Crack | Multiple Microcracks | Multiple Microcracks | Multiple Microcracks | Multiple Microcracks |
| CDW-8 | No Crack | Multiple Microcracks | Multiple Microcracks | Multiple Microcracks | Multiple Microcracks |
| CDW-9 | No Crack | No Crack | No Crack | No Crack | No Crack |
| CDW-10 | No Crack | No Crack | No Crack | No Crack | No Crack |
| CDW-11 | No Crack | No Crack | No Crack | No Crack | No Crack |
| CDW-12 | No Crack | No Crack | No Crack | No Crack | No Crack |
| CDW-13 | No Crack | No Crack | Few Microcracks | Multiple Microcracks | Multiple Microcracks |
| CDW-14 | No Crack | No Crack | No Crack | No Crack | No Crack |

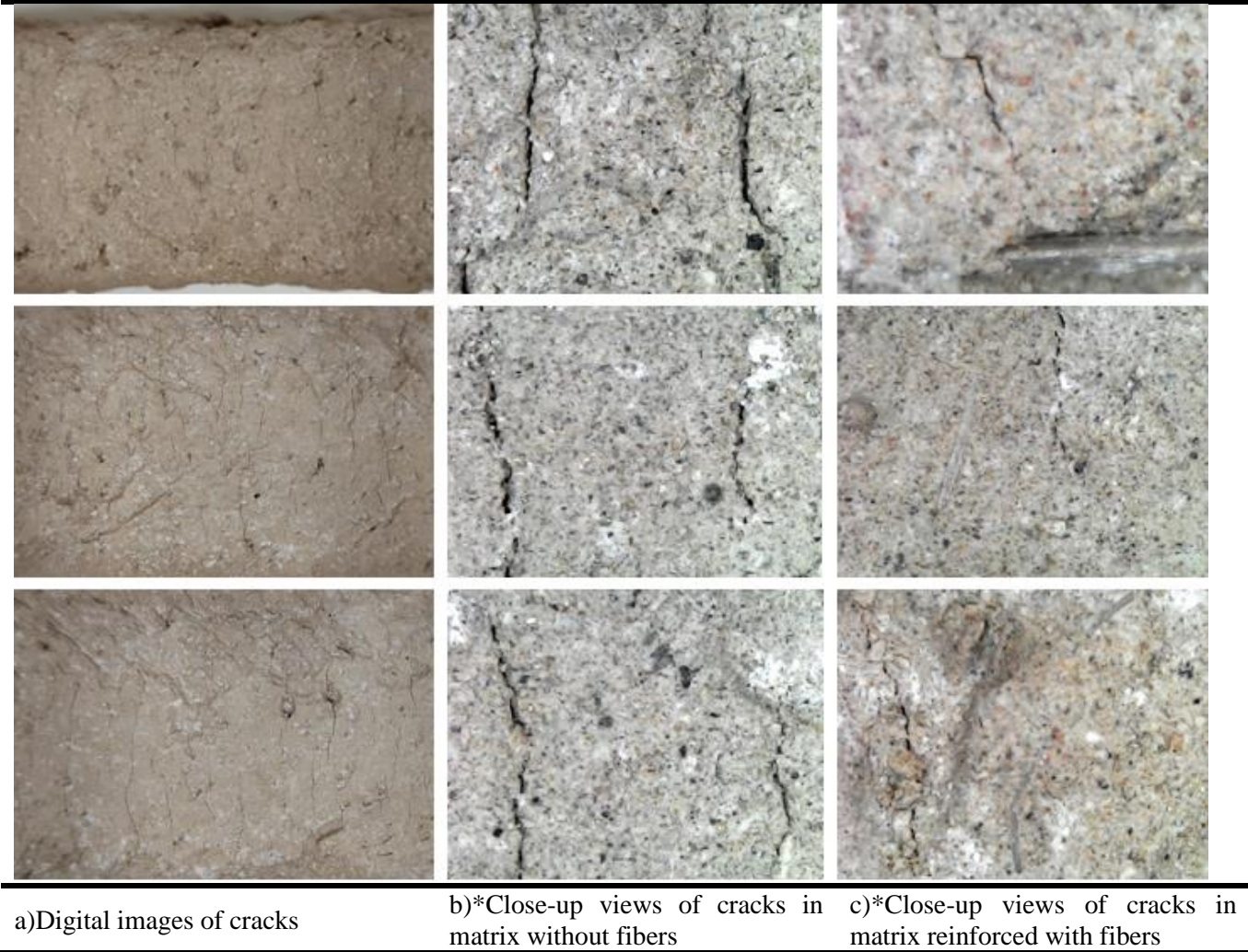
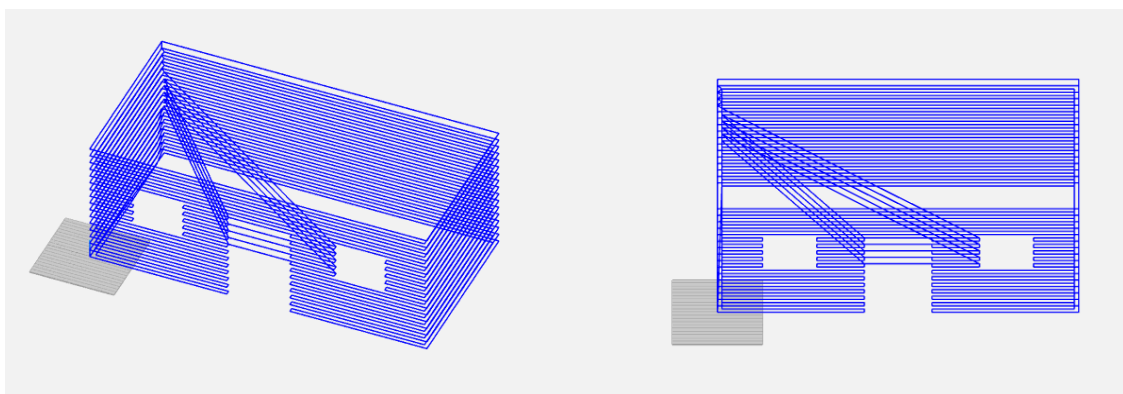


Figure 4.23. Representative digital images and close-up views of cracks occurred in 3D-printed filaments. (*area of $3.2 \times 2.4 \text{ mm}^2$)

4.3.3.6. Sustainable 3D Printing: Harnessing CDW-Based Geopolymer Technology

The application of 3D-printing at a laboratory scale was executed utilizing a gantry type 3D printer to showcase the viability of printing CDW-based geopolymer mortars developed in the present study. In the first step, the design for the small-scale house was created using a computer-aided design program, and from there, the G-codes required for printing the structure were generated (Fig 4.24.a). Subsequently, the structure was 3D-printed to assess its printing performance. The assessment focused on factors including shape retention, construction ease, extrusion capability, and the correlation between the intended design and the actual printed structure. As depicted in Figure 4.24.c, the CDW-based geopolymer mixture designated as CDW-1 demonstrates satisfactory performance with regard to buildability, shape retention, and extrudability. This observation underscores the promising potential for upcycling construction and demolition wastes through the synthesis of geopolymers using advanced 3D printing technology. The printed structure exhibited identical geometry to the design, and no defects, discontinuities, ruptures, or cracks were noticed during the printing. Furthermore, when the images of the samples taken from bond region of printed walls (Figure 4.24.b) were examined, it was observed that the layers were completely integrated, and no cold joints were encountered, indicating adequate adhesion between layers. Proper adhesion without gaps/cracks/discontinuities has been observed between printed layers both in the vertical and horizontal directions. In other words, when printing adjacent double walls (horizontal printing) or layers on top of each other (vertical printing), sufficient interlayer adhesion has been observed.



a)



b)



c)

Figure 4.24. Visualization of a) G-code for the designed structure in software, b) bond region of consecutive layers, c) 3D-printed structure.

4.4. Reinforcement Strategies and Modular System for 3D-Printed CDW-Based Geopolymer Structures

In this part, the performance of printed structures made of the mixes developed within the thesis scope, various reinforcement strategies, and a preliminary study on the modular system's applicability in the 3D-AM system were examined.

4.4.1. Introduction

Upon reviewing the extensive body of existing studies on 3D-AM, in this study, research has been performed on reinforcement strategies and modular systems for 3D-printed structures made of CDW-based geopolymer, an area with relatively few studies in the literature. This study brings forth innovation through novel materials tailored for 3D-AM and a fresh perspective on the 3D-AM process, embracing both reinforcement and modular

manufacturing methodologies. Within the scope of the study, brick and concrete waste from CDW and industrial waste-based slag and silica fume were utilized in the mixture design. The geopolymer mixture was activated with a 5M NaOH solution, and recycled aggregates were used as aggregates to achieve a higher recycling rate. Various reinforcing strategies (e.g. fiber and steel reinforced printed structures), different wall designs (e.g. simple box, zigzag, reinforced inner wall), and distinct applications intended to increase interlayer bond strength between hardened and fresh layer (e.g. wetting, chipping, and shear stud), and a modular system for 3D-AM were examined. The impact of the tested parameters on the mechanical features of CDW-based 3D-printed structures was thoroughly examined by performing compressive, three-point bending, and direct tensile tests. It is believed that the findings of this research will contribute to the current literature by demonstrating the effectiveness of reinforcement techniques on 3D-printed structures and the applicability of the modular system in 3D-AM system. Besides that, the outcomes of this study are believed to make a significant contribution to the current state-of-the-art, as the findings provide comprehensive insights and knowledge about 3D-AM applications.

4.4.2. Experimental Studies

4.4.2.1. Materials and mixture design

This research utilized a 3D-printable CDW-based geopolymer mixture with a flow diameter ranging between 16 and 16.5 cm, measured by following ASTM C1437-15. The details regarding the mixture used were tabulated in Table 4.8. The dry composition of the mixture consists of 55% BW, 15% CW, 25% BFS, and 5% SF. These proportions were determined considering the authors' previous studies [256]. The mixtures were activated with a 5M NaOH solution. The mixtures maintain an aggregate/binder ratio of 1, and the water/binder ratio is set at 0.44.

Table 4.8. Details of geopolymer mortar mixture (1000g precursor).

| Precursors | | | | Alkaline Activator | | Aggregate | W/B ratio | Flow Diameter (cm) |
|------------|--------|------------------------|--------|--------------------|------------|-----------|-----------|--------------------|
| CDW-based | | Industrial Waste-based | | NaOH | | RCA (g) | | |
| BW (g) | CW (g) | BFS (g) | SF (g) | Molarity (M) | Amount (g) | | | |
| 550 | 150 | 250 | 50 | 5 | 88 | 1000 | 0.44 | 16.0-16.5 cm |

4.4.2.2. Specimen preparation

Gantry type printer was used during the printing operation. Information regarding the printer (with an effective printing area of 100×100×40 cm [width × length × height]), the mortar conveying pump (a screw pump with a 20 L capacity and capable of generating pressure up to 25 bar) can be found in the recent works of the authors [77,91,128]. The printing operation was conducted at a printing rate of 50 mm/s using a 19 mm circular nozzle. Each layer printed has a height of 16 mm and a thickness of 40mm.

As part of study, the reinforcement for printed structures was explored to enhance their capacity to bear tensile stress throughout their service life. Because, unreinforced concrete-like brittle materials are susceptible to tensile stress, and addressing this vulnerability is a key focus of the research. In this context, firstly, an effort was made to introduce fibers into the material, a process considered relatively more straightforward and practical compared to alternative methods. To accomplish this, polypropylene fibers were added to the mixture at a weight ratio of 0.5 to binders. Additionally, similar to conventional reinforced concretes, the load-bearing capacity and behavior under the load of the printed products were examined by introducing reinforcement steel rebar between the layers. To determine the frequency of reinforcement, initially, a single reinforcement steel rebar was placed in the center of a 6-layered wall element, and as an alternative, a total of 5 reinforcement steel rebars were placed at each layer junction for the same structure. The reinforcement positioning took place concurrently with the printing process, without any printing time interval between layers. The diameter of the reinforcement used was chosen as 5 mm, considering the layer thickness of the printed structure. Overall, within this framework, four approaches were tested, comprising 6-layered reference specimens (BS coded specimens), a fiber-reinforced specimen (BS-FR coded specimens), single steel-reinforced specimens (BS-SSR coded specimens), and multiple steel-reinforced specimens (BS-MSR coded specimens), all featuring a length of 480 mm and a thickness of 40 mm. The details of these products are illustrated in Figure 4.25.

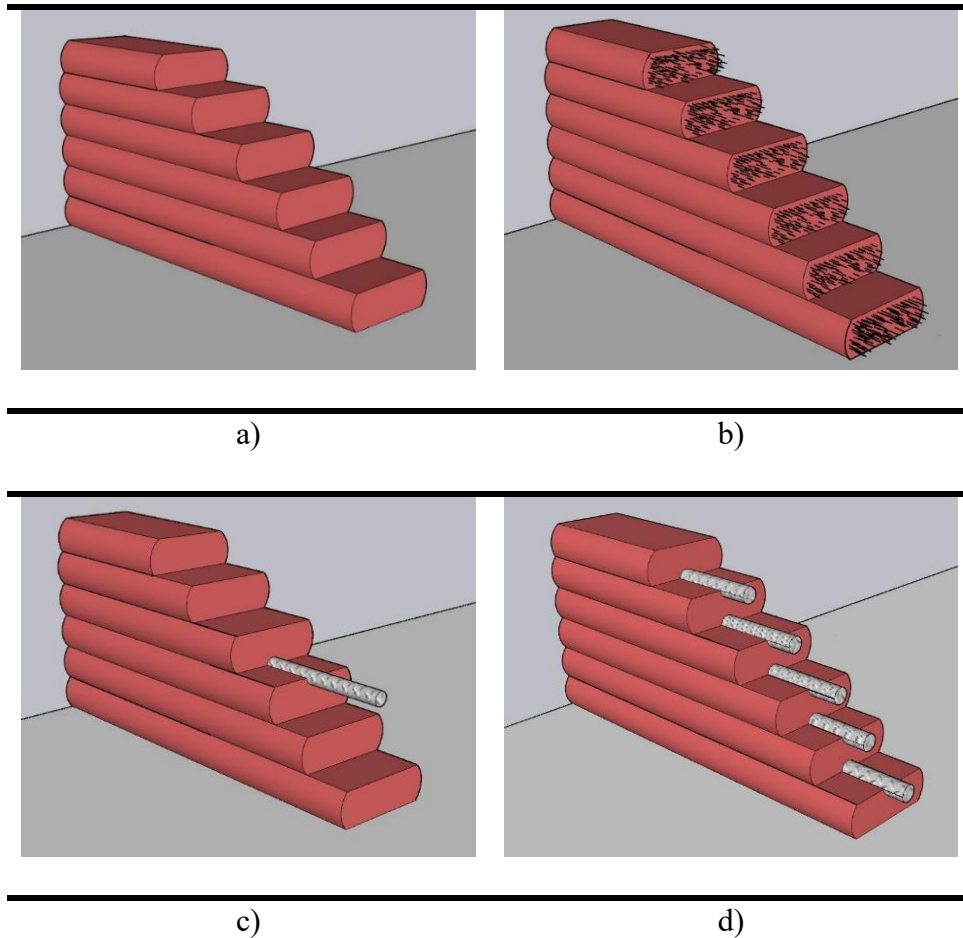


Figure 4.25. Schematic representation of printed specimen a) 6-layered reference (BS), b) fiber-reinforced (BS-FR), c) single steel-reinforced (BS-SSR), d) multiple steel-reinforced (BS-MSR).

In addition to the reinforcement, the impact of inner wall plans on the mechanical features of the wall was examined as load transferring between layers is fundamental in 3D-printed structures. In this context, three practical methods have been tested. These include i) the hollow inner wall, characterized by a basic box wall structure, ii) the zigzag inner wall, also known as a crosslinked or triangular truss, and iii) the reinforced inner wall, also referred to as a crosstie reinforced wall. All wall designs are three-layered, with dimensions of 240 mm in length, 140 mm in height, and 48 mm in thickness. In the zigzag-type wall, truss transitions were created at approximately 60-degree angles. For the laterally reinforced walls, a 5 mm ribbed construction steel was used at 48 mm intervals between two wall elements to ensure the transfer of load. The details of these products were displayed in Figure 4.26.

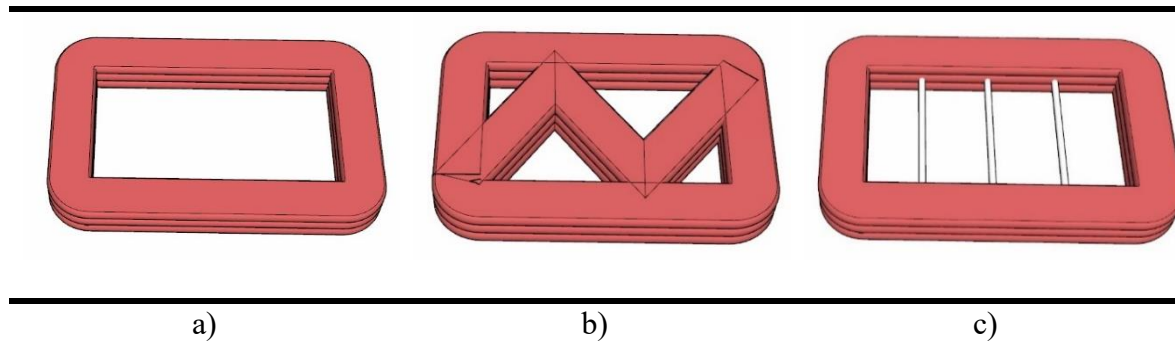


Figure 4.26. Schematic representation of a) simple box wall (OOP-B), b) zigzag inner wall (OOP-Z), c) crosstie reinforced wall (OOP-RS).

In 3D-AM applications, it is emphasized that bond strength is a crucial factor in addition to the mechanical properties of the used material. Insufficient bonding yields that failure occurs in the bond region rather than the matrix of the printed products under loading. Insufficient bonding arises from various variables, such as the rheological features of the material, printing time intervals, material aging, etc. The printing of a fresh layer onto a hardened layer is the most crucial situation among these cases and requires careful attention. This can be attributed to i) different shrinkage performances of layers printed at different times, ii) a lesser amount of interacted bond areas between layers, and iii) reduced orientation capacity to rearrange the surfaces of the layers due to the enhanced stiffness of the hardened layer, preventing intermixing with the subsequent layer [105]. Considering the necessity of addressing this issue specific to 3D-AM, this study focused on the application of interlayer wetting, interlayer chipping, and interlayer shear studs as relatively easy-to-implement methods to enhance the bond strength of the printed structure. Five different structures were explored to examine the impact of printing parameters on the bonding performance of 3D-printed structures. Initially, a continuous 6-layered structure was printed without any printing time interval, representing full composite action (FCA). Furthermore, scenarios were examined where three layers were printed initially, followed by the printing of three additional layers one day later. In this context, four variations were considered: the first involved no further treatment (i.e., partial composite action PCA), the second included wetting the surface before printing additional layers (i.e., partial composite action modification 1 PCA-W), the third comprised chipping the surface while still fresh, followed by printing three new layers after a one-day waiting period (i.e., partial composite action modification 2 PCA-C), and the fourth involved adding shear studs (a diameter of 5 mm and at intervals of 60 mm, with a length of 30 mm.) to the fresh surface, followed by printing

new layers after waiting for one day (i.e., partial composite action modification 3 PCA-S). These variations aimed to simulate different conditions and assess their effectiveness on the bonding strength of the printed structures. All printed structures are 6-layered, with dimensions of 480 mm in length, 96 mm in height, and 40 mm in thickness. The details of these products were demonstrated in Figure 4.27.

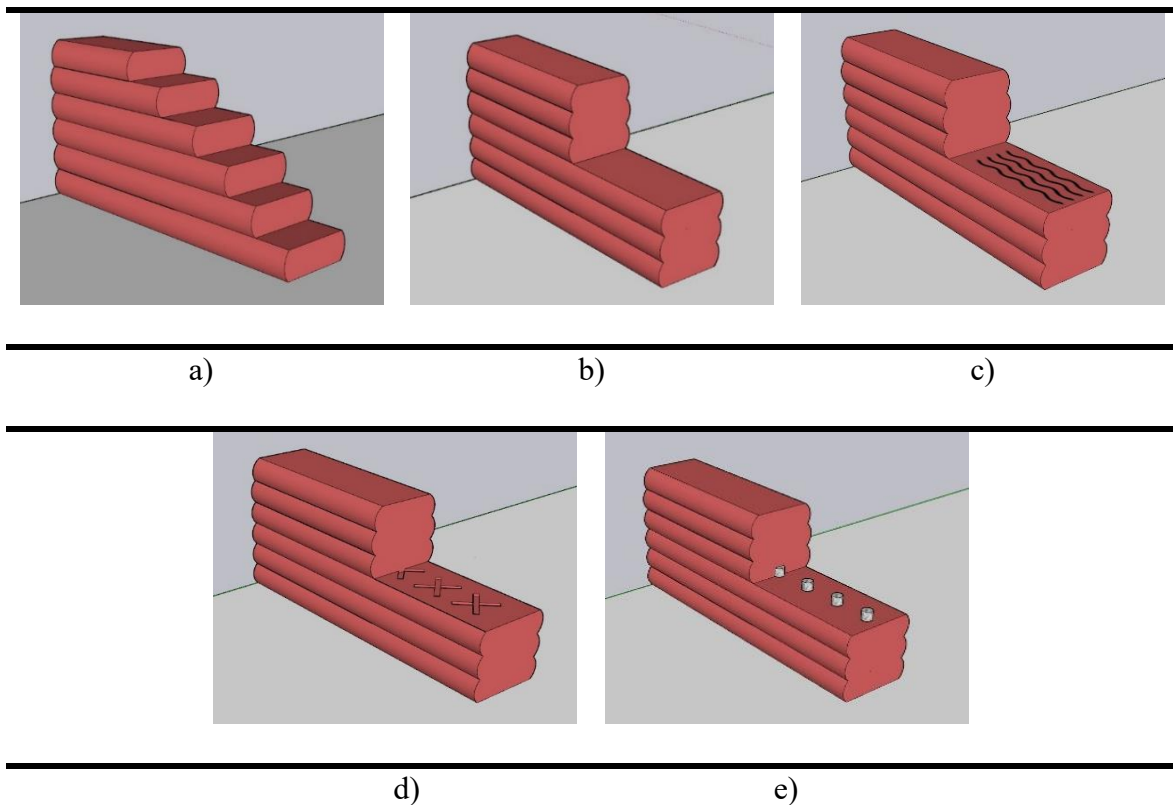


Figure 4.27. Schematic representation of a) continuously printed 6-layered specimen (FCA), b) 3+3 printed specimen with no treatment (PCA), c) 3+3 printed specimen with wetting treatment (PCA-W), d) 3+3 printed specimen with chipping treatment (PCA-C), e) 3+3 printed specimen with shear studs (PCA-S).

The 3D-printed structures require the transfer of the expensive printing and the concrete mixing and pumping equipment, negatively affect their practical application. Therefore, there is a trend to form 3D-printed structures by building them using modular 3D-printed structural elements. This application necessitates proper joint details between modular structural elements. To this end, considering the advantages of prefabrication, an investigation was conducted on whether elements manufactured with 3D-AM can be prefabricated and modular. This was explored by attempting to use a reinforced wet connection for the 3D-printed wall. Detailed monolithic (MW) and modular (MoDW) wall

elements, reinforced with mesh reinforcement (150 mm×150 mm, diameter of 5 mm), were presented in Figure 4.28. Both structures are 4-layered with dimensions of 600 mm in length, 150 mm in height, and 64 mm in thickness. The modular structure has been 3D-printed as two identical parts and connected to each other with a wet joint, the details of which were shown in the Figure 4.28. The CDW-based geopolymer mixture has been used in the wet joint region.

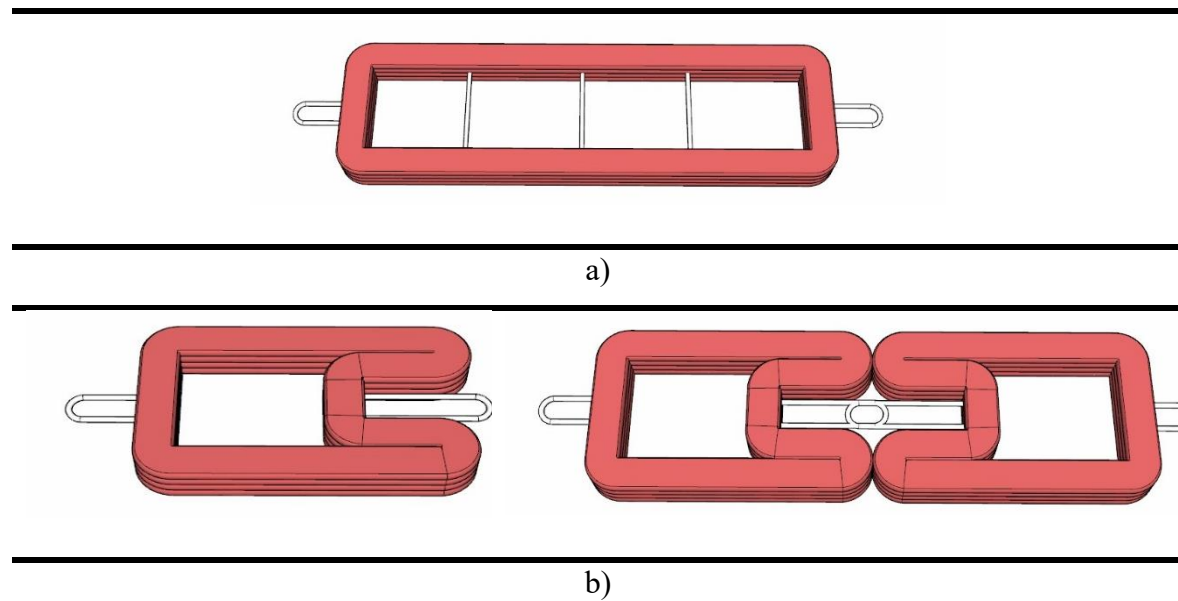


Figure 4.28. Schematic representation of a) monolithic 3D-printed wall (MW), b) modular 3D-printed wall (MoDW) and joint details.

4.4.2.3. Testing methods

Three-Point Bending Test

Three-point bending test was carried out on 3D-printed structures by using a deformation-controlled electro-mechanical test device at a crosshead velocity of 0.05 mm/s in accordance with ASTM C78. The span of the samples was segmented into two equal sections, and the locations for applying loads were precisely determined. Since the tested surface was flat, and there was no hindrance in distributing the load, additional capping was not applied for the 6-layered specimens and monolithic printed specimens. The tested specimens, produced through 3D printing, consisted of six layers with dimensions of 480 mm in length, 96 mm in height and 40 mm in thickness. The illustration of the three-point bending test for 3D-printed structures were given in Figure 4.29. Two replicates of 3D-printed structures were tested, and results were averaged. Tests were performed along the direction parallel to reinforcements and perpendicular to the reinforced wet joint in order to check the

contribution of these strategies. The test results have been utilized in the investigation of reinforcing 3D printed structures and enhancing the bond strength.



6-layered printed specimen

Figure 4.29. Three-point bending test setup.

Compressive Strength Test

Compressive strength test was carried out on 3D-printed structures by using a deformation-controlled electro-mechanical test device at a speed of 0.05 mm/s to investigate the effect of inner wall design on the load bearing capacity and stress transfer capacity of walls. Tests were conducted on 3D-printed wall elements consisting of three layers, measuring 240 mm in length, 140 mm in height, and 48 mm in thickness. Prior to testing, cappings were applied to the surfaces with indentations and protrusions, ensuring a homogeneous stress distribution. Two replicates of 3D-printed structures were tested, and results were averaged. All the specimens were tested in direction parallel to reinforcements and lattice orientations to examine the contribution of these modifications. The illustration of the compressive strength test can be found in Figure 4.30.



| | | |
|----|----|----|
| a) | b) | c) |
|----|----|----|

Figure 4.30. Compressive strength test setup for a) simple box wall (OOP-B), b) zigzag inner wall (OOP-Z), c) cross-tie reinforced wall (OOP-RS).

Direct Tensile Test

To investigate the effectiveness of modular approaches in 3D-printed structures, direct tensile tests were conducted on monolithic and modular specimens. To conduct the test, hooks were attached to the mesh reinforcement within the printed structure, and the experiment was performed by applying tensile force after clamping the hooks to the jaws of the test device at both ends. This process was conducted at a rate of 0.05 mm/s by deformation-controlled electro-mechanical test device. The illustration of the direct tensile strength test can be found in Figure 4.31. Two replicates of 3D-printed structures were tested, and the results were averaged.

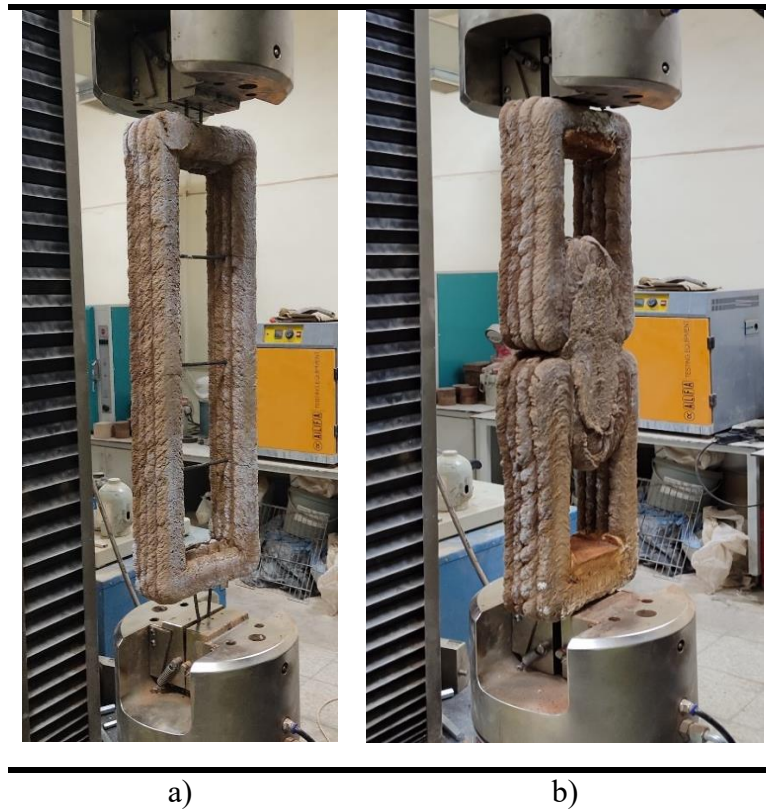


Figure 4.31. Direct tensile test setup for a) monolithic 3D-printed wall (MW), b) modular 3D-printed wall (MoDW).

4.4.3. Experimental Results and Discussion

4.4.3.1. Reinforcing Strategies for Bending Strength

In this study, the strengthening of 3D-printed structures was investigated to improve their ability to withstand tensile stress. In this context, three-point bending test was applied to the printed structures. The force-displacement representative curves of the samples that most closely corresponds to the average values are illustrated in Figure 4.32. According to the obtained results, the bending capacities for the BS, BS-FR, BS-SSR and BS-MSR specimens are recorded as 2.50kN, 2.61kN, 3.16kN and 6.58kN, respectively. While BS-FR specimen showed similar behavior compared to the BS specimen, both BS-SSR and BS-MSR specimens showed a significant enhancement in the strength (by ratio of approximately 26% and 163%, respectively) and the displacement ductility. In addition, the energy dissipation capacities of BS-SSR and BS-MSR specimens increased significantly.

It is clear from Figure 4.32 that the inclusion of fiber to the matrix has no notable effect on the strength and behavior of structure under loading, although it was anticipated to observe performance enhancement because of the role of fibers as inter-discontinuity sutures and ability of inhibiting the crack growth by bridging the cracks [224]. It could be concluded that the provided fiber (i.e., a weight ratio of 0.5 to binders) was not enough to change the mechanical features of the printed specimen possibly because of percentages of the utilized fibers and the off-axis orientation of fibers, resulting in lower bridging behavior [257]. However, the steel reinforcement formed a sufficient bond strength with the 3D-printed concrete to form a composite material with an enhanced mechanical properties and more ductile bending behavior. The inclusion of only one steel reinforcement (i.e., reinforcement ratio of 0.0051, which is approximately 1.5 times the minimum reinforcement ratio given in ACI318-19) affected the bending behavior of the 3D-printed concrete considerably. In addition, the BS-MSR specimen had superior performance over the other alternatives, since with the increase in reinforcement in the cross-section, greater load-bearing capacity and ductility were achieved. But this specimen was not neither a feasible nor a practical alternative considering the reinforcement ratio in the tested layered structure. Consequently, the BS-SSR specimen was a promising alternative to enhance the bending behavior of the printed elements.

The observed damages of the BS, BS-FR, BS-SSR and BS-MSR specimens are summarized in Figure 4.33. The BS specimen showed a typical bending crack at the midspan. This crack

reached the top of the specimen quickly, which caused the collapse of the specimen. Similarly, the BS-FR specimen showed a major flexure crack, and the placed fiber could not prevent the excessive crack mouth opening under the effect of vertical load due to possibly the selected fiber-to-binder ratio, physical and mechanical properties of fiber length. Therefore, no enhancement was observed in the bending behavior. The BS-SSR specimen had similar major flexure crack, yet the placed longitudinal reinforcement avoided the excessive crack mouth opening and caused an increase in both load and displacement capacities. Unlike other specimens, the BS-MSR specimen showed a first shear crack between the support and the applied load due to excessive longitudinal reinforcement. Then, the flexural cracks also formed in the midspan, and the specimen failed due to loss of integrity at the midspan.

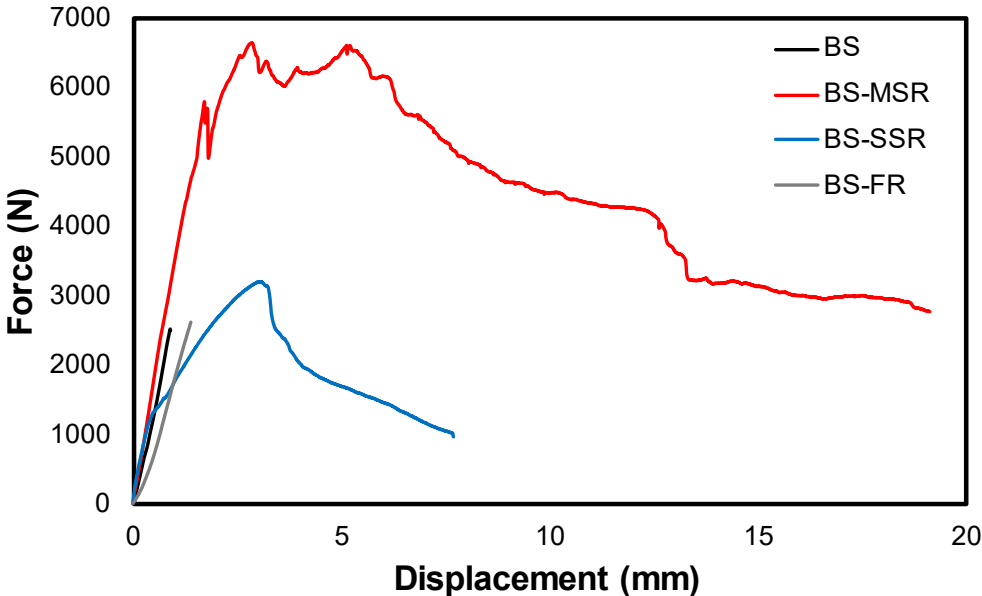


Figure 4.32. Bending strength: Three-point bending test results.





Figure 4.33. Typical failure patterns of bended specimens a) BS specimen, b) BS-FR specimen, c) BS-SSR specimen, d) BS-MSR specimen.

4.4.3.2. Reinforcing Strategies for Out-of-plane Strength

The impact of inner wall design on the out-of-plane mechanical strength of the wall was investigated, as the transfer of load between layers would be crucial in out-of-plane direction of the 3D-printed structures. The force-displacement curves for specimens are presented in Figure 4.34. Each data point in Figure 4.34 displays the representative curve of the samples that most closely corresponds to the average values obtained from the results of the compressive tests. The capacities for the OOP-B, OOP-RS and OOP-Z specimens are recorded as 62.9kN, 79.5kN and 120.8kN, respectively. According to the results obtained, application of lateral reinforcement (OOP-RS) to a box section (OOP-B) would result in a more stable load transfer, enhancing the capacity approximately 26%. Moreover, the formation of lattice throughout the wall geometry increased the capacity compared to a box section by nearly 92%. Therefore, the out-of-plane capacity of 3D-printed walls could be modified significantly by altering the cross-sectional geometry to lattice from box section at the expense of increasing the required material and printing time by approximately 55%. The application of crossties to the cross-sectional geometry is more feasible and economical compared to Zigzag wall design. Figure 4.34 clearly illustrates that all the alternative reinforcement and cross-section details (i.e., OOP-RS and OOP-Z specimens) compared to a box geometry (i.e., OOP-B specimen) resulted in the increase in both stiffness and strength. However, the displacement capacity of specimens tended to reduce slightly (i.e., approximately 15%) due to these modifications.

The observed damages of the OOP-B, OOP-RS and OOP-Z specimens are summarized in Figure 4.35. The OOP-B specimen carried compressive loads until one of its web components crushed. The failure of this specimen was sudden and brittle. The OOP-RS specimen also showed a brittle behavior but this specimen failed not only due to the crushing of the web but some part of the flange also incorporated the failure load owing to the cross-ties. The OOP-Z specimen had more capacity as the compressive load in out-of-plane direction was carried by more web component due to lattice formation. The lattices enhanced the load capacity, but they would not cause a ductile behavior.

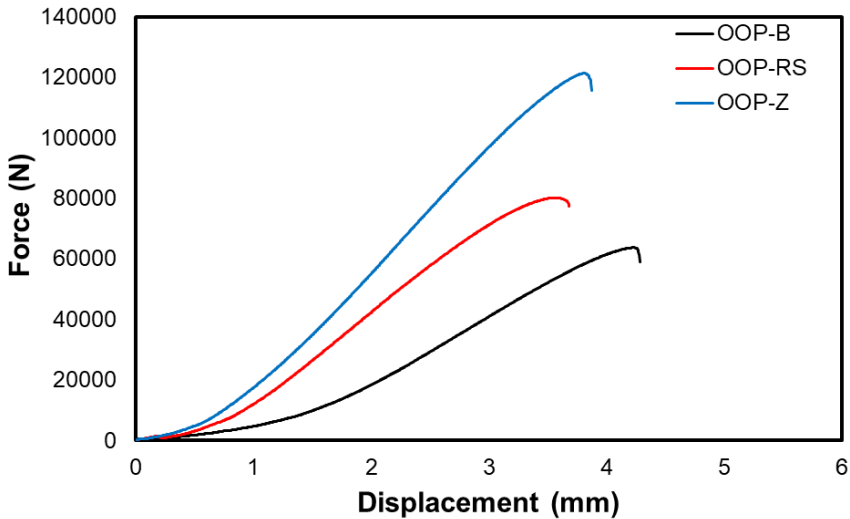


Figure 4.34. Out-of-plane strength: Compressive test results.

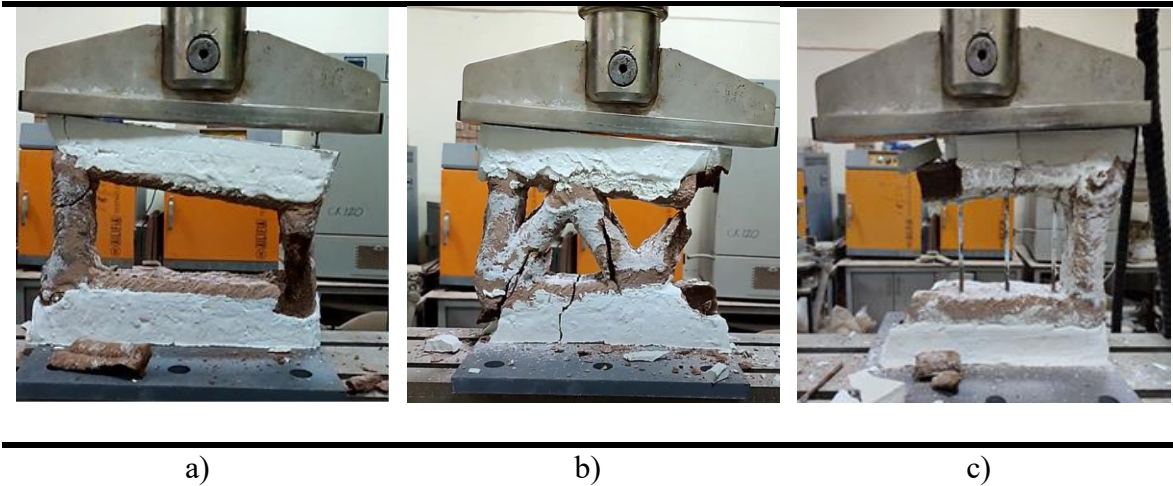


Figure 4.35. Typical failure patterns under compressive loading a) OOP-B specimen, b) OOP-Z specimen, and c) OOP-RS specimen.

4.4.3.3. Reinforcing Strategies for Interlayer Bond Strength

The 3D-printing process has a problem related to the full composite action due to its nature (i.e., time intervals during printing process). This problem is more pronounced in real time applications as the time required to print the next layer is more, which reduces the bond between the previous and the newly printed layer. Considering this, in this study, the effect of different interlayer treatments was investigated. The force-displacement curves for each specimen are illustrated in Figure 4.36. Data point in Figure represents the sample curve that closely matches the mean values obtained from the results of the tests. The capacities for the FCA, PCA, PCA-W, PCA-C and PCA-S specimens are 2.50kN, 1.18kN, 1.95kN, 1.98kN and 2.02kN, respectively. According to the results, no interface treatment (i.e., PCA specimen) would result in nearly 53% reduction in the capacity whereas the wetting (PCA-W specimen), the chipping (PCA-C specimen) and shear stud placement (PCA-S specimen) enhanced the interface capacity nearly 70% compared to no interface treatment scenario (i.e., PCA specimen), reaching approximately 80% of the capacity of the FCA specimen.

It can easily be inferred from Figure 4.36 that the behavior of each specimen is similar in the initial elastic region. However, the stiffness and the strength of each specimen varied based on the quality of the interface bond. The larger vertical shear demands increased the moment on each specimen, which in return resulted in an elevated horizontal shear through each interface. When the horizontal shear demand reached the shear strength of the interface, there exists horizontal slip between layers causing the failure of composite action. After this point, the two layers are not connected to each other anymore, reducing the strength and stiffness. It is clear that the FCA specimen represent an enhanced stiffness and strength compared to the other PCA specimens (Figure 4.36). This is because; the FCA specimen is the theoretically extremum point. However, in field application condition, there is no FCA specimen due to the limitations of 3D-printing. Therefore, the best approach is to develop interface treatment strategies that give close strength and stiffness to the FCA specimen. From the strength point of view, PCA-W, PCA-C and PCA-S specimens resulted in very similar behavior. However, the stiffness of the PCA-S specimen was better than PCA-W and PCA-C specimens. As expected, PCA specimen showed the least strength and stiffness because this specimen was designed to show the characteristics for the lowest possible scenarios (other extremum point). The potential cause for observing inferior performance in PCA specimens compared to FCA may be attributed to several factors. Firstly, the enhanced stiffness of the initial layer in PCA could lead to the formation of macropores and a reduced

number of interacted bond areas between layers [104,105,258,259]. Moreover, the heightened stiffness may limit the orientation capacity, preventing effective rearrangement of layer surfaces and hindering intermixing with subsequent layers [258,260]. Besides, there might be a loss of moisture content in the fresh layer due to water absorption by the hardened layer, leading to decreased ion mobility and insufficient formation of geopolymerization products between layers [261]. Additionally, non-uniform shrinkage between layers could also play a role in weakening bond strength [115,262], as shrinkage performance of CDW-based geopolymers are upper intermediate level [256]. Wetting treatment in interlayer region provided enhanced bending capacity since as stated by Sanjayan et al. [261], adequate surface moisture is essential to maintain the required workability or malleability of the concrete, enabling the development of inter-layer bonds; conversely, a dry surface lacks the necessary workability for bond formation. Moreover, given the higher intermediate water absorption of CDW-based geopolymer, wetting the surface hinders water absorption from the fresh mixture by the hardened structure. This, in turn, facilitates proper ion mobility in the interlayer region, favoring the process of geopolymerization and enhanced adhesion between the layers. Additionally, the chipping process was observed to be advantageous for enhancing bond strength, as anticipated. This is attributed to the additional surface area generated in the bond region through chipping, promoting sufficient bonding between layers. Similarly, shear stud implementation between layers provided enhanced interlayer mechanical performance as it provided structural integrity and load share between layers, and prevention of slip of layers [263]. Given the application limitation with a nozzle height of 16 mm, shear studs can only connect one freshly poured layer to a hardened layer. To optimize the observed enhancement, it may be beneficial to increase the frequency of shear stud application across multiple layers. However, careful consideration must be given to factors such as time constraints and the precision/requirement of workmanship to ensure effective implementation. Overall, the effect of shear stud was the most promising alternative as far as the stiffness and strength characteristic enhancement of the interface. However, PCA-W could also be recommended due to its practical superiority over other alternatives.

The observed damages of the FCA, PCA, PCA-W, PCA-C and PCA-S specimens are given in Figure 4.37. The FCA specimen had no slip at the interface causing a nearly vertical flexure crack at the mid span. However, the PCA specimen had a completely two specimens split by the cold joint formed at the mid-height of the specimen after the bond at the mid-

height was broken due to larger horizontal shear demands caused by the moment demands. Both PCA-W and PCA-C specimens showed a better bond between interfaces. This better interface behavior was proved by the observed shorter slip region. In addition, the shear stud placement in the PCA-S specimen also improved the interface bond, resulting in a reduced slip deformation.

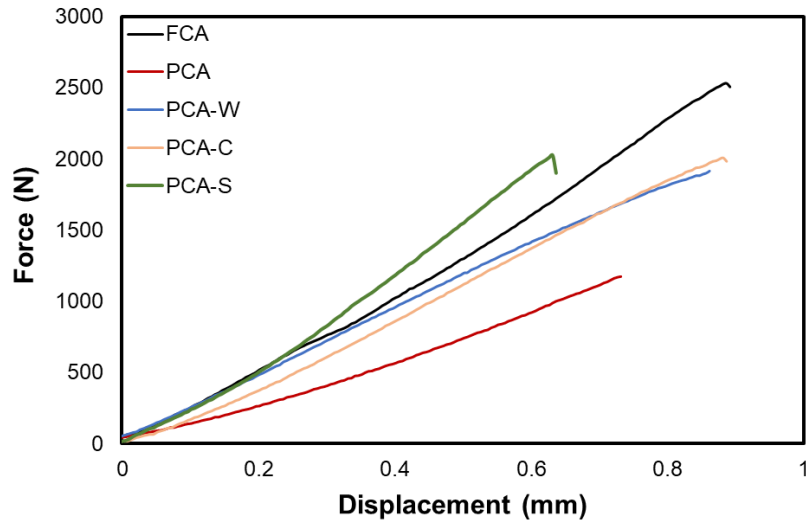
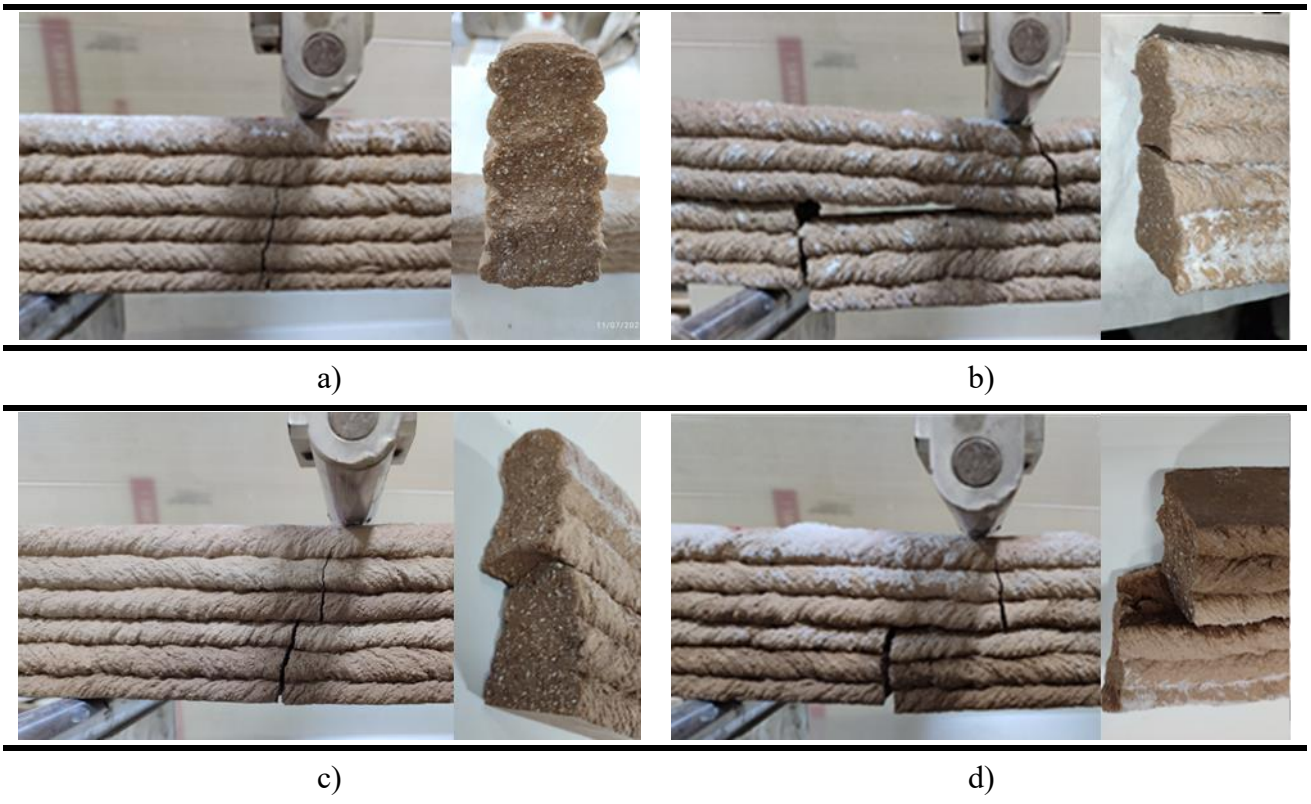


Figure 4.36. Interlayer bond strength: Three-point bending test results.





e)

Figure 4.37. Typical failure patterns of bended specimens a) FCA specimen, b) PCA specimen, c) PCA-W specimen, d) PCA-C specimen, e) PCA-S specimen.

4.4.3.4. Modular System

Exploring the benefits of prefabrication, an inquiry was undertaken to determine if components produced through 3D-AM could be prefabricated and constructed using modular structural elements. The force-displacement curves for each specimen are presented in Figure 4.38. Each data point displayed in Figure corresponds to the representative curve of the samples that best approximates the mean values obtained from the results of the tensile tests. The tensile capacities of the MW and MoDW specimens are 2.19 kN and 2.21 kN, respectively. Essentially, the MW and MoDW specimens had 7.91 mm and 7.46 mm displacement capacities, respectively. In other words, the difference in the displacement capacities was only 6%. Therefore, the tested modular connection (MoDW specimen) successfully transfers the same tensile load as its non-modular counterpart (MW specimen).

The observed damages of the MW and MoDW specimens are illustrated in Figure 4.39. The joint for the modular construction of the 3D-printed structural components showed no damage localized around the designed joint region. The capacity was lost due to the damage at the 3D-printed parts of each specimen (i.e., MW and MoDW specimens). This observation proved that the joint was capable of transferring the tensile force demands. In addition, the deformations of each specimen at the failure point were very close to each other, implying that there was no slip at the joint.

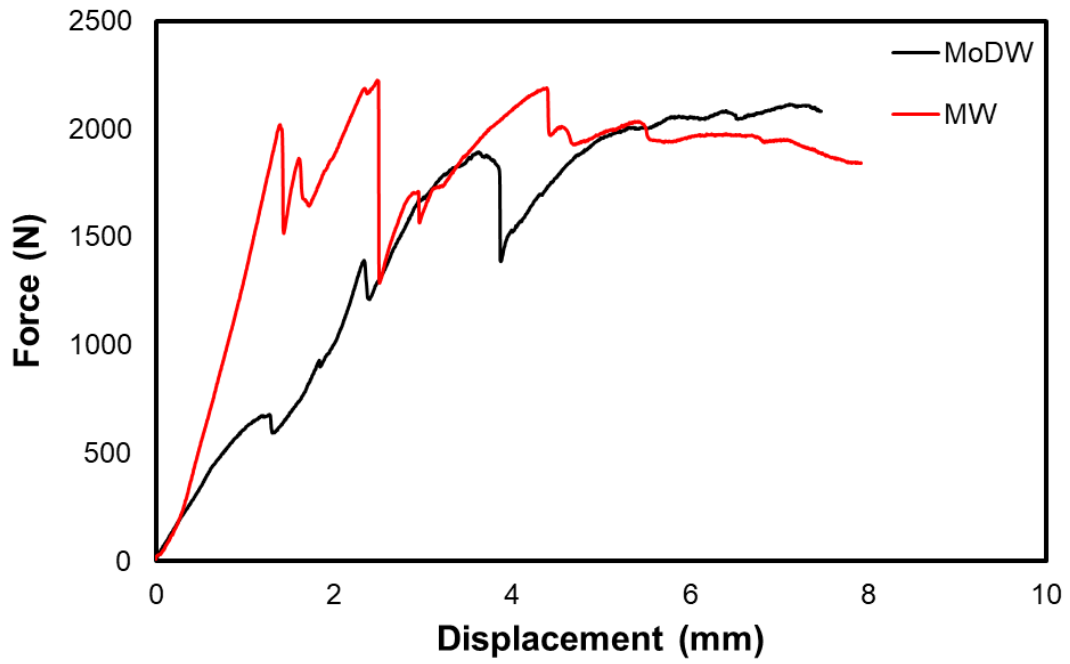


Figure 4.38. Modular construction: Tensile test results.

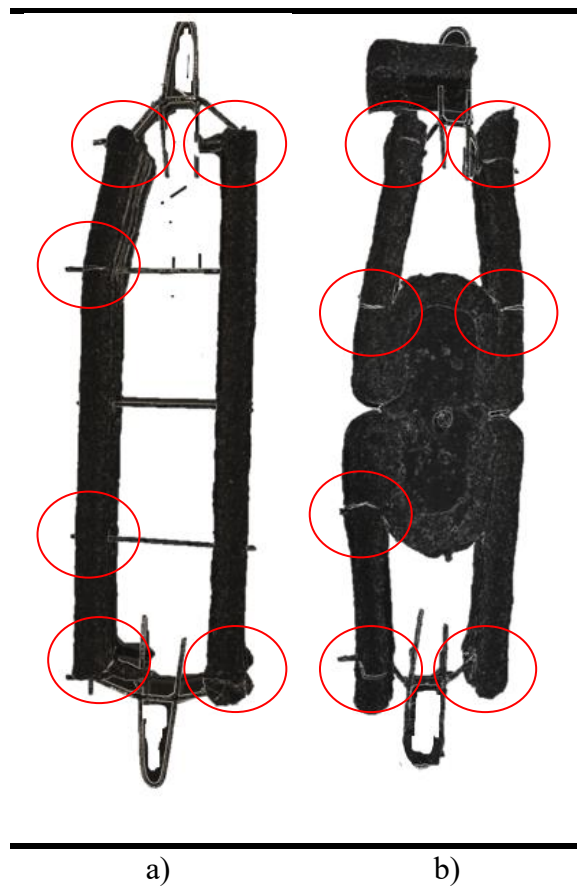


Figure 4.39. Typical failure patterns of a) MW specimen, b) MoDW specimen.

4.4.3.5. Advancing Sustainable 3D-AM in the Built Environment

The findings related to reinforcing strategies and modular systems in 3D-AM for CDW-based geopolymer systems significantly broaden the application scope of 3D-AM in the built environment. Utilizing CDW helps mitigate the environmental impact of construction activities by reducing the need for raw materials like Portland cement and aggregates, consequently lowering CO₂ emissions and energy consumption during ingredient processing. Moreover, valorizing CDW in building materials reduces potential water, land, and air contamination from deposition areas, conserves land from becoming disposal sites, and creates opportunities for agricultural applications. In addition to that, integrating 3D-printing of CDW-based geopolymer systems with reinforcing strategies expands application areas of 3D-AM in built environment by facilitating the production of robust structural elements that are suitable for diverse structural applications. This allows for the construction of single- or multi-storey buildings, medium-sized bridges, and more, using CDW-based geopolymers via 3D-AM technology. This approach offers enhanced cost and time effectiveness, rapid manufacturing, and the disposal of waste through a value-added approach, particularly beneficial in developing countries where CDWs are often deposited on clean lands or used in low-tech applications. Furthermore, implementing off-site production with a modular approach in 3D-AM enhances the advantages provided by the 3D-AM technology. It facilitates continuous and practical production, mitigating issues related to on-site installation of 3D printers and weather condition-based restrictions. It is expected that a facility to be established near waste deposition sites will enable the utilization of CDW in a value-added manner through the 3D-AM process, thereby facilitating the production of prefabricated/modular structural elements. This, in turn, is anticipated to contribute to a more sustainable implementation of 3D-AM in the built environment. Considering the deterioration of infrastructure worldwide and the resulting demolition waste, as well as the CDW generated from new construction and renovation to meet the needs of a growing population, along with the waste arising from destructive natural disasters such as earthquakes, the tested reinforcing strategies, and modular manufacturing approaches for 3D-AM within the scope of the study become even more crucial.

5. CONCLUSION

The results of the research conducted within the framework of the dissertation study and the details of these studies, which were shared in the previous chapters, are summarized separately for each section below.

5.1. Effect of Industrial Waste-Based Precursors on Performance of CDW-Based Geopolymer Paste

- Inclusion of industrial waste-based precursors into the CDW-based geopolymer mixtures yielded an increment in the flowability of the mixtures and provided longer open time performance. While the FA was the most effective precursor in terms of enhancement of workability, SF incorporation resulted in relatively lower enhancement among industrial wastes. However, SF incorporation caused more decrement in shear yield stress compared to the others.
- Industrial waste containing mixtures exhibited higher mechanical performance compared to the 100% CDW-based geopolymer mixtures, regardless of type and substitution rate of industrial wastes. Among industrial waste substituted mixtures, the compressive strength results of SF-incorporated ones were the highest, while those of FA-incorporated ones were the lowest.
- Although 100% CDW-based geopolymer system had less environmental burden, the mixture using FA, BFS and SF followed very closely behind. The main distinct parameters on the LCA results were raised from the transportation related impacts. While influence of water, CDW treatment and BFS, FA and SF on the environmental impact categories were almost negligible, NaOH, Ca(OH)₂, transportation and electricity were the components that have the greatest effects.
- The promising results were obtained from the industrial waste-based precursors by using them in CDW-based geopolymer providing enhancement of engineering properties (e.g., better workability and enhanced compressive strength) without endangering the environmental burden of the mixture which can be used further in the studies related with advanced manufacturing technologies.

5.2. Low-Alkaline Activated CDW-Based Geopolymer Mortars

- The 4M NaOH concentration was found to be insufficient for early strength (1-day) development, regardless of the precursor content. However, the mixtures activated with 4M NaOH eventually achieved a strength at further ages, indicating the adequateness of alkalinity for long-term geopolymerization. Nonetheless, this was accompanied by an increased level of shrinkage. Increasing the NaOH molarity from 4M to 8M generally improved the engineering features and effectiveness of the CDW-based geopolymer mixtures, regardless of the precursor content. However, a NaOH molarity of 5M was found to be the optimal choice, as it provided adequate alkalinity for early strength development.
- 100% CDW-based geopolymer mixtures showed lower mechanical and durability performance and exhibited vulnerability to water ingress and incapable of enduring freeze-thaw. Nonetheless, inclusion of BFS improved the mechanical, transport and durability performance of CDW-based geopolymer mixtures. But increasing the size and amount of RCAs led to a reduction in the performance of CDW-based geopolymer. This negative impact was effectively mitigated by substituting SF in the mixtures.
- Even with reduced alkalinity and the incorporation of calcium- and silicon-based precursors, the challenge of efflorescence persists in CDW-based geopolymer mixtures, particularly concerning their visual appearance. Overall, the CDW-based geopolymer mixture demonstrated remarkable compressive strength of 24.9 MPa and flexural strength of 4.7 MPa at the end of the 28-day ambient curing period along with superior durability performance.

5.3. 3D-Printable CDW-based Geopolymer: Investigating the Effects of Additives on Engineering Properties

- The fresh and hardened properties of CDW-based geopolymer can be customized for specific applications by incorporating additives.
- Nano SiO₂ and Al₂O₃, Na₂SiO₃, BA, and CAC were identified as beneficial additives for improving the mechanical performance of the low-activity CDW-based geopolymer. Remarkably, with the use of additives, compressive strength reached 29.8 MPa, while flexural strength achieved 5.4 after a 28-day ambient curing period.

- The efflorescence performance of CDW-based geopolymer mortar was observed to be closely linked to the strength, permeability, and inherent characteristics (such as chemical content) of its ingredients. Effective mitigation of efflorescence was achieved through the incorporation of nano SiO₂ and Al₂O₃, GNP, MC, Na₂SiO₃, CaO, CAC, and Ca(OH)₂. Furthermore, crack mitigation was successfully addressed by the inclusion of MC, Na₂SiO₃, CaO, CAC, and Ca(OH)₂.
- The formulated CDW-based geopolymer mixture can be effectively printed using a 3D printer, demonstrating satisfactory characteristics in terms of buildability, shape retention, and extrudability.
- Overall, a comprehensive testing methodology revealed the efficiency of chemical additives in influencing the features of CDW-based geopolymer, making them potential candidates for enhancing its characteristics and tackling identified challenges. However, detailed investigations into dosage and combinations are essential for a thorough understanding of their impact.
- It is crucial to emphasize that the results are highly likely to vary with the presence of different types, contents and origin of precursors. This aspect opens an appealing path for future research pursuits. Beyond the challenges posed by shrinkage-induced cracks and efflorescence in CDW-based geopolymers, the energy-intensive nature and carbon footprint associated with the alkaline activator process, safety concerns at higher alkaline dosages, durability issues stemming from crack formation, and potential variations in CDW-precursors can be identified as potential limitations or challenges that may hinder widespread utilization of CDW-based geopolymer.

5.4. Reinforcement Strategies and Modular System for 3D-Printed CDW-Based Geopolymer Structures

- The incorporation of polypropylene fiber at a weight ratio of 0.5% alongside binders exhibited negligible effect on the strength and structural behavior of printed structures under loading. In contrast, the introduction of steel reinforcement resulted in a substantial enhancement in bending capacity. Notably, single steel reinforcement contributed to an impressive 26% improvement, while structures employing multiple steel reinforcements demonstrated a significant increase of 163%.

- The modification of cross-sectional geometry has a considerable impact on the out-of-plane capacity of 3D-printed walls. The results indicate that introducing lateral reinforcement (OOP-RS) to a box section (OOP-B) leads to a more stable load transfer, resulting in an enhanced capacity by approximately 26%. Furthermore, the incorporation of a lattice structure throughout the wall geometry proves to be even more effective, yielding an impressive 92% increase in capacity compared to a conventional box section.
- The observed impact of the printing time interval on the interlayer mechanical performance of 3D-printed CDW-based geopolymer structures is noteworthy. Specifically, a substantial 53% decrement in capacity was noted, highlighting the sensitivity of mechanical properties to the printing time interval.
- The applied reinforcing strategies, including wetting, chipping, and shear stud implementation, demonstrated a substantial enhancement in interface bond strength capacity. Specifically, there was an impressive 80% increase compared to scenarios where no interface treatment was applied.
- Tests conducted on the modular system revealed that the examined modular connection efficiently transmits an equivalent tensile load compared to its non-modular counterpart, displaying similar failure behavior. These findings are promising, underscoring the potential application of modular systems in 3D-AM construction.
- The utilization of CDWs in value-added geopolymer production, coupled with innovative, fast, environmentally friendly, and economical methods of 3D-AM, integrating reinforcing strategies in the 3D-AM process to enable the construction of robust and more diverse structures, and integrating prefabrication methods into the 3D-AM process to make it even more environmentally friendly, economical, and rapid, is expected to open up new avenues for 3D-AM in the built environment.

6. REFERENCES

- [1] P.J.M. Monteiro, S.A. Miller, A. Horvath, Towards sustainable concrete, *Nat Mater* 16 (2017) 698–699.
- [2] S.A. Miller, V.M. John, S.A. Pacca, A. Horvath, Carbon dioxide reduction potential in the global cement industry by 2050, *Cem Concr Res* 114 (2018) 115–124. <https://doi.org/10.1016/J.CEMCONRES.2017.08.026>.
- [3] C. Chen, R. Xu, D. Tong, X. Qin, J. Cheng, J. Liu, B. Zheng, L. Yan, Q. Zhang, A striking growth of CO₂ emissions from the global cement industry driven by new facilities in emerging countries, *Environmental Research Letters* 17 (2022) 044007.
- [4] Supriya, R. Chaudhury, U. Sharma, P.C. Thapliyal, L.P. Singh, Low-CO₂ emission strategies to achieve net zero target in cement sector, *J Clean Prod* 417 (2023) 137466. <https://doi.org/10.1016/J.JCLEPRO.2023.137466>.
- [5] U. UNEP, Emissions gap report 2020, UN, 2021.
- [6] T. Watari, Z. Cao, S. Hata, K. Nansai, Efficient use of cement and concrete to reduce reliance on supply-side technologies for net-zero emissions, *Nat Commun* 13 (2022) 4158. <https://doi.org/10.1038/s41467-022-31806-2>.
- [7] M.L. Nehdi, A. Marani, L. Zhang, Is net-zero feasible: Systematic review of cement and concrete decarbonization technologies, *Renewable and Sustainable Energy Reviews* 191 (2024) 114169. <https://doi.org/10.1016/J.RSER.2023.114169>.
- [8] H. Wu, J. Zuo, G. Zillante, J. Wang, H. Yuan, Status quo and future directions of construction and demolition waste research: A critical review, *J Clean Prod* 240 (2019) 118163. <https://doi.org/10.1016/J.JCLEPRO.2019.118163>.
- [9] J. Solís-Guzmán, M. Marrero, M.V. Montes-Delgado, A. Ramírez-de-Arellano, A Spanish model for quantification and management of construction waste, *Waste Management* 29 (2009) 2542–2548. <https://doi.org/10.1016/J.WASMAN.2009.05.009>.
- [10] M. Yazdani, K. Kabirifar, B.E. Frimpong, M. Shariati, M. Mirmozaffari, A. Boskabadi, Improving construction and demolition waste collection service in an urban area using a simheuristic approach: A case study in Sydney, Australia, *J Clean Prod* 280 (2021) 124138. <https://doi.org/10.1016/J.JCLEPRO.2020.124138>.
- [11] D. Delgado Camacho, P. Clayton, W.J. O'Brien, C. Seepersad, M. Juenger, R. Ferron, S. Salamone, Applications of additive manufacturing in the construction industry – A

- forward-looking review, *Autom Constr* 89 (2018) 110–119. <https://doi.org/10.1016/J.AUTCON.2017.12.031>.
- [12] T.D. Ngo, A. Kashani, G. Imbalzano, K.T.Q. Nguyen, D. Hui, Additive manufacturing (3D printing): A review of materials, methods, applications and challenges, *Compos B Eng* 143 (2018) 172–196. <https://doi.org/10.1016/J.COMPOSITESB.2018.02.012>.
- [13] J. Wei, K. Cen, Empirical assessing cement CO₂ emissions based on China's economic and social development during 2001–2030, *Science of The Total Environment* 653 (2019) 200–211. <https://doi.org/10.1016/J.SCITOTENV.2018.10.371>.
- [14] N.A. Madloul, R. Saidur, M.S. Hossain, N.A. Rahim, A critical review on energy use and savings in the cement industries, *Renewable and Sustainable Energy Reviews* 15 (2011) 2042–2060. <https://doi.org/10.1016/J.RSER.2011.01.005>.
- [15] J.F. Xie, Y.X. Huang, W.W. Li, X.N. Song, L. Xiong, H.Q. Yu, Efficient electrochemical CO₂ reduction on a unique chrysanthemum-like Cu nanoflower electrode and direct observation of carbon deposit, *Electrochim Acta* 139 (2014) 137–144. <https://doi.org/10.1016/J.ELECTACTA.2014.06.034>.
- [16] M. Alhawat, A. Ashour, G. Yildirim, A. Aldemir, M. Sahmaran, Properties of geopolymers sourced from construction and demolition waste: A review, *Journal of Building Engineering* 50 (2022) 104104. <https://doi.org/10.1016/J.JOBE.2022.104104>.
- [17] O.H. Zinkaah, A. Araba, M. Alhawat, Performance of ACI code for predicting the flexural capacity and deflection of reinforced geopolymer concrete beams, in: *IOP Conf Ser Mater Sci Eng*, IOP Publishing, 2021: p. 012067.
- [18] Y.H.M. Amran, R. Alyousef, H. Alabduljabbar, M. El-Zeadani, Clean production and properties of geopolymer concrete; A review, *J Clean Prod* 251 (2020) 119679. <https://doi.org/10.1016/J.JCLEPRO.2019.119679>.
- [19] K. Neupane, D. Chalmers, P. Kidd, High-strength geopolymer concrete-properties, advantages and challenges, *Advances in Materials* 7 (2018) 15–25.
- [20] X. Jiang, R. Xiao, M. Zhang, W. Hu, Y. Bai, B. Huang, A laboratory investigation of steel to fly ash-based geopolymer paste bonding behavior after exposure to elevated temperatures, *Constr Build Mater* 254 (2020) 119267. <https://doi.org/10.1016/J.CONBUILDMAT.2020.119267>.

- [21] M. Lahoti, P. Narang, K.H. Tan, E.H. Yang, Mix design factors and strength prediction of metakaolin-based geopolymer, *Ceram Int* 43 (2017) 11433–11441. <https://doi.org/10.1016/J.CERAMINT.2017.06.006>.
- [22] M. Rostami, K. Behfarnia, The effect of silica fume on durability of alkali activated slag concrete, *Constr Build Mater* 134 (2017) 262–268. <https://doi.org/10.1016/J.CONBUILDMAT.2016.12.072>.
- [23] B.V. Rangan, Design and manufacture of flyash-based geopolymer concrete, *Concrete in Australia* 34 (2008) 37–43.
- [24] D.M. Roy, Alkali-activated cements Opportunities and challenges, *Cem Concr Res* 29 (1999) 249–254. [https://doi.org/10.1016/S0008-8846\(98\)00093-3](https://doi.org/10.1016/S0008-8846(98)00093-3).
- [25] F. Pacheco-Torgal, J. Castro-Gomes, S. Jalali, Alkali-activated binders: A review: Part 1. Historical background, terminology, reaction mechanisms and hydration products, *Constr Build Mater* 22 (2008) 1305–1314. <https://doi.org/10.1016/J.CONBUILDMAT.2007.10.015>.
- [26] J. Davidovits, Geopolymers: inorganic polymeric new materials, *J Therm Anal Calorim* 37 (1991) 1633–1656.
- [27] J.R. Van Wazer, Equilibria and kinetics in inorganic polymerizations, *Inorg. Macromol. Rev* 1 (1970) 89–99.
- [28] E. Gartner, Industrially interesting approaches to “low-CO₂” cements, *Cem Concr Res* 34 (2004) 1489–1498. <https://doi.org/10.1016/J.CEMCONRES.2004.01.021>.
- [29] H. Rahier, B. Van Mele, M. Biesemans, J. Wastiels, X. Wu, Low-temperature synthesized aluminosilicate glasses, *J Mater Sci* 31 (1996) 71–79. <https://doi.org/10.1007/BF00355128>.
- [30] A. Palomo, J.I. López de la Fuente, Alkali-activated cementitious materials: Alternative matrices for the immobilisation of hazardous wastes: Part I. Stabilisation of boron, *Cem Concr Res* 33 (2003) 281–288. [https://doi.org/10.1016/S0008-8846\(02\)00963-8](https://doi.org/10.1016/S0008-8846(02)00963-8).
- [31] P. Duxson, A. Fernández-Jiménez, J.L. Provis, G.C. Lukey, A. Palomo, J.S.J. van Deventer, Geopolymer technology: the current state of the art, *J Mater Sci* 42 (2007) 2917–2933. <https://doi.org/10.1007/s10853-006-0637-z>.
- [32] S. Mallicoat, P. Sarin, W.M. Kriven, Novel, Alkali-Bonded, Ceramic Filtration Membranes, *Developments in Advanced Ceramics and Composites: Ceramic Engineering and Science Proceedings* 26 (2005) 37–44.

- [33] Y. Bao, M.W. Grutzeck, C.M. Jantzen, Preparation and properties of hydroceramic waste forms made with simulated hanford low-activity waste, *Journal of the American Ceramic Society* 88 (2005) 3287–3302.
- [34] V.D. Glukhovskiy, *Gruntosilikaty (soil silicates)* Gosstroyizdat, Kiev, Ukraine (1959).
- [35] A. Fernández-Jiménez, A. Palomo, M. Criado, Microstructure development of alkali-activated fly ash cement: a descriptive model, *Cem Concr Res* 35 (2005) 1204–1209. <https://doi.org/10.1016/J.CEMCONRES.2004.08.021>.
- [36] A. Fernández-Jiménez, A. Palomo, I. Sobrados, J. Sanz, The role played by the reactive alumina content in the alkaline activation of fly ashes, *Microporous and Mesoporous Materials* 91 (2006) 111–119. <https://doi.org/10.1016/J.MICROMESO.2005.11.015>.
- [37] J.L. Provis, G.C. Lukey, J.S.J. Van Deventer, Do geopolymers actually contain nanocrystalline zeolites? A reexamination of existing results, *Chemistry of Materials* 17 (2005) 3075–3085.
- [38] J.L. Provis, P. Duxson, J.S.J. van Deventer, G.C. Lukey, The Role of Mathematical Modelling and Gel Chemistry in Advancing Geopolymer Technology, *Chemical Engineering Research and Design* 83 (2005) 853–860. <https://doi.org/10.1205/CHERD.04329>.
- [39] J.S.J. van Deventer, J.L. Provis, P. Duxson, G.C. Lukey, Reaction mechanisms in the geopolymeric conversion of inorganic waste to useful products, *J Hazard Mater* 139 (2007) 506–513. <https://doi.org/10.1016/J.JHAZMAT.2006.02.044>.
- [40] T.W. Swaddle, J. Salerno, P.A. Tregloan, Aqueous aluminates, silicates, and aluminosilicates, *Chem Soc Rev* 23 (1994) 319–325.
- [41] T.W. Swaddle, Silicate complexes of aluminum(III) in aqueous systems, *Coord Chem Rev* 219–221 (2001) 665–686. [https://doi.org/10.1016/S0010-8545\(01\)00362-9](https://doi.org/10.1016/S0010-8545(01)00362-9).
- [42] R. Aiello, F. Crea, A. Nastro, B. Subotić, F. Testa, Influence of cations on the physicochemical and structural properties of aluminosilicate gel precursors. Part 1. Chemical and thermal properties, *Zeolites* 11 (1991) 767–775. [https://doi.org/10.1016/S0144-2449\(05\)80054-5](https://doi.org/10.1016/S0144-2449(05)80054-5).
- [43] I.I. Ivanova, R. Aiello, J.B. Nagy, F. Crea, E.G. Derouane, N. Dumont, A. Nastro, B. Subotić, F. Testa, Influence of cations on the physicochemical and structural properties of aluminosilicate gel precursors: II. Multinuclear magnetic resonance characterization, *Microporous Materials* 3 (1994) 245–257. [https://doi.org/10.1016/0927-6513\(94\)00036-0](https://doi.org/10.1016/0927-6513(94)00036-0).

- [44] J. Faimon, Oscillatory silicon and aluminum aqueous concentrations during experimental aluminosilicate weathering, *Geochim Cosmochim Acta* 60 (1996) 2901–2907. [https://doi.org/10.1016/0016-7037\(96\)00130-5](https://doi.org/10.1016/0016-7037(96)00130-5).
- [45] P. Duxson, G.C. Lukey, J.S.J. van Deventer, Physical evolution of Na-geopolymer derived from metakaolin up to 1000 C, *J Mater Sci* 42 (2007) 3044–3054.
- [46] P. Duxson, J.L. Provis, G.C. Lukey, S.W. Mallicoat, W.M. Kriven, J.S.J. Van Deventer, Understanding the relationship between geopolymer composition, microstructure and mechanical properties, *Colloids Surf A Physicochem Eng Asp* 269 (2005) 47–58. <https://doi.org/10.1016/J.COLSURFA.2005.06.060>.
- [47] I. Garcia-Lodeiro, A. Palomo, A. Fernández-Jiménez, An overview of the chemistry of alkali-activated cement-based binders, *Handbook of Alkali-Activated Cements, Mortars and Concretes* (2015) 19–47. <https://doi.org/10.1533/9781782422884.1.19>.
- [48] F. Farooq, X. Jin, M. Faisal Javed, A. Akbar, M. Izhar Shah, F. Aslam, R. Alyousef, Geopolymer concrete as sustainable material: A state of the art review, *Constr Build Mater* 306 (2021) 124762. <https://doi.org/10.1016/J.CONBUILDMAT.2021.124762>.
- [49] I. Garcia-Lodeiro, A. Palomo, A. Fernández-Jiménez, Crucial insights on the mix design of alkali-activated cement-based binders, *Handbook of Alkali-Activated Cements, Mortars and Concretes* (2015) 49–73. <https://doi.org/10.1533/9781782422884.1.49>.
- [50] P. Chindaprasirt, T. Chareerat, V. Sirivivatnanon, Workability and strength of coarse high calcium fly ash geopolymer, *Cem Concr Compos* 29 (2007) 224–229. <https://doi.org/10.1016/J.CEMCONCOMP.2006.11.002>.
- [51] P. Nath, P.K. Sarker, Effect of GGBFS on setting, workability and early strength properties of fly ash geopolymer concrete cured in ambient condition, *Constr Build Mater* 66 (2014) 163–171. <https://doi.org/10.1016/J.CONBUILDMAT.2014.05.080>.
- [52] P.S. Deb, P. Nath, P.K. Sarker, The effects of ground granulated blast-furnace slag blending with fly ash and activator content on the workability and strength properties of geopolymer concrete cured at ambient temperature, *Materials & Design* (1980-2015) 62 (2014) 32–39. <https://doi.org/10.1016/J.MATDES.2014.05.001>.
- [53] S. Saha, C. Rajasekaran, Enhancement of the properties of fly ash based geopolymer paste by incorporating ground granulated blast furnace slag, *Constr Build Mater* 146 (2017) 615–620. <https://doi.org/10.1016/J.CONBUILDMAT.2017.04.139>.
- [54] I. Ismail, S.A. Bernal, J.L. Provis, R. San Nicolas, S. Hamdan, J.S.J. Van Deventer, Modification of phase evolution in alkali-activated blast furnace slag by the

- incorporation of fly ash, *Cem Concr Compos* 45 (2014) 125–135. <https://doi.org/10.1016/J.CEMCONCOMP.2013.09.006>.
- [55] U. Rattanasak, P. Chindaprasirt, Influence of NaOH solution on the synthesis of fly ash geopolymer, *Miner Eng* 22 (2009) 1073–1078. <https://doi.org/10.1016/J.MINENG.2009.03.022>.
- [56] D. Hardjito, S.E. Wallah, D.M.J. Sumajouw, B.V. Rangan, On the development of fly ash-based geopolymer concrete, *Materials Journal* 101 (2004) 467–472.
- [57] E. Ul Haq, S. Kunjalukkal Padmanabhan, A. Licciulli, Synthesis and characteristics of fly ash and bottom ash based geopolymers—A comparative study, *Ceram Int* 40 (2014) 2965–2971. <https://doi.org/10.1016/J.CERAMINT.2013.10.012>.
- [58] L. Chen, Z. Wang, Y. Wang, J. Feng, Preparation and properties of alkali activated metakaolin-based geopolymer, *Materials* 9 (2016) 767.
- [59] T.A. Aiken, J. Kwasny, W. Sha, M.N. Soutsos, Effect of slag content and activator dosage on the resistance of fly ash geopolymer binders to sulfuric acid attack, *Cem Concr Res* 111 (2018) 23–40. <https://doi.org/10.1016/J.CEMCONRES.2018.06.011>.
- [60] A. Albidah, M. Alghannam, H. Abbas, T. Almusallam, Y. Al-Salloum, Characteristics of metakaolin-based geopolymer concrete for different mix design parameters, *Journal of Materials Research and Technology* 10 (2021) 84–98. <https://doi.org/10.1016/J.JMRT.2020.11.104>.
- [61] B.H. Mo, H. Zhu, X.M. Cui, Y. He, S.Y. Gong, Effect of curing temperature on geopolymerization of metakaolin-based geopolymers, *Appl Clay Sci* 99 (2014) 144–148. <https://doi.org/10.1016/J.CLAY.2014.06.024>.
- [62] M. Zhang, M. Zhao, G. Zhang, T. El-Korchi, M. Tao, A multiscale investigation of reaction kinetics, phase formation, and mechanical properties of metakaolin geopolymers, *Cem Concr Compos* 78 (2017) 21–32. <https://doi.org/10.1016/J.CEMCONCOMP.2016.12.010>.
- [63] H. Wang, H. Li, F. Yan, Synthesis and mechanical properties of metakaolinite-based geopolymer, *Colloids Surf A Physicochem Eng Asp* 268 (2005) 1–6. <https://doi.org/10.1016/J.COLSURFA.2005.01.016>.
- [64] S. Kumar, R. Kumar, S.P. Mehrotra, Influence of granulated blast furnace slag on the reaction, structure and properties of fly ash based geopolymer, *J Mater Sci* 45 (2010) 607–615. <https://doi.org/10.1007/s10853-009-3934-5>.
- [65] Q. Wan, F. Rao, S. Song, R.E. García, R.M. Estrella, C.L. Patiño, Y. Zhang, Geopolymerization reaction, microstructure and simulation of metakaolin-based

- geopolymers at extended Si/Al ratios, *Cem Concr Compos* 79 (2017) 45–52. <https://doi.org/10.1016/J.CEMCONCOMP.2017.01.014>.
- [66] P. Cong, L. Mei, Using silica fume for improvement of fly ash/slag based geopolymer activated with calcium carbide residue and gypsum, *Constr Build Mater* 275 (2021) 122171. <https://doi.org/10.1016/J.CONBUILDMAT.2020.122171>.
- [67] P. Duan, C. Yan, W. Zhou, Compressive strength and microstructure of fly ash based geopolymer blended with silica fume under thermal cycle, *Cem Concr Compos* 78 (2017) 108–119. <https://doi.org/10.1016/J.CEMCONCOMP.2017.01.009>.
- [68] Y. Aygörmez, O. Canpolat, M.M. Al-mashhadani, M. Uysal, Elevated temperature, freezing-thawing and wetting-drying effects on polypropylene fiber reinforced metakaolin based geopolymer composites, *Constr Build Mater* 235 (2020) 117502. <https://doi.org/10.1016/J.CONBUILDMAT.2019.117502>.
- [69] G. Liang, H. Zhu, Z. Zhang, Q. Wu, Effect of rice husk ash addition on the compressive strength and thermal stability of metakaolin based geopolymer, *Constr Build Mater* 222 (2019) 872–881. <https://doi.org/10.1016/J.CONBUILDMAT.2019.06.200>.
- [70] M.S. Aslam, B. Huang, L. Cui, Review of construction and demolition waste management in China and USA, *J Environ Manage* 264 (2020) 110445. <https://doi.org/10.1016/J.JENVMAN.2020.110445>.
- [71] Z. Wu, A.T.W. Yu, L. Shen, Investigating the determinants of contractor's construction and demolition waste management behavior in Mainland China, *Waste Management* 60 (2017) 290–300. <https://doi.org/10.1016/J.WASMAN.2016.09.001>.
- [72] H. Duan, T.R. Miller, G. Liu, V.W.Y. Tam, Construction debris becomes growing concern of growing cities, *Waste Management* 83 (2019) 1–5. <https://doi.org/10.1016/J.WASMAN.2018.10.044>.
- [73] U.S.E.P. Agency, *Advancing Sustainable Materials Management: 2018 Fact Sheet—Assessing Trends in Materials Generation and Management in the United States*, (2020).
- [74] M. Wahlström, J. Bergmans, T. Teittinen, J. Bachér, A. Smeets, A. Paduart, *Construction and Demolition Waste: challenges and opportunities in a circular economy*, Waste and Materials in a Green Economy; European Environment Agency: Copenhagen, Denmark (2020).

- [75] S.O. Ajayi, L.O. Oyedele, Policy imperatives for diverting construction waste from landfill: Experts' recommendations for UK policy expansion, *J Clean Prod* 147 (2017) 57–65. <https://doi.org/10.1016/J.JCLEPRO.2017.01.075>.
- [76] C.S. Poon, A.T.W. Yu, L.H. Ng, On-site sorting of construction and demolition waste in Hong Kong, *Resour Conserv Recycl* 32 (2001) 157–172. [https://doi.org/10.1016/S0921-3449\(01\)00052-0](https://doi.org/10.1016/S0921-3449(01)00052-0).
- [77] O. Şahin, H. İlcan, A.T. Ateşli, A. Kul, G. Yıldırım, M. Şahmaran, Construction and demolition waste-based geopolymers suited for use in 3-dimensional additive manufacturing, *Cem Concr Compos* 121 (2021) 104088. <https://doi.org/10.1016/J.CEMCONCOMP.2021.104088>.
- [78] M.B. Ali, R. Saidur, M.S. Hossain, A review on emission analysis in cement industries, *Renewable and Sustainable Energy Reviews* 15 (2011) 2252–2261. <https://doi.org/10.1016/J.RSER.2011.02.014>.
- [79] A.M. Zeyad, H.M. Magbool, B.A. Tayeh, A.R. Garcez de Azevedo, A. Abutaleb, Q. Hussain, Production of geopolymer concrete by utilizing volcanic pumice dust, *Case Studies in Construction Materials* 16 (2022) e00802. <https://doi.org/10.1016/J.CSCM.2021.E00802>.
- [80] H. Ulugöl, M.F. Günal, İ.Ö. Yaman, G. Yıldırım, M. Şahmaran, Effects of self-healing on the microstructure, transport, and electrical properties of 100% construction- and demolition-waste-based geopolymer composites, *Cem Concr Compos* 121 (2021) 104081. <https://doi.org/10.1016/J.CEMCONCOMP.2021.104081>.
- [81] H. Ulugöl, A. Kul, G. Yıldırım, M. Şahmaran, A. Aldemir, D. Figueira, A. Ashour, Mechanical and microstructural characterization of geopolymers from assorted construction and demolition waste-based masonry and glass, *J Clean Prod* 280 (2021) 124358. <https://doi.org/10.1016/J.JCLEPRO.2020.124358>.
- [82] G. Yıldırım, A. Kul, E. Özçelikci, M. Şahmaran, A. Aldemir, D. Figueira, A. Ashour, Development of alkali-activated binders from recycled mixed masonry-originated waste, *Journal of Building Engineering* 33 (2021) 101690. <https://doi.org/10.1016/J.JOBE.2020.101690>.
- [83] A. ALAHVERDI, E. NajafiKani, Construction wastes as raw materials for geopolymer binders, (2009).
- [84] L. Reig, M.M. Tashima, L. Soriano, M. V Borrachero, J. Monzó, J. Payá, Alkaline activation of ceramic waste materials, *Waste Biomass Valorization* 4 (2013) 729–736.

- [85] K. Komnitsas, D. Zaharaki, A. Vlachou, G. Bartzas, M. Galetakis, Effect of synthesis parameters on the quality of construction and demolition wastes (CDW) geopolymers, *Advanced Powder Technology* 26 (2015) 368–376. <https://doi.org/10.1016/J.APT.2014.11.012>.
- [86] A. Vásquez, V. Cárdenas, R.A. Robayo, R.M. de Gutiérrez, Geopolymer based on concrete demolition waste, *Advanced Powder Technology* 27 (2016) 1173–1179. <https://doi.org/10.1016/J.APT.2016.03.029>.
- [87] H.M. Khater, Effect of calcium on geopolymerization of aluminosilicate wastes, *Journal of Materials in Civil Engineering* 24 (2012) 92–101.
- [88] A. Allahverdi, E.N. Kani, Use of construction and demolition waste (CDW) for alkali-activated or geopolymer cements, *Handbook of Recycled Concrete and Demolition Waste* (2013) 439–475. <https://doi.org/10.1533/9780857096906.3.439>.
- [89] E. Ozcelikci, A. Kul, M.F. Gunal, B.F. Ozel, G. Yildirim, A. Ashour, M. Sahmaran, A comprehensive study on the compressive strength, durability-related parameters and microstructure of geopolymer mortars based on mixed construction and demolition waste, *J Clean Prod* 396 (2023) 136522. <https://doi.org/10.1016/J.JCLEPRO.2023.136522>.
- [90] M. Vafaei, A. Allahverdi, P. Dong, N. Bassim, M. Mahinroosta, Resistance of red clay brick waste/phosphorus slag-based geopolymer mortar to acid solutions of mild concentration, *Journal of Building Engineering* 34 (2021) 102066. <https://doi.org/10.1016/J.JOBE.2020.102066>.
- [91] H. Ilcan, O. Sahin, A. Kul, G. Yildirim, M. Sahmaran, Rheological properties and compressive strength of construction and demolition waste-based geopolymer mortars for 3D-Printing, *Constr Build Mater* 328 (2022) 127114. <https://doi.org/10.1016/J.CONBUILDMAT.2022.127114>.
- [92] H. Ilcan, O. Sahin, A. Kul, E. Ozcelikci, M. Sahmaran, Rheological property and extrudability performance assessment of construction and demolition waste-based geopolymer mortars with varied testing protocols, *Cem Concr Compos* 136 (2023) 104891. <https://doi.org/10.1016/J.CEMCONCOMP.2022.104891>.
- [93] O. Mahmoodi, H. Siad, M. Lachemi, S. Dadsetan, M. Sahmaran, Development of normal and very high strength geopolymer binders based on concrete waste at ambient environment, *J Clean Prod* 279 (2021) 123436. <https://doi.org/10.1016/J.JCLEPRO.2020.123436>.

- [94] S.A. Khan, A. Kul, O. Şahin, M. Şahmaran, S.G. Al-Ghamdi, M. Koç, Energy-environmental performance assessment and cleaner energy solutions for a novel Construction and Demolition Waste-based geopolymer binder production process, *Energy Reports* 8 (2022) 14464–14475. <https://doi.org/10.1016/J.EGYR.2022.10.345>.
- [95] N. Mir, S.A. Khan, A. Kul, O. Sahin, M. Sahmaran, M. Koc, Life cycle assessment of construction and demolition waste-based geopolymers suited for use in 3-dimensional additive manufacturing, *Clean Eng Technol* 10 (2022) 100553. <https://doi.org/10.1016/J.CLET.2022.100553>.
- [96] O. Mahmoodi, H. Siad, M. Lachemi, M. Şahmaran, Comparative life cycle assessment analysis of mono, binary and ternary construction and demolition wastes-based geopolymer binders, *Mater Today Proc* (2023). <https://doi.org/10.1016/J.MATPR.2023.05.658>.
- [97] O. Mahmoodi, H. Siad, M. Lachemi, S. Dadsetan, M. Sahmaran, Development of ceramic tile waste geopolymer binders based on pre-targeted chemical ratios and ambient curing, *Constr Build Mater* 258 (2020) 120297. <https://doi.org/10.1016/J.CONBUILDMAT.2020.120297>.
- [98] C.L. Hwang, M.D. Yehualaw, D.H. Vo, T.P. Huynh, A. Largo, Performance evaluation of alkali activated mortar containing high volume of waste brick powder blended with ground granulated blast furnace slag cured at ambient temperature, *Constr Build Mater* 223 (2019) 657–667. <https://doi.org/10.1016/J.CONBUILDMAT.2019.07.062>.
- [99] J. Tan, Ö. Cizer, B. Vandevyvere, J. De Vlieger, H. Dan, J. Li, Efflorescence mitigation in construction and demolition waste (CDW) based geopolymer, *Journal of Building Engineering* 58 (2022) 105001. <https://doi.org/10.1016/J.JOBE.2022.105001>.
- [100] H. Kloft, M. Empelmann, N. Hack, E. Herrmann, D. Lowke, Reinforcement strategies for 3D-concrete-printing, *Civil Engineering Design* 2 (2020) 131–139.
- [101] F. Hamidi, F. Aslani, Additive manufacturing of cementitious composites: Materials, methods, potentials, and challenges, *Constr Build Mater* 218 (2019) 582–609. <https://doi.org/10.1016/J.CONBUILDMAT.2019.05.140>.
- [102] S.H. Khajavi, M. Tetik, A. Mohite, A. Peltokorpi, M. Li, Y. Weng, J. Holmström, Additive Manufacturing in the Construction Industry: The Comparative

- Competitiveness of 3D Concrete Printing, *Applied Sciences* 11 (2021).
<https://doi.org/10.3390/app11093865>.
- [103] A. Al Rashid, S.A. Khan, S. G. Al-Ghamdi, M. Koç, Additive manufacturing: Technology, applications, markets, and opportunities for the built environment, *Autom Constr* 118 (2020) 103268. <https://doi.org/10.1016/J.AUTCON.2020.103268>.
- [104] H. İlcan, H. Özkılıç, M.S. Tuğluca, M. Şahmaran, Interlayer mechanical performance of 3D-printed cementitious systems: A comprehensive study on operational and material parameters, *Constr Build Mater* 419 (2024) 135463. <https://doi.org/10.1016/J.CONBUILDMAT.2024.135463>.
- [105] H. Özkılıç, H. İlcan, E. Aminipour, M.S. Tuğluca, A. Aldemir, M. Şahmaran, Bond properties and anisotropy performance of 3D-printed construction and demolition waste-based geopolymers: Effect of operational- and material-oriented parameters, *Journal of Building Engineering* 78 (2023) 107688. <https://doi.org/10.1016/J.JOBE.2023.107688>.
- [106] S.H. Ghaffar, J. Corker, M. Fan, Additive manufacturing technology and its implementation in construction as an eco-innovative solution, *Autom Constr* 93 (2018) 1–11. <https://doi.org/10.1016/J.AUTCON.2018.05.005>.
- [107] P. Wu, J. Wang, X. Wang, A critical review of the use of 3-D printing in the construction industry, *Autom Constr* 68 (2016) 21–31. <https://doi.org/10.1016/J.AUTCON.2016.04.005>.
- [108] R. Maskuriy, A. Selamat, P. Maresova, O. Krejcar, O.O. David, Industry 4.0 for the Construction Industry: Review of Management Perspective, *Economies* 7 (2019). <https://doi.org/10.3390/economies7030068>.
- [109] C. profile Denmark, European Construction Sector Observatory, (2021).
- [110] Integrating digital innovations in the construction sector: The case of 3D Printing and Drones in construction, 2019. <https://ec.europa.eu/docsroom/documents/34517/attachments/1/translations/en/renditions/native> (accessed February 16, 2024).
- [111] G. Ma, R. Buswell, W.R. Leal da Silva, L. Wang, J. Xu, S.Z. Jones, Technology readiness: A global snapshot of 3D concrete printing and the frontiers for development, *Cem Concr Res* 156 (2022) 106774. <https://doi.org/10.1016/J.CEMCONRES.2022.106774>.
- [112] S. El-Sayegh, L. Romdhane, S. Manjikian, A critical review of 3D printing in construction: benefits, challenges, and risks, *Archives of Civil and Mechanical Engineering* 20 (2020) 34. <https://doi.org/10.1007/s43452-020-00038-w>.

- [113] R. Robayo-Salazar, R. Mejía de Gutiérrez, M.A. Villaquirán-Caicedo, S. Delvasto Arjona, 3D printing with cementitious materials: Challenges and opportunities for the construction sector, *Autom Constr* 146 (2023) 104693. <https://doi.org/10.1016/J.AUTCON.2022.104693>.
- [114] S.K. Kaliyavaradhan, P.S. Ambily, P.R. Prem, S.B. Ghodke, Test methods for 3D printable concrete, *Autom Constr* 142 (2022) 104529. <https://doi.org/10.1016/J.AUTCON.2022.104529>.
- [115] G.M. Moelich, J. Kruger, R. Combrinck, Plastic shrinkage cracking in 3D printed concrete, *Compos B Eng* 200 (2020) 108313. <https://doi.org/10.1016/J.COMPOSITESB.2020.108313>.
- [116] M. Chougan, S. Hamidreza Ghaffar, M. Jahanzat, A. Albar, N. Mujaddedi, R. Swash, The influence of nano-additives in strengthening mechanical performance of 3D printed multi-binder geopolymer composites, *Constr Build Mater* 250 (2020) 118928. <https://doi.org/10.1016/J.CONBUILDMAT.2020.118928>.
- [117] A. Kashani, T.D. Ngo, Optimisation of mixture properties for 3D printing of geopolymer concrete, in: *Isarc. Proceedings of the International Symposium on Automation and Robotics in Construction*, IAARC Publications, 2018: pp. 1–8.
- [118] B. Panda, S.C. Paul, N.A.N. Mohamed, Y.W.D. Tay, M.J. Tan, Measurement of tensile bond strength of 3D printed geopolymer mortar, *Measurement* 113 (2018) 108–116. <https://doi.org/10.1016/J.MEASUREMENT.2017.08.051>.
- [119] B. Panda, C. Unluer, M.J. Tan, Investigation of the rheology and strength of geopolymer mixtures for extrusion-based 3D printing, *Cem Concr Compos* 94 (2018) 307–314. <https://doi.org/https://doi.org/10.1016/j.cemconcomp.2018.10.002>.
- [120] B. Panda, S. Chandra Paul, M. Jen Tan, Anisotropic mechanical performance of 3D printed fiber reinforced sustainable construction material, *Mater Lett* 209 (2017) 146–149. <https://doi.org/10.1016/J.MATLET.2017.07.123>.
- [121] S. Al-Qutaifi, A. Nazari, A. Bagheri, Mechanical properties of layered geopolymer structures applicable in concrete 3D-printing, *Constr Build Mater* 176 (2018) 690–699. <https://doi.org/10.1016/J.CONBUILDMAT.2018.04.195>.
- [122] B. Nematollahi, M. Xia, S.H. Bong, J. Sanjayan, Hardened properties of 3D printable ‘one-part’ geopolymer for construction applications, in: *First RILEM International Conference on Concrete and Digital Fabrication–Digital Concrete 2018*, Springer, 2019: pp. 190–199.

- [123] B. Panda, M.J. Tan, Experimental study on mix proportion and fresh properties of fly ash based geopolymer for 3D concrete printing, *Ceram Int* 44 (2018) 10258–10265. <https://doi.org/https://doi.org/10.1016/j.ceramint.2018.03.031>.
- [124] S. Muthukrishnan, S. Ramakrishnan, J. Sanjayan, Effect of alkali reactions on the rheology of one-part 3D printable geopolymer concrete, *Cem Concr Compos* 116 (2021) 103899. <https://doi.org/10.1016/J.CEMCONCOMP.2020.103899>.
- [125] G. Ma, Z. Li, L. Wang, G. Bai, Micro-cable reinforced geopolymer composite for extrusion-based 3D printing, *Mater Lett* 235 (2019) 144–147. <https://doi.org/10.1016/J.MATLET.2018.09.159>.
- [126] K. Pasupathy, S. Ramakrishnan, J. Sanjayan, 3D concrete printing of eco-friendly geopolymer containing brick waste, *Cem Concr Compos* 138 (2023) 104943. <https://doi.org/10.1016/J.CEMCONCOMP.2023.104943>.
- [127] G. Ma, Y. Yan, M. Zhang, J. Sanjayan, Effect of steel slag on 3D concrete printing of geopolymer with quaternary binders, *Ceram Int* 48 (2022) 26233–26247. <https://doi.org/10.1016/J.CERAMINT.2022.05.305>.
- [128] N.C. Demiral, M. Ozkan Ekinci, O. Sahin, H. Ilcan, A. Kul, G. Yildirim, M. Sahmaran, Mechanical anisotropy evaluation and bonding properties of 3D-printable construction and demolition waste-based geopolymer mortars, *Cem Concr Compos* 134 (2022) 104814. <https://doi.org/10.1016/J.CEMCONCOMP.2022.104814>.
- [129] D. Chaiyotha, W. Kantawong, P. Payakanitia, S. Pinitsoontorn, P. Chindaprasirt, Finding optimized conditions for 3D printed high calcium fly ash based alkali-activated mortar, *Case Studies in Construction Materials* 18 (2023) e01976. <https://doi.org/10.1016/J.CSCM.2023.E01976>.
- [130] A. Kazemian, X. Yuan, E. Cochran, B. Khoshnevis, Cementitious materials for construction-scale 3D printing: Laboratory testing of fresh printing mixture, *Constr Build Mater* 145 (2017) 639–647. <https://doi.org/10.1016/J.CONBUILDMAT.2017.04.015>.
- [131] Y. Kim, H.-J. Kong, V. Li, Design of Engineered Cementitious Composite (ECC) Suitable for Wet-mix Shotcreting, *ACI Mater J* 100 (2003).
- [132] B. Nematollahi, P. Vijay, J. Sanjayan, A. Nazari, M. Xia, V.N. Nerella, V. Mechtcherine, Effect of Polypropylene Fibre Addition on Properties of Geopolymers Made by 3D Printing for Digital Construction, *Materials* 11 (2018) 2352. <https://doi.org/10.3390/ma11122352>.

- [133] G. Tabilo-Munizaga, G. V. Barbosa-Cánovas, Rheology for the food industry, *J Food Eng* 67 (2005) 147–156. <https://doi.org/10.1016/J.JFOODENG.2004.05.062>.
- [134] Y. Chen, S. Chaves Figueiredo, Ç. Yalçınkaya, O. Çopuroğlu, F. Veer, E. Schlangen, The Effect of Viscosity-Modifying Admixture on the Extrudability of Limestone and Calcined Clay-Based Cementitious Material for Extrusion-Based 3D Concrete Printing, *Materials* 12 (2019) 1374. <https://doi.org/10.3390/ma12091374>.
- [135] X. Zhou, Z. Li, M. Fan, H. Chen, Rheology of semi-solid fresh cement pastes and mortars in orifice extrusion, *Cem Concr Compos* 37 (2013) 304–311. <https://doi.org/10.1016/J.CEMCONCOMP.2013.01.004>.
- [136] J.J. Benbow, J. Bridgwater, The influence of formulation on extrudate structure and strength, *Chem Eng Sci* 42 (1987) 753–766. [https://doi.org/10.1016/0009-2509\(87\)80035-0](https://doi.org/10.1016/0009-2509(87)80035-0).
- [137] R. v Mises, *Mechanik der festen Körper im plastisch-deformablen Zustand*, Nachrichten von Der Gesellschaft Der Wissenschaften Zu Göttingen, Mathematisch-Physikalische Klasse 1913 (1913) 582–592.
- [138] J.B. Guinee, Handbook on life cycle assessment operational guide to the ISO standards, *Int J Life Cycle Assess* 7 (2002) 311–313. <https://doi.org/10.1007/BF02978897>.
- [139] M. Goedkoop, M. Oele, A. Schrywer, M. Vieira, *SimaPro Database Manual: Methods Library*, 2008.
- [140] R. Bajpai, K. Choudhary, A. Srivastava, K.S. Sangwan, M. Singh, Environmental impact assessment of fly ash and silica fume based geopolymer concrete, *J Clean Prod* 254 (2020) 120147. <https://doi.org/https://doi.org/10.1016/j.jclepro.2020.120147>.
- [141] G. Habert, J.B. d’Espinose de Lacaillerie, N. Roussel, An environmental evaluation of geopolymer based concrete production: reviewing current research trends, *J Clean Prod* 19 (2011) 1229–1238. <https://doi.org/https://doi.org/10.1016/j.jclepro.2011.03.012>.
- [142] S. Yaseri, G. Hajiaghahi, F. Mohammadi, M. Mahdikhani, R. Farokhzad, The role of synthesis parameters on the workability, setting and strength properties of binary binder based geopolymer paste, *Constr Build Mater* 157 (2017) 534–545. <https://doi.org/10.1016/J.CONBUILDMAT.2017.09.102>.
- [143] O. Mahmoodi, H. Siad, M. Lachemi, M. Sahmaran, Synthesis and optimization of binary systems of brick and concrete wastes geopolymers at ambient environment,

- Constr Build Mater 276 (2021) 122217.
<https://doi.org/10.1016/J.CONBUILDMAT.2020.122217>.
- [144] Z. Duan, S. Hou, J. Xiao, A. Singh, Rheological properties of mortar containing recycled powders from construction and demolition wastes, *Constr Build Mater* 237 (2020) 117622. <https://doi.org/10.1016/J.CONBUILDMAT.2019.117622>.
- [145] S. Samantasinghar, S.P. Singh, Fresh and Hardened Properties of Fly Ash–Slag Blended Geopolymer Paste and Mortar, *Int J Concr Struct Mater* 13 (2019) 47. <https://doi.org/10.1186/s40069-019-0360-1>.
- [146] O. Boukendakdji, E.-H. Kadri, S. Kenai, Effects of granulated blast furnace slag and superplasticizer type on the fresh properties and compressive strength of self-compacting concrete, *Cem Concr Compos* 34 (2012) 583–590. <https://doi.org/https://doi.org/10.1016/j.cemconcomp.2011.08.013>.
- [147] O. Boukendakdji, S. Kenai, E.H. Kadri, F. Rouis, Effect of slag on the rheology of fresh self-compacted concrete, *Constr Build Mater* 23 (2009) 2593–2598. <https://doi.org/https://doi.org/10.1016/j.conbuildmat.2009.02.029>.
- [148] M.A. Megat Johari, J.J. Brooks, S. Kabir, P. Rivard, Influence of supplementary cementitious materials on engineering properties of high strength concrete, *Constr Build Mater* 25 (2011) 2639–2648. <https://doi.org/https://doi.org/10.1016/j.conbuildmat.2010.12.013>.
- [149] J.J. Brooks, M.A. Megat Johari, M. Mazloom, Effect of admixtures on the setting times of high-strength concrete, *Cem Concr Compos* 22 (2000) 293–301. [https://doi.org/https://doi.org/10.1016/S0958-9465\(00\)00025-1](https://doi.org/https://doi.org/10.1016/S0958-9465(00)00025-1).
- [150] J. Shang, J.-G. Dai, T.-J. Zhao, S.-Y. Guo, P. Zhang, B. Mu, Alternation of traditional cement mortars using fly ash-based geopolymer mortars modified by slag, *J Clean Prod* 203 (2018) 746–756. <https://doi.org/https://doi.org/10.1016/j.jclepro.2018.08.255>.
- [151] J. Tan, J. Cai, X. Li, J. Pan, J. Li, Development of eco-friendly geopolymers with ground mixed recycled aggregates and slag, *J Clean Prod* 256 (2020) 120369. <https://doi.org/https://doi.org/10.1016/j.jclepro.2020.120369>.
- [152] N.R. Rakhimova, R.Z. Rakhimov, Alkali-activated cements and mortars based on blast furnace slag and red clay brick waste, *Mater Des* 85 (2015) 324–331. <https://doi.org/https://doi.org/10.1016/j.matdes.2015.06.182>.

- [153] C.K. Yip, G.C. Lukey, J.S.J. van Deventer, The coexistence of geopolymetric gel and calcium silicate hydrate at the early stage of alkaline activation, *Cem Concr Res* 35 (2005) 1688–1697. <https://doi.org/10.1016/j.cemconres.2004.10.042>.
- [154] S. Ferreiro, D. Herfort, J.S. Damtoft, Effect of raw clay type, fineness, water-to-cement ratio and fly ash addition on workability and strength performance of calcined clay – Limestone Portland cements, *Cem Concr Res* 101 (2017) 1–12. <https://doi.org/10.1016/j.cemconres.2017.08.003>.
- [155] R. Kurda, J. de Brito, J.D. Silvestre, Influence of recycled aggregates and high contents of fly ash on concrete fresh properties, *Cem Concr Compos* 84 (2017) 198–213. <https://doi.org/10.1016/J.CEMCONCOMP.2017.09.009>.
- [156] P. Chindapasirt, S. Homwuttiwong, V. Sirivivatnanon, Influence of fly ash fineness on strength, drying shrinkage and sulfate resistance of blended cement mortar, *Cem Concr Res* 34 (2004) 1087–1092. <https://doi.org/10.1016/J.CEMCONRES.2003.11.021>.
- [157] F.A. Mustapha, A. Sulaiman, R.N. Mohamed, S.A. Umara, The effect of fly ash and silica fume on self-compacting high-performance concrete, *Mater Today Proc* 39 (2021) 965–969. <https://doi.org/10.1016/J.MATPR.2020.04.493>.
- [158] A. Jain, R. Gupta, S. Chaudhary, Sustainable development of self-compacting concrete by using granite waste and fly ash, *Constr Build Mater* 262 (2020) 120516. <https://doi.org/10.1016/J.CONBUILDMAT.2020.120516>.
- [159] W.E. Elemam, A.H. Abdelraheem, M.G. Mahdy, A.M. Tahwia, Optimizing fresh properties and compressive strength of self-consolidating concrete, *Constr Build Mater* 249 (2020) 118781. <https://doi.org/10.1016/J.CONBUILDMAT.2020.118781>.
- [160] T. Yang, H. Zhu, Z. Zhang, X. Gao, C. Zhang, Q. Wu, Effect of fly ash microsphere on the rheology and microstructure of alkali-activated fly ash/slag pastes, *Cem Concr Res* 109 (2018) 198–207. <https://doi.org/10.1016/J.CEMCONRES.2018.04.008>.
- [161] J. Qiu, Y. Zhao, J. Xing, X. Sun, Fly Ash/Blast Furnace Slag-Based Geopolymer as a Potential Binder for Mine Backfilling: Effect of Binder Type and Activator Concentration, *Advances in Materials Science and Engineering* 2019 (2019) 2028109. <https://doi.org/10.1155/2019/2028109>.
- [162] F.A. Memon, M.F. Nuruddin, N. Shafiq, Effect of silica fume on the fresh and hardened properties of fly ash-based self-compacting geopolymer concrete, *International Journal of Minerals, Metallurgy, and Materials* 20 (2013) 205–213.

- [163] R.P. Batista, A.C.C. Trindade, P.H.R. Borges, F. de A. Silva, Silica fume as precursor in the development of sustainable and high-performance MK-based alkali-activated materials reinforced with short PVA fibers, *Front Mater* 6 (2019) 77.
- [164] A.A. Ramezani-pour, M.A. Moeini, Mechanical and durability properties of alkali activated slag coating mortars containing nanosilica and silica fume, *Constr Build Mater* 163 (2018) 611–621. <https://doi.org/10.1016/J.CONBUILDMAT.2017.12.062>.
- [165] A. Wetzel, B. Middendorf, Influence of silica fume on properties of fresh and hardened ultra-high performance concrete based on alkali-activated slag, *Cem Concr Compos* 100 (2019) 53–59. <https://doi.org/10.1016/J.CEMCONCOMP.2019.03.023>.
- [166] C. Jithendra, S. Elavenil, Effects of Silica Fume on Workability and Compressive Strength Properties of Aluminosilicate Based Flowable Geopolymer Mortar under Ambient Curing, *Silicon* 12 (2020) 1965–1974. <https://doi.org/10.1007/s12633-019-00308-0>.
- [167] X. Dai, S. Aydın, M.Y. Yardımcı, K. Lesage, G. De Schutter, Rheology and microstructure of alkali-activated slag cements produced with silica fume activator, *Cem Concr Compos* 125 (2022) 104303. <https://doi.org/10.1016/J.CEMCONCOMP.2021.104303>.
- [168] J.G.S. Van Jaarsveld, J.S.J. Van Deventer, G.C. Lukey, The effect of composition and temperature on the properties of fly ash- and kaolinite-based geopolymers, *Chemical Engineering Journal* 89 (2002) 63–73. [https://doi.org/10.1016/S1385-8947\(02\)00025-6](https://doi.org/10.1016/S1385-8947(02)00025-6).
- [169] A.S. Faried, W.H. Sofi, A.-Z. Taha, M.A. El-Yamani, T.A. Tawfik, Mix Design Proposed for Geopolymer Concrete Mixtures Based on Ground Granulated Blast furnace slag, *Australian Journal of Civil Engineering* 18 (2020) 205–218. <https://doi.org/10.1080/14488353.2020.1761513>.
- [170] S.A. Bernal, E.D. Rodríguez, R. Mejía de Gutiérrez, M. Gordillo, J.L. Provis, Mechanical and thermal characterisation of geopolymers based on silicate-activated metakaolin/slag blends, *J Mater Sci* 46 (2011) 5477–5486. <https://doi.org/10.1007/s10853-011-5490-z>.
- [171] C. Shi, R.L. Day, A calorimetric study of early hydration of alkali-slag cements, *Cem Concr Res* 25 (1995) 1333–1346. [https://doi.org/10.1016/0008-8846\(95\)00126-W](https://doi.org/10.1016/0008-8846(95)00126-W).
- [172] O. Mahmoodi, H. Siad, M. Lachemi, S. Dadsetan, M. Sahmaran, Optimization of brick waste-based geopolymer binders at ambient temperature and pre-targeted

- chemical parameters, *J Clean Prod* 268 (2020) 122285. <https://doi.org/10.1016/J.JCLEPRO.2020.122285>.
- [173] I. Garcia-Lodeiro, A. Palomo, A. Fernández-Jiménez, D.E. Macphee, Compatibility studies between N-A-S-H and C-A-S-H gels. Study in the ternary diagram Na₂O–CaO–Al₂O₃–SiO₂–H₂O, *Cem Concr Res* 41 (2011) 923–931. <https://doi.org/https://doi.org/10.1016/j.cemconres.2011.05.006>.
- [174] W. Valencia-Saavedra, R. Robayo-Salazar, R. de Gutiérrez, Alkali-Activated Hybrid Cements Based on Fly Ash and Construction and Demolition Wastes Using Sodium Sulfate and Sodium Carbonate, *Molecules* 26 (2021). <https://doi.org/10.3390/molecules26247572>.
- [175] S.R. Da Silva, J.J. de O. Andrade, A Review on the Effect of Mechanical Properties and Durability of Concrete with Construction and Demolition Waste (CDW) and Fly Ash in the Production of New Cement Concrete, *Sustainability* 14 (2022). <https://doi.org/10.3390/su14116740>.
- [176] S. Songpiriyakij, T. Pulngern, P. Pungpremtrakul, C. Jaturapitakkul, Anchorage of steel bars in concrete by geopolymer paste, *Mater Des* 32 (2011) 3021–3028. <https://doi.org/10.1016/J.MATDES.2011.01.048>.
- [177] P. Chindaprasirt, P. Paisitsrisawat, U. Rattanasak, Strength and resistance to sulfate and sulfuric acid of ground fluidized bed combustion fly ash–silica fume alkali-activated composite, *Advanced Powder Technology* 25 (2014) 1087–1093. <https://doi.org/10.1016/J.APT.2014.02.007>.
- [178] S.H. Kang, Y. Jeong, M.O. Kim, J. Moon, Pozzolanic reaction on alkali-activated Class F fly ash for ambient condition curable structural materials, *Constr Build Mater* 218 (2019) 235–244. <https://doi.org/10.1016/J.CONBUILDMAT.2019.05.129>.
- [179] J.C. Knudson, G.B. Crane, R.S. Briggs, Atmospheric Emissions from Chlor-alkali Manufacture, Environmental Protection Agency, Air Pollution Control Office, 1971.
- [180] M.A. Villaquirán-Caicedo, R. Mejía de Gutiérrez, Comparison of different activators for alkaline activation of construction and demolition wastes, *Constr Build Mater* 281 (2021) 122599. <https://doi.org/10.1016/J.CONBUILDMAT.2021.122599>.
- [181] H. Ilcan, O. Sahin, Z. Unsal, E. Ozcelikci, A. Kul, N. Cağatay Demiral, M. Ozkan Ekinici, M. Sahmaran, Effect of industrial waste-based precursors on the fresh, hardened and environmental performance of construction and demolition wastes-based geopolymers, *Constr Build Mater* 394 (2023) 132265. <https://doi.org/10.1016/J.CONBUILDMAT.2023.132265>.

- [182] D.W. Zhang, D. min Wang, Z. Liu, F. zhu Xie, Rheology, agglomerate structure, and particle shape of fresh geopolymer pastes with different NaOH activators content, *Constr Build Mater* 187 (2018) 674–680. <https://doi.org/10.1016/J.CONBUILDMAT.2018.07.205>.
- [183] K. Vance, A. Dakhane, G. Sant, N. Neithalath, Observations on the rheological response of alkali activated fly ash suspensions: the role of activator type and concentration, *Rheol Acta* 53 (2014) 843–855. <https://doi.org/10.1007/s00397-014-0793-z>.
- [184] H. Jiang, M. Fall, E. Yilmaz, Y. Li, L. Yang, Effect of mineral admixtures on flow properties of fresh cemented paste backfill: Assessment of time dependency and thixotropy, *Powder Technol* 372 (2020) 258–266. <https://doi.org/10.1016/J.POWTEC.2020.06.009>.
- [185] A.F.H. Sherwani, K.H. Younis, R.W. Arndt, Fresh, Mechanical, and Durability Behavior of Fly Ash-Based Self Compacted Geopolymer Concrete: Effect of Slag Content and Various Curing Conditions, *Polymers (Basel)* 14 (2022) 3209.
- [186] T. Raju, K.P. Ramaswamy, B. Saraswathy, Effects of slag and superplasticizers on alkali activated geopolymer paste, in: *IOP Conf Ser Earth Environ Sci*, IOP Publishing, 2020: p. 012042.
- [187] M.B. Leite, J.G.L. Figueire do Filho, P.R.L. Lima, Workability study of concretes made with recycled mortar aggregate, *Mater Struct* 46 (2013) 1765–1778.
- [188] L. Evangelista, J. de Brito, Mechanical behaviour of concrete made with fine recycled concrete aggregates, *Cem Concr Compos* 29 (2007) 397–401. <https://doi.org/10.1016/J.CEMCONCOMP.2006.12.004>.
- [189] G.F. Huseien, J. Mirza, M. Ismail, M.W. Hussin, M.A.M. Arrifin, A.A. Hussein, The effect of sodium hydroxide molarity and other parameters on water absorption of geopolymer mortars, *Indian J. Sci. Technol* 9 (2016) 1–7.
- [190] A. Abdullah, K. Hussin, M.M.A.B. Abdullah, Z. Yahya, W. Sochacki, R.A. Razak, K. Błoch, H. Fansuri, The Effects of various concentrations of NaOH on the inter-particle gelation of a fly ash geopolymer aggregate, *Materials* 14 (2021) 1111.
- [191] H. İlcan, Investigation Of The Rheological and Workability Properties Of Construction and Demolition Waste Based Geopolymer Mortars, (2021).
- [192] K. Ghosh, P. Ghosh, Effect of % Na₂O and % SiO₂ on apperent porosity and sorptivity of fly ash based geopolymer, *IOSR J. Eng* 2 (2012) 96–101.

- [193] J.L. Provis, R.J. Myers, C.E. White, V. Rose, J.S.J. Van Deventer, X-ray microtomography shows pore structure and tortuosity in alkali-activated binders, *Cem Concr Res* 42 (2012) 855–864. <https://doi.org/10.1016/J.CEMCONRES.2012.03.004>.
- [194] Y. Hu, Z. Tang, W. Li, Y. Li, V.W.Y. Tam, Physical-mechanical properties of fly ash/GGBFS geopolymer composites with recycled aggregates, *Constr Build Mater* 226 (2019) 139–151. <https://doi.org/10.1016/J.CONBUILDMAT.2019.07.211>.
- [195] I. Ismail, S.A. Bernal, J.L. Provis, R. San Nicolas, D.G. Brice, A.R. Kilcullen, S. Hamdan, J.S.J. Van Deventer, Influence of fly ash on the water and chloride permeability of alkali-activated slag mortars and concretes, *Constr Build Mater* 48 (2013) 1187–1201. <https://doi.org/10.1016/J.CONBUILDMAT.2013.07.106>.
- [196] Z. Ma, Q. Tang, H. Wu, J. Xu, C. Liang, Mechanical properties and water absorption of cement composites with various fineness and contents of waste brick powder from C&D waste, *Cem Concr Compos* 114 (2020) 103758. <https://doi.org/10.1016/J.CEMCONCOMP.2020.103758>.
- [197] B. Skariah Thomas, J. Yang, A. Bahurudeen, S.N. Chinnu, J.A. Abdalla, R.A. Hawileh, H.M. Hamada, Geopolymer concrete incorporating recycled aggregates: A comprehensive review, *Cleaner Materials* 3 (2022) 100056. <https://doi.org/10.1016/J.CLEMA.2022.100056>.
- [198] F.U.A. Shaikh, H. Odoh, A.B. Than, Effect of nano silica on properties of concretes containing recycled coarse aggregates, *Proceedings of the Institution of Civil Engineers-Construction Materials* 168 (2015) 68–76.
- [199] N.S. Martys, C.F. Ferraris, Capillary transport in mortars and concrete, *Cem Concr Res* 27 (1997) 747–760. [https://doi.org/10.1016/S0008-8846\(97\)00052-5](https://doi.org/10.1016/S0008-8846(97)00052-5).
- [200] B. Dündar, M.S. Tuğluca, H. İlcan, O. Şahin, M. Şahmaran, The effects of various operational- and materials-oriented parameters on the carbonation performance of low-quality recycled concrete aggregate, *Journal of Building Engineering* 68 (2023) 106138. <https://doi.org/10.1016/J.JOBE.2023.106138>.
- [201] M. Hongqiang, C. Hongyu, Z. Hongguang, S. yangyang, N. Yadong, H. Qingjie, H. Zetao, Study on the drying shrinkage of alkali-activated coal gangue-slag mortar and its mechanisms, *Constr Build Mater* 225 (2019) 204–213. <https://doi.org/10.1016/J.CONBUILDMAT.2019.07.258>.

- [202] Z. Xu, J. Yue, G. Pang, R. Li, P. Zhang, S. Xu, Influence of the activator concentration and solid/liquid ratio on the strength and shrinkage characteristics of alkali-activated slag geopolymer pastes, *Advances in Civil Engineering 2021* (2021) 1–11.
- [203] Y. Zhang, H. Liu, T. Ma, G. Gu, C. Chen, J. Hu, Understanding the changes in engineering behaviors and microstructure of FA-GBFS based geopolymer paste with addition of silica fume, *Journal of Building Engineering* 70 (2023) 106450. <https://doi.org/10.1016/J.JOBE.2023.106450>.
- [204] G. Sadeghian, K. Behfarnia, M. Teymouri, Drying shrinkage of one-part alkali-activated slag concrete, *Journal of Building Engineering* 51 (2022) 104263. <https://doi.org/10.1016/J.JOBE.2022.104263>.
- [205] X. Liu, E. Liu, Y. Fu, Reduction in Drying Shrinkage and Efflorescence of Recycled Brick and Concrete Fine Powder–Slag-Based Geopolymer, *Applied Sciences* 13 (2023) 2997.
- [206] K. Mermerdaş, Z. Algin, Ekmen, Experimental assessment and optimization of mix parameters of fly ash-based lightweight geopolymer mortar with respect to shrinkage and strength, *Journal of Building Engineering* 31 (2020) 101351. <https://doi.org/10.1016/J.JOBE.2020.101351>.
- [207] W. Xu, Z. Tang, Y. Song, Y. Xie, B. Lei, H. Yu, G. Long, M. Kai, Drying shrinkage of geopolymeric recycled aggregate concrete, *Constr Build Mater* 395 (2023) 132220. <https://doi.org/10.1016/J.CONBUILDMAT.2023.132220>.
- [208] F. Matakah, T. Salem, M. Shaafaey, P. Soroushian, Drying shrinkage of alkali activated binders cured at room temperature, *Constr Build Mater* 201 (2019) 563–570. <https://doi.org/10.1016/J.CONBUILDMAT.2018.12.223>.
- [209] H. Wu, C. Wang, Z. Ma, Drying shrinkage, mechanical and transport properties of sustainable mortar with both recycled aggregate and powder from concrete waste, *Journal of Building Engineering* 49 (2022) 104048. <https://doi.org/10.1016/J.JOBE.2022.104048>.
- [210] M. Albitar, M.S. Mohamed Ali, P. Visintin, M. Drechsler, Durability evaluation of geopolymer and conventional concretes, *Constr Build Mater* 136 (2017) 374–385. <https://doi.org/10.1016/J.CONBUILDMAT.2017.01.056>.
- [211] E. Yener, C. Karaaslan, Curing time and temperature effect on the resistance to wet-dry cycles of fly ash added pumice based geopolymer, *Cement Based Composites* 1 (2020) 19–25.

- [212] A. Fakhrabadi, M. Ghadakpour, A.J. Choobbasti, S.S. Kutanaei, Evaluating the durability, microstructure and mechanical properties of a clayey-sandy soil stabilized with copper slag-based geopolymer against wetting-drying cycles, *Bulletin of Engineering Geology and the Environment* 80 (2021) 5031–5051. <https://doi.org/10.1007/s10064-021-02228-z>.
- [213] B. Nikmehr, R. Al-Ameri, A state-of-the-art review on the incorporation of recycled concrete aggregates in geopolymer concrete, *Recycling* 7 (2022) 51.
- [214] B. Zhang, H. Zhu, P. Feng, P. Zhang, A review on shrinkage-reducing methods and mechanisms of alkali-activated/geopolymer systems: Effects of chemical additives, *Journal of Building Engineering* 49 (2022) 104056. <https://doi.org/10.1016/J.JOBE.2022.104056>.
- [215] E. Bahşi, O. Şahin, H. İlcan, B. Uzal, M.F. Günal, G. Yıldırım, M. Şahmaran, Role of inclusion size distribution of titanium dioxide on the nitrogen oxides reduction capability and microstructural characteristics of cementitious systems, *Constr Build Mater* 318 (2022) 125992. <https://doi.org/10.1016/J.CONBUILDMAT.2021.125992>.
- [216] P. Duan, C. Yan, W. Luo, W. Zhou, Effects of adding nano-TiO₂ on compressive strength, drying shrinkage, carbonation and microstructure of fluidized bed fly ash based geopolymer paste, *Constr Build Mater* 106 (2016) 115–125. <https://doi.org/10.1016/J.CONBUILDMAT.2015.12.095>.
- [217] T. Phoo-ngernkham, P. Chindaprasirt, V. Sata, S. Hanjitsuwan, S. Hatanaka, The effect of adding nano-SiO₂ and nano-Al₂O₃ on properties of high calcium fly ash geopolymer cured at ambient temperature, *Mater Des* 55 (2014) 58–65. <https://doi.org/10.1016/J.MATDES.2013.09.049>.
- [218] P. Zhang, J. Su, J. Guo, S. Hu, Influence of carbon nanotube on properties of concrete: A review, *Constr Build Mater* 369 (2023) 130388. <https://doi.org/10.1016/J.CONBUILDMAT.2023.130388>.
- [219] H. Du, H.J. Gao, S.D. Pang, Improvement in concrete resistance against water and chloride ingress by adding graphene nanoplatelet, *Cem Concr Res* 83 (2016) 114–123. <https://doi.org/10.1016/J.CEMCONRES.2016.02.005>.
- [220] J.H. Ideker, K.L. Scrivener, H. Fryda, B. Touzo, Calcium Aluminate Cements, *Lea's Chemistry of Cement and Concrete* (2019) 537–584. <https://doi.org/10.1016/B978-0-08-100773-0.00012-5>.
- [221] A.M. Kalinkin, B.I. Gurevich, M.S. Myshenkov, M. V Chislov, E. V Kalinkina, I.A. Zvereva, Z. Cherkezova-Zheleva, D. Paneva, V. Petkova, Synthesis of Fly Ash-Based

- Geopolymers: Effect of Calcite Addition and Mechanical Activation, *Minerals* 10 (2020). <https://doi.org/10.3390/min10090827>.
- [222] P. Lertwattanakul, G. Sua-iam, N. Makul, Effects of calcium carbonate powder on the fresh and hardened properties of self-consolidating concrete incorporating untreated rice husk ash, *J Clean Prod* 172 (2018) 3265–3278. <https://doi.org/10.1016/J.JCLEPRO.2017.10.336>.
- [223] S. V Patankar, Y.M. Ghugal, S.S. Jamkar, Mix design of fly ash based geopolymer concrete, in: *Advances in Structural Engineering: Materials, Volume Three*, Springer, 2015: pp. 1619–1634.
- [224] K. Behfarnia, M. Rostami, Mechanical properties and durability of fiber reinforced alkali activated slag concrete, *Journal of Materials in Civil Engineering* 29 (2017) 04017231.
- [225] Y. Cui, D. Wang, Effects of Water on Pore Structure and Thermal Conductivity of Fly Ash-Based Foam Geopolymers, *Advances in Materials Science and Engineering* 2019 (2019) 3202794. <https://doi.org/10.1155/2019/3202794>.
- [226] Y.F. Cao, Z. Tao, Z. Pan, R. Wuhler, Effect of calcium aluminate cement on geopolymer concrete cured at ambient temperature, *Constr Build Mater* 191 (2018) 242–252. <https://doi.org/10.1016/J.CONBUILDMAT.2018.09.204>.
- [227] A. Aboulayt, M. Riahi, M. Ouazzani Touhami, H. Hannache, M. Gomina, R. Moussa, Properties of metakaolin based geopolymer incorporating calcium carbonate, *Advanced Powder Technology* 28 (2017) 2393–2401. <https://doi.org/10.1016/J.APT.2017.06.022>.
- [228] B.B. Jindal, R. Sharma, The effect of nanomaterials on properties of geopolymers derived from industrial by-products: A state-of-the-art review, *Constr Build Mater* 252 (2020) 119028. <https://doi.org/10.1016/J.CONBUILDMAT.2020.119028>.
- [229] T. Alomayri, Experimental study of the microstructural and mechanical properties of geopolymer paste with nano material (Al₂O₃), *Journal of Building Engineering* 25 (2019) 100788. <https://doi.org/10.1016/J.JOBE.2019.100788>.
- [230] Y. Cui, H. Hao, J. Li, W. Chen, Effect of adding methylcellulose on mechanical and vibration properties of geopolymer paste and hybrid fiber-reinforced geopolymer composite, *Journal of Materials in Civil Engineering* 32 (2020) 04020166.
- [231] M. Komljenović, Z. Baščarević, V. Bradić, Mechanical and microstructural properties of alkali-activated fly ash geopolymers, *J Hazard Mater* 181 (2010) 35–42. <https://doi.org/10.1016/J.JHAZMAT.2010.04.064>.

- [232] M.M.A.B. Abdullah, H. Kamarudin, M. Binhussain, R. Razak, Z. Yahya, Effect of Na₂SiO₃/NaOH Ratios and NaOH Molarities on Compressive Strength of Fly-Ash-Based Geopolymer, *ACI Mater J* 109 (2012) 503–508.
- [233] P. Risdanareni, J.J. Ekaputri, Triwulan, The influence of alkali activator concentration to mechanical properties of geopolymer concrete with trass as a filler, in: *Materials Science Forum*, Trans Tech Publ, 2015: pp. 125–134.
- [234] F. Matakah, R. Aqel, A. Ababneh, Enhancement of the Mechanical Properties of Kaolin Geopolymer Using Sodium Hydroxide and Calcium Oxide, *Procedia Manuf* 44 (2020) 164–171. <https://doi.org/10.1016/J.PROMFG.2020.02.218>.
- [235] X. Chen, J. Zhang, M. Lu, B. Chen, S. Gao, J. Bai, H. Zhang, Y. Yang, Study on the effect of calcium and sulfur content on the properties of fly ash based geopolymer, *Constr Build Mater* 314 (2022) 125650. <https://doi.org/10.1016/J.CONBUILDMAT.2021.125650>.
- [236] X. Zhao, C. Liu, L. Zuo, L. Wang, Q. Zhu, M. Wang, Investigation into the effect of calcium on the existence form of geopolymerized gel product of fly ash based geopolymers, *Cem Concr Compos* 103 (2019) 279–292. <https://doi.org/10.1016/J.CEMCONCOMP.2018.11.019>.
- [237] M.H. El Ouni, A. Raza, H. Haider, M. Arshad, B. Ali, Enhancement of mechanical and toughness properties of carbon fiber-reinforced geopolymer pastes comprising nano calcium oxide, *Journal of the Australian Ceramic Society* 58 (2022) 1375–1387. <https://doi.org/10.1007/s41779-022-00764-9>.
- [238] M. Vafaei, A. Allahverdi, Influence of calcium aluminate cement on geopolymerization of natural pozzolan, *Constr Build Mater* 114 (2016) 290–296. <https://doi.org/10.1016/J.CONBUILDMAT.2016.03.204>.
- [239] A. Fernández-Jiménez, A. Palomo, T. Vazquez, R. Vallepu, T. Terai, K. Ikeda, Alkaline activation of blends of metakaolin and calcium aluminate, *Journal of the American Ceramic Society* 91 (2008) 1231–1236.
- [240] M.L. Granizo, S. Alonso, M.T. Blanco-Varela, A. Palomo, Alkaline activation of metakaolin: effect of calcium hydroxide in the products of reaction, *Journal of the American Ceramic Society* 85 (2002) 225–231.
- [241] T. Tracz, J. Śliwiński, Effect of cement paste content and w/c ratio on concrete water absorption, *Cement Wapno Beton* 17 (2012).
- [242] G.L. Golewski, Assessing of water absorption on concrete composites containing fly ash up to 30 % in regards to structures completely immersed in water, *Case Studies*

- in *Construction Materials* 19 (2023) e02337.
<https://doi.org/10.1016/J.CSCM.2023.E02337>.
- [243] E. Güneyisi, M. Gesoğlu, T. Ozturan, K. Mermerdaş, E. Özbay, Properties of Mortars with Natural Pozzolana and Limestone-Based Blended Cements, *ACI Mater J* 108 (2011) 493–500.
- [244] A.K. Saha, P.K. Sarker, Durability characteristics of concrete using ferronickel slag fine aggregate and fly ash, *Magazine of Concrete Research* 70 (2018) 865–874.
- [245] E.U. CCAA, Cement Concrete & Aggregates Australia, 2010, Website: Http://Www.Ccaa.Com.Au/LCA/Case_studies/WarehouseBuilding/Operation_vs_construction.Php (2009).
- [246] Y. Benachour, C.A. Davy, F. Skoczylas, H. Houari, Effect of a high calcite filler addition upon microstructural, mechanical, shrinkage and transport properties of a mortar, *Cem Concr Res* 38 (2008) 727–736.
<https://doi.org/10.1016/J.CEMCONRES.2008.02.007>.
- [247] H. Chen, X. Chen, W. Tan, P. Wu, Y. Zhang, Durability performance of waste glass powder and calcium oxide added sodium carbonate-activated slag mortar, *Mater Today Commun* 36 (2023) 106472.
<https://doi.org/10.1016/J.MTCOMM.2023.106472>.
- [248] M. Vafaei, A. Allahverdi, High strength geopolymer binder based on waste-glass powder, *Advanced Powder Technology* 28 (2017) 215–222.
<https://doi.org/10.1016/J.APT.2016.09.034>.
- [249] E. Najafi Kani, A. Allahverdi, J.L. Provis, Efflorescence control in geopolymer binders based on natural pozzolan, *Cem Concr Compos* 34 (2012) 25–33.
<https://doi.org/10.1016/J.CEMCONCOMP.2011.07.007>.
- [250] M. Mastali, P. Kinnunen, A. Dalvand, R. Mohammadi Firouz, M. Illikainen, Drying shrinkage in alkali-activated binders – A critical review, *Constr Build Mater* 190 (2018) 533–550. <https://doi.org/10.1016/J.CONBUILDMAT.2018.09.125>.
- [251] X. Zhu, X. Kang, J. Deng, K. Yang, L. Yu, C. Yang, A comparative study on shrinkage characteristics of graphene oxide (GO) and graphene nanoplatelets (GNPs) modified alkali-activated slag cement composites, *Mater Struct* 54 (2021) 106.
<https://doi.org/10.1617/s11527-021-01695-w>.
- [252] C. Ridtirud, P. Chindaprasirt, K. Pimraksa, Factors affecting the shrinkage of fly ash geopolymers, *International Journal of Minerals, Metallurgy, and Materials* 18 (2011) 100–104. <https://doi.org/10.1007/s12613-011-0407-z>.

- [253] P.L. Nasatto, F. Pignon, J.L.M. Silveira, M.E.R. Duarte, M.D. Nosedá, M. Rinaudo, Methylcellulose, a Cellulose Derivative with Original Physical Properties and Extended Applications, *Polymers (Basel)* 7 (2015) 777–803. <https://doi.org/10.3390/polym7050777>.
- [254] X.H. Yuan, W. Chen, Z.A. Lu, H. Chen, Shrinkage compensation of alkali-activated slag concrete and microstructural analysis, *Constr Build Mater* 66 (2014) 422–428. <https://doi.org/10.1016/J.CONBUILDMAT.2014.05.085>.
- [255] X. Zhu, D. Tang, K. Yang, Z. Zhang, Q. Li, Q. Pan, C. Yang, Effect of Ca(OH)₂ on shrinkage characteristics and microstructures of alkali-activated slag concrete, *Constr Build Mater* 175 (2018) 467–482. <https://doi.org/10.1016/J.CONBUILDMAT.2018.04.180>.
- [256] H. İlcan, A.O. Demirbaş, H. Ulugöl, M. Şahmaran, Low-alkaline activated construction and demolition waste-based geopolymers, *Constr Build Mater* 411 (2024) 134546. <https://doi.org/10.1016/J.CONBUILDMAT.2023.134546>.
- [257] M.S. Tuğluca, E. Özdoğru, H. İlcan, E. Özçelikci, H. Ulugöl, M. Şahmaran, Characterization of chemically treated waste wood fiber and its potential application in cementitious composites, *Cem Concr Compos* 137 (2023) 104938. <https://doi.org/10.1016/J.CEMCONCOMP.2023.104938>.
- [258] Y. Chen, K. Jansen, H. Zhang, C. Romero Rodriguez, Y. Gan, O. Çopuroğlu, E. Schlangen, Effect of printing parameters on interlayer bond strength of 3D printed limestone-calcined clay-based cementitious materials: An experimental and numerical study, *Constr Build Mater* 262 (2020) 120094. <https://doi.org/10.1016/J.CONBUILDMAT.2020.120094>.
- [259] Y. Xu, Q. Yuan, Z. Li, C. Shi, Q. Wu, Y. Huang, Correlation of interlayer properties and rheological behaviors of 3DPC with various printing time intervals, *Addit Manuf* 47 (2021) 102327. <https://doi.org/10.1016/J.ADDMA.2021.102327>.
- [260] B. Panda, N.A. Noor Mohamed, S.C. Paul, G.V.P. Bhagath Singh, M.J. Tan, B. Šavija, The Effect of Material Fresh Properties and Process Parameters on Buildability and Interlayer Adhesion of 3D Printed Concrete, *Materials* 12 (2019). <https://doi.org/10.3390/ma12132149>.
- [261] J.G. Sanjayan, B. Nematollahi, M. Xia, T. Marchment, Effect of surface moisture on inter-layer strength of 3D printed concrete, *Constr Build Mater* 172 (2018) 468–475. <https://doi.org/10.1016/J.CONBUILDMAT.2018.03.232>.

- [262] K. Federowicz, M. Kaszyńska, A. Zieliński, M. Hoffmann, Effect of Curing Methods on Shrinkage Development in 3D-Printed Concrete, *Materials* 13 (2020). <https://doi.org/10.3390/ma13112590>.
- [263] S. Qian, V.C. Li, Influence of concrete material ductility on shear response of stud connections, *ACI Mater J* 103 (2006) 60.